AAR Expansion; Effect of Reinforcement, Specimen Type, and Temperature

Task 1-B

December 2017

by

Victor E. Saouma
Damon Howard
David Graff
Mohammad Amin Hariri-Ardebili

University of Colorado, Boulder

NRC-HQ-60-14-G-0010: Reports

1-A: *Design of an AAR Prone Concrete Mix for Large Scale Testing*
1-B: *AAR Expansion; Effect of Reinforcement, Specimen Type, and Temperature*
1-C: *Effect of AAR on Shear Strength of Panels*
2: *Diagnosis & Prognosis of AAR in Existing Structures*
3-a: *Effect of AAR on the Capacity of a Shear Wall Subjected to Reverse Cyclic Loading*
3-b: *Probabilistic Based Nonlinear Seismic Analysis of Nuclear Containment Vessel Structures with AAR*

Contents

List of Figures

List of Tables

NOTE

This report follows a preceding one which addressed the reactive concrete mix design and culminated with the casting of the specimens off-campus.

It will address the ensuing on-campus activities: curing of the specimens, followed by testing.

1 Introduction

1.1 Motivation

Alkali-silica reactions (ASR) have been known to cause degradation in concrete (Stanton, 1940). Cracking and damage due to ASR has been observed in large scale concrete structures such as bride piers, dams, and nuclear power plants in recent years (Morenon et al., 2017) (Saouma et al., 2016). To understand how these structures will be affected on the global scale, it is important to understand how concrete responds on the material level in various configurations and conditions.

The overall research goal, which this thesis is only a portion of, is to quantify the risks to concrete nuclear power plant containment structures affected by alkali silica reactions (ASR) during a seismic event by quantifying the effects of ASR expansion on the shear strength of the concrete. In order to do this, representative model concrete shear specimens with reactive aggregates and increased alkalinity are cast and stored in a high heat and humidity environment to accelerate ASR degradation and reach a target expansion of 0.5% as quickly as possible. Once the expansion goal is reached, specimens are loaded in shear across their cross section under confining pressure. Results are compared to control specimens of the same size and concrete mix with ASR suppressed through the addition of lithium nitrate during concrete mixing.

1.2 Research Objective

There are two main research objectives that this thesis will cover. The first is to promote ASR expansion in shear specimens, prisms, and blocks until they expand to a target level. The second will make up the bulk of this report consists of the studying how six different reinforcement configurations or two different storage temperatures will effect the expansion of the specimen

First, this report will outline the process of promoting and tracking ASR swelling in the reactive concrete specimens throughout this experiment. Using datum discs, DEMEC strain guages, internal temperature sensors, strain guages, a ambient temperature and humidity data logger, and pH sensors, a large amount of expansion and supplemental data has been collected. Data provides a multitude of opportunities to understand how expansion is progressing towards the ultimate expansion goal of 0.5%. These tools enabled tracking the expansion of the specimens and recognition of any corrective actions that needed to be taken.

For the second research objective, a number of prisms and blocks were cast at the same time and from the same concrete mixes as the shear specimens. To study the reinforcement effects on expansion, prisms and shear specimens are either reinforced with axial reinforcement or unreinforced while the blocks are reinforced with six different reinforcement configurations. Additionally, blocks and prisms are stored at two different temperature levels; 100°F or 70°F. Tracking the ASR expansion at these different temperatures will show

how the different temperature levels affect ASR expansion.

1.3 Report Organization

This report consists of nine chapters and an appendix. This chapter presents the motivations behind the project and the objectives of the thesis. The chapters that follow detail the process of developing ASR in concrete, collecting expansion data, and analysis of that data.

Chapter 2 is a review of previous research completed on this topic. A brief overview of alkali-silica reaction and the factors influencing its production are presented. Studies of reinforcement and environmental effects on ASR afflicted concrete are also listed that inform the predictions of outcomes for this thesis.

Chapter 3 gives a brief summary of casting the concrete specimens. This chapter gives an inventory of the specimens, reinforcement, location, and the data collection devices with which they are outfitted. Also included is an description of the conditions in which the specimens are cured and the tools to achieve those conditions.

Chapter 4 discusses the tools used to monitor the ASR expansion and the crack indexes during the curing process. Included is the method for data collection, processing, and presented in a way that conclusions can be made.

Chapter 5 has pictures of specimens.

Chapter 6 and 7 will present the measured expansions and crack indexes respectively.

Chapter 8 presents the predicted outcomes of the project developed from the research collected in Chapter 2. Results of the processed expansion and supplementary data collected during the course of the project are presented. Discussion of synthesized results and how they compare to the predictions is given.

Chapter 9 is the conclusion of the thesis which summarizes the work completed, the observations that have been made, and recommendations for future work.

Finally, the appendix will show the individual expansion curves of each sample.

2 Literature Review

2.1 Introduction

Alkali-silica reactions (ASR) were first recognized as a deleterious process in concrete by Stanton (1940). Three components are required to form ASR; reactive minerals in aggregates, sufficient alkalinity from cement, and adequate moisture to hydrate the produced gel. ASR occurs when alkali material such as sodium (Na^+) or potassium (K^+) ions are released from the cement to react with silica (SiO_2) released from reactive aggregate to form a gel. In the presence of water, the gel expands to initially fill the pores of the concrete and eventually form cracks throughout the cement paste and aggregate (Hobbs, 1988). The chemical equation showing this process is shown below (Saouma and Perotti, 2006).

$$xSiO_2 + yNa(K)OH \rightarrow Na_ySiXO_{z,aq}$$
$$Na(K)_ySi_xO_{z,aq} + H_2O \rightarrow Na(K)_ySi_xO_zwH_2O$$

ASR is most often seen in large civil engineering structures that are subject to significant loading, such as bridge piers or dams (Morenon et al., 2017). More recently, there is evidence of ASR occurring in nuclear power plants (Saouma et al., 2016). ASR expansion can lead to damage and cracks in structures resulting in a decrease of their stability, safety, and performance.

Determining if a given aggregate is capable of causing ASR and ASR's effect on concrete's mechanical properties such as compressive strength, tensile strength, modulus of elasticity, and modulus of rupture has previously been studied (Swamy and Al-Asali, 1988). As mentioned previously, the ultimate goal of the overall experiment is to quantify the effects of ASR expansion on the shear strength of the concrete, of which there is little research. Saouma et al. (2016) theorizes that as concrete degrades, the shear strength should be decreased since the concrete is degrading at the material level. However, they state that ASR induces additional compressive stress, similar to a prestressing, which will increase the shear resistance of the concrete. Additionally, ASR expansion is likely to reduce crack openings during shear loading, increasing aggregate interlock and providing additional shear resistance. Understanding the factors that promote ASR expansion allows the creation ASR expansion in shear specimens rapidly and efficiently to study the effects on shear strength.

2.2 Parameters Influencing ASR Expansion in Laboratory Testing

Many factors can cause variability in the rate of ASR expansion during accelerated laboratory testing. Aggregate type, size, and grading, cement type, and mix design all play an important role in the expansion of concrete. These factors as part of the ongoing research objectives of this project were previously studied

by Saouma, Sparks, and Graff (2016). While these variables do affect ASR expansion, they are outside the scope of this thesis since they have previously been set. Each specimen is made of the same mix design so these variables are not differentiating factors. Therefore, all the parameters that influence ASR discussed here are ones that can be altered during the "curing" stage of the project after the specimens have been cast.

(Lindgård et al., 2012) completed a literature review that evaluates the influence of exposure conditions during storage and curing. The following are the parameters that can impact ASR production during the curing phase:

- Internal Moisture Conditions
- Alkali Leaching
- Specimen Wrapping
- Externally Added Alkalis
- Storage Temperature

As stated previously, moisture is required for ASR swelling to occur by hydrating the silica gel. Storing specimens over water in sealed containers were found to reduce expansion by Blanks and Meissner (1946). Lindgård found wrapping specimens in a wetted absorbent material, such as burlap or cotton, can have a pronounced effect on ASR expansion by either reducing or promoting alkali leaching. The composition of the wetting solution impacts which will occur. Water alone can promote the leaching of alkalinity. Samples wrapped in cloth wetted with 1.0M or 0.1M NaOH. Specimens exposed to higher alkalinity solution showed 25% more expansion than unwrapped samples and 3.5 times more than prisms wrapped with de-ionized water. Wrapping with 0.1M NaOH did not significantly prevent alkali leaching but the effects on expansions were negligible. Temperature also plays a significant role in the amount of ASR expansion. Since this is one of the parameters being studied in this thesis, its effects are discussed more in depth in Section 2.3.

2.3 Effects of Temperature

One of the principal parameters affecting the expansion of ASR effected concrete is the temperature of the specimens. ASR is a thermodynamically driven reaction and the temperature of the concrete has a great affect on the rate of expansion (Larive, 1998). Concretes stored at elevated temperatures show a faster initial expansion and higher ultimate expansion than those stored at room temperature, Figure 2.1 (Swamy and Al-Asali, 1988).

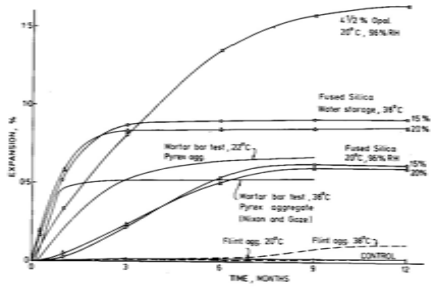

Figure 2.1: Results of Temperature Effect on ASR Expansion (Swamy and Al-Asali, 1988)

As temperature increases, the solubility of SiO_2, and subsequently the reaction rate, also increases. This forms a greater amount of silica gel producing higher expansion. This magnitude of this effect varies for

different types of silica-rich aggregates and can even activate seemingly "non-reactive" aggregates at high temperatures (Lindgård et al., 2012).

There is a substantial difference between accelerated lab testing and ASR formation in real life structures. Ideker et al. (2012) found that in testing 17 coarse aggregates, five were found to not be deleterious using ASTM C1260 (2000) (Accelerated Mortar Bar Test) but were found to be substantially reactive when subjected to ASTM C1293 (2008) and outdoor exposure block testing. In an attempt to accurately compare the effects of real-life environmental effects on ASR expansion, Fournier et al. (2009) compared the expansion of identical blocks in Ottawa, Canada and Austin, Texas showing that ASR expansion occurs at a higher rate in warmer climates than cooler climates.

Additionally, ASR expansion can vary within a structure according to the exposure conditions. Cores taken from exposed portions structures (such as from the extremities of an abutment wall or foundation) afflicted with ASR in expansion tests in laboratory conditions showed greater cracking than unexposed portions. This is due to exposure freeze-thaw and wetting-drying cycles which effect the concrete near the structure's extremities and accelerate ASR cracking (Bérubé et al., 2005).

2.4 Effects of Reinforcement

One parameter affecting ASR expansion not listed by (Lindgård et al., 2012) is the internal restraint due to embedded reinforcement. Reinforcement can have a pronounced effect on ASR by providing a restraint against the expansion by absorbing the produced strain into the reinforcement. Unlike the parameters listed above, reinforcement does not impact the chemical reaction but restrains the effects of the reaction.

In accelerated mortar bar tests, modified to produce a reinforced specimen using wire reinforcement, (Musaoglu, Turanli, and Saritas, 2014) found reinforcement had a considerable effect on expansion when compared to unreinforced specimens. Mortar bars with no reinforcement and reinforcements ratios of 0.045%, 0.08%, and 0.125% were tested, Figure 2.2. As the reinforcement ratio increased, expansion decreased at a greater rate. Only moderate levels of reinforcement were necessary to produce large decreases in expansion. Additionally, ASR expansion was further reduced by the inclusion of a prestressing force on the wire reinforcement.

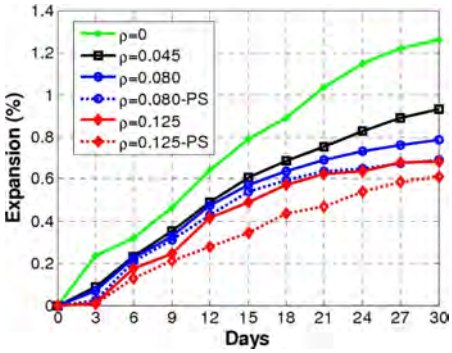

Figure 2.2: Reinforcement and prestressing effects on expansion, (Musaoglu, Turanli, and Saritas, 2014)

Morenon et al. (2017) studied the effects of strain and stress induced by restraints due to reinforcement in one, two, or three directions on ASR expansion. The inclusion of steel reinforcement in long concrete cylinders reduced expansion up to 50% in the reinforced direction while increasing strain in the orthogonal

direction by up to 30%, Figure 2.3 and 2.4. Expansion caused increased stress in the reinforcement to the point of debonding.

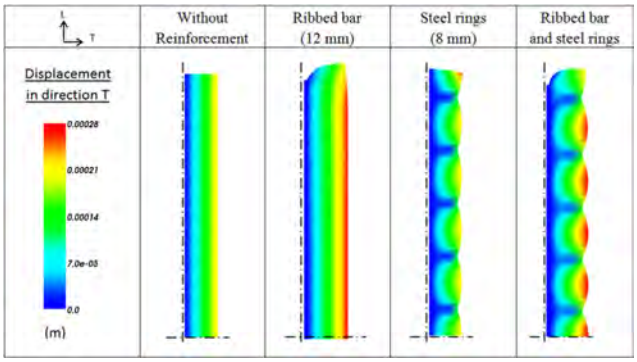

Figure 2.3: Reinforcement effects on expansion (Musaoglu, Turanli, and Saritas, 2014)

	Without Reinforcement (WR)	Ribbed bars (12 mm)	Steel rings (8 mm)	Ribbed bars and steel rings
$\frac{\varepsilon_L}{\varepsilon_{WR}}$	**1**	From **0.3** *(close to the top)* to **0.5** *(close to the axis of symmetry)*	**1.3**	From **0.4** *(close to the top)* to **0.6** *(close to the axis of symmetry)*
$\frac{\varepsilon_T}{\varepsilon_{WR}}$	**1**	**1.2**	From **0.5** *(inside a ring)* to **1.0** *(between rings)*	From **0.65** *(inside a ring)* to **1.25** *(between rings)*
$\sigma_{MINconcrete}$ (MPa)	**0**	**−1.8** *(parallel to the longitudinal axis)*	**−0.7** *(perpendicular to the longitudinal axis)*	**−3.3** *(between the bar and a ring)*
$\sigma_{MAXsteel}$ (MPa)	–	**195**	**110**	**300**

Figure 2.4: Reinforcement effects on expansion (Musaoglu, Turanli, and Saritas, 2014)

In real world bridge structures afflicted with ASR, less expansion is found in the direction of reinforcement. Columns experience less vertical expansion than horizontal and beams experience less horizontal expansion that vertical, corresponding the direction of the prestressing cables (Bérubé et al., 2005). In both of these cases, the direction of reinforcement is also the direction of loading that can act as confinement. External confining pressure has been shown to restrict ASR expansion in many cases by Dunant and Scrivener (2012), Gautam et al. (2017), and Multon and Toutlemonde (2006).

2.5 Larive's Expansion Equation

Larive (1998) tested more than 600 specimens with various mixtures and ambient and mechanical conditions and proposed a numerical model for the expansion of the concrete at a point in time given in Equation 2.1.

$$\xi(t,\theta) = \frac{1-\exp(-\frac{t}{\tau_c(\theta)})}{1+\exp\left(-\frac{(t-\tau_l(\theta))}{\tau_c(\theta)}\right)} \tag{2.1}$$

τ_l is the latency time which corresponds to the inflection point. τ_c is the characteristic time and is defined in terms of the intersection of the tangent at τ_l with the asymptotic unit value of ξ, Figure 2.5.

Equations for τ_l and τ_c is given in Equation 2.2

$$\begin{aligned} \tau_l(\theta) &= \tau_l(\theta_0)\exp\left[U_l\left(\tfrac{1}{\theta}-\tfrac{1}{\theta_0}\right)\right] \\ \tau_c(\theta) &= \tau_c(\theta_0)\exp\left[U_c\left(\tfrac{1}{\theta}-\tfrac{1}{\theta_0}\right)\right] \end{aligned} \tag{2.2}$$

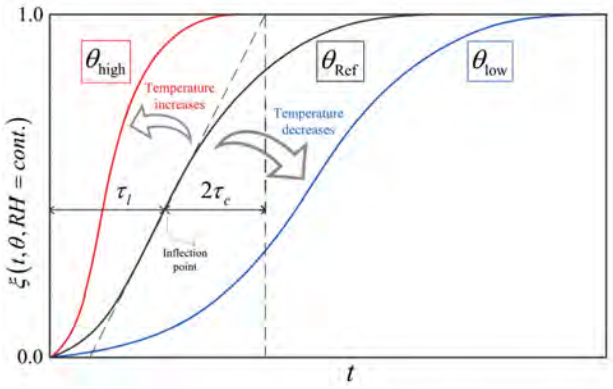

Figure 2.5: Definition of latency and characteristic times (Saouma and Perotti, 2006)

expressed in terms of the absolute temperature ($\theta^oK = 273 + T^oC$) and the corresponding activation energies. U_l and U_c are the activation energies, minimum energy required to trigger the reaction for the latency and characteristic times, respectively. From Larive's tests, universal activation energy values were determined to be 9400 ± 500K and 5400 ± 500K (Saouma and Perotti, 2006). These equations are compared to the actual collected data to evaluate to the validity of the numerical model in Section 6.4.

2.6 AAR and Crack Indices

At the macroscopic scale, an indication about the expansion of the concrete can be derived from the crack-index (LCPC, 1997). The crack-index is determined by measuring the crack width along pre-drawn lines, Fig. 2.6 and is expressed as crack-width per measured length. However, it has to be kept in mind that the formation of the cracks may not be attributable solely to AAR. Still, the crack index indicates a concrete expansion at the studied location in mm/m.

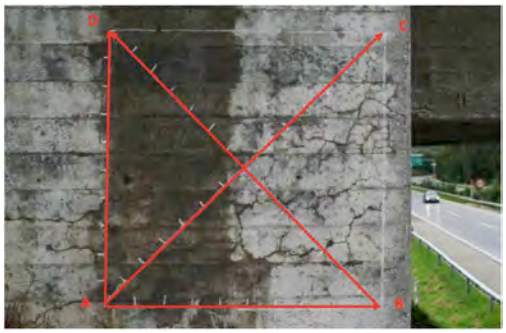

Figure 2.6: Determination of the crack-index along the lines A-B, A-C, A-D and B-C. Side of the square = 1 m, Leemann and Griffa (2013)

This page intentionally left blank.

3 Casting and Curing

3.1 Casting

The verification of reactive aggregates and development of the concrete mix used to create the specimens for this experiment has previously been completed and documented by Saouma, Sparks, and Graff (2016). This document includes the quantities of coarse and fine aggregate, water, cement, and admixtures for each batch. Additionally, mixed concrete properties such as slump, air content, unit weight, and water-cement ratio are detailed.

On May 2nd and 4th, 2016 the specimens to be used in this program were cast at Fall Line Inspections in Denver, CO. Over these two days, 6.27 cubic yards of concrete mixed and poured into forms to create 16 shear specimens, 15 blocks, 24 prisms, 9 wedge splitting test specimens, and multiple cylinders. Figures 3.1 to 3.7 provide a brief overview of the casting process including form building and transportation, aggregate preparation, concrete mixing, filling forms, and curing.

Figure 3.1 shows the 16 shear specimen forms after being built, transporting them the Fall Line, and their organization in preparation for casting. In Figure 3.2 coarse and fine aggregates are mixed to ensure constant moisture throughout the aggregates while batching and mixing since some surface aggregates could have dried. The aggregates are then loaded into the batcher in Figure 3.3. The batcher provides the designated weight of each aggregate in Figure 3.4 and transports them to the mixer via conveyor belt. Cement is manually weighed beforehand and added to the conveyor belt at the same time. Water is also weighed before mixing and added to the mixer after the cement and aggregate. After the cement is mixed, Figure 3.5 shows the wet concrete poured out of the mixer into a bucket for easy transportation to the forms. Figure 3.6 shows slump and air content tests performed before filling forms ensuring adequate wet concrete properties are obtained. Finally, the forms are filled, and concrete is vibrated in Figure 3.7. Afterwards, concrete is covered with wet burlap to prevent shrinkage cracking.

Figure 3.1: Wood forms built, transported, and organized at casting location

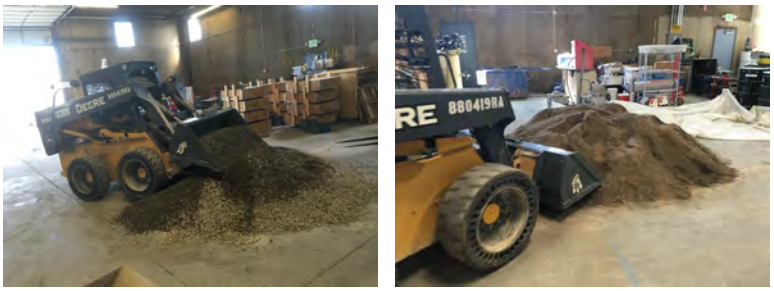

Figure 3.2: Mixing aggregates for consistent moisture content

Figure 3.3: Loading aggregates into batcher

Figure 3.4: Adding water, aggregates, cement, and admixtures to mixer

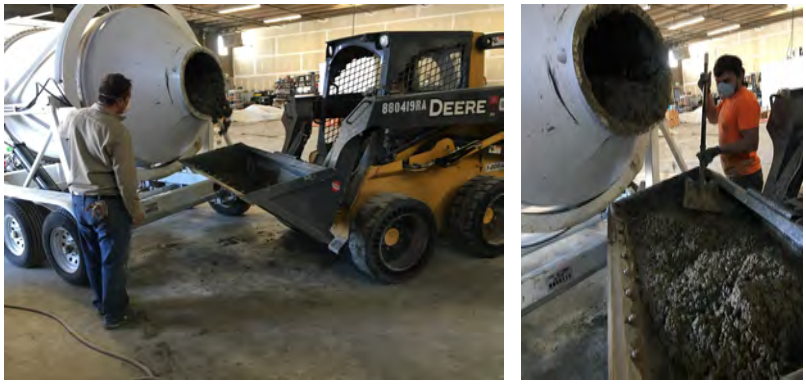

Figure 3.5: Pouring mixed cement from mixer for testing and transportation to forms

Figure 3.6: Measuring concrete slump and air content

Figure 3.7: Filling forms, vibrating concrete, and covering with wetted burlap

Table 3.1 gives the slump of each concrete batch cast. Batch 2 had a lower slump than the other batches and is outside the target range for the concrete mix. Due to time and material restraints, the concrete was still used and poured into forms. A discussion on how the low slump of batch 2 affects the ASR expansion results is in Section 8.7.

Batch Number	Slump (in)
1	5.5
2	2.25
3	6.0
4	4.75

Table 3.1: Slump of each concrete batch

3.2 Concrete Compressive Strength Testing

The concrete from each batch is tested to ensure that the concrete has reached the target 28-day compressive strength of 4,000 psi. 7 and 28 days after casting, three 4" cylinders from each concrete batch were tested in the 110-kip testing machine according to ASTM, C39 (2016), Figure 3.8. For each cylinder, three measurements were taken of the cylinder's diameter and length then placed in the testing machine under force controlled loading until failure. Table 3.2 shows the average 7 and 28 day strength of each concrete

batch. Note that all batches meet the target compressive strength.

Figure 3.8: Compression Testing

Batch Number	Average 7-Day f'c (ksi)	Average 28-Day f'c (ksi)
1	2.64	5.99
2	4.13	4.98
3	3.67	4.21
4	4.83	5.71

Table 3.2: Average 7 and 28 Day Compressive Strength

3.3 Curing

A critical part of this program is creating an environment that is conducive to creating the alkali-silica reaction in the concrete (or "curing" the concrete) as quickly as possible. Previous research has shown that ASR develops at a greater rate in conditions of high heat and humidity (Swamy and Al-Asali, 1988). Leeching of alkalinity from the concrete is prevented by either wrapping the specimens in burlap and wetting with aqueous sodium hydroxide (NaOH) or submerging the specimens in aqueous NaOH. Additional blocks and prisms are stored in ambient temperature conditions.

Given the large number of shear specimens, numerous blocks, prisms, and cylinders, the fog room at the University of Colorado Boulder's structures testing lab is used to accelerate ASR in the specimens. The fog room provides a contained space of adequate size to store the specimens at 100°F and 95% relative humidity. Specimens that are stored at ambient temperatures are stored in plastic containers on the floor of the structures lab.

3.4 Test Specimens

A variety of test specimens were cast to learn more about ASR expansion in concrete and the effects on concrete's mechanical properties. The shear specimens are cast to determine ASR's effect on shear strength.

Blocks and prisms are used to track expansion and to study the environmental and reinforcement effects on ASR. Cylinders and wedge splitting test specimens provide data about ASR's effect on other mechanical properties of the deteriorated concrete.

3.4.1 Shear Specimens

Shear specimens are 42" long, 30" tall, and 10" thick. The concrete of the shear specimens can be divided into two groups, reactive and non-reactive. Reactive samples contain aggregates with high silica content and have been dosed with additional sodium hydroxide that will accelerate the reaction. These specimens are stored in the university's fog room at 100°F and 95% relative humidity to facilitate the development of ASR in the concrete. To provide the concrete with as much alkalinity as possible, specimens will be wrapped in burlap and wetted with 1.0M sodium hydroxide. More detailed information about the fog room is given in section 3.5.

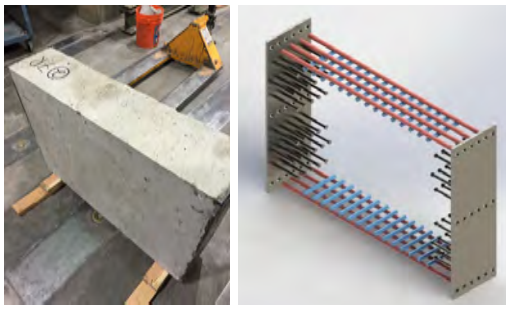

(a) Specimen (b) Internal reinforcement

Figure 3.9: Shear Specimen

The non-reactive samples contain the same reactive aggregates with lithium nitrate added which suppresses ASR from occurring. These specimens will serve as a control to compare the shear strength of the reactive specimens. Non-reactive specimens are also stored in the fog room but are not wetted with sodium hydroxide.

Most shear specimens are reinforced in the longitudinal and transverse directions shown in Figure 3.9(b). Longitudinal reinforcement is four #6 bars and transverse reinforcement consists of eleven #7 bars providing a reinforcement ratio of 0.52% and 0.59%, respectively. Three reactive and two non-reactive specimens are unreinforced to investigate the effects of reinforcement on shear strength in ASR afflicted concrete.

Certain specimens are outfitted with temperature sensors and strain gauges to collect useful data about the expansion progress. Table 5.1 provides a complete list of specimen batches, reactivity, and location. The table also identifies temperature sensor ID and strain gauge identification, if any.

Table 3.3: Shear Specimens

Batch	ID	Reactive	Rebars	Temp. ID	Strain Gauge	Loc.
1	1	Y	Y			FR
	2		Y	1		
	3		Y			
2	4	Y	N			
	5		Y			
	6		Y	2	9	
	7		Y			
	8		N			
3	9	Y	Y		10	
	10		Y	3		
	11		Y			
	12		N			
4	13	No	Y			
	14		Y	4		
	15		N			
	16		N			

3.4.2 Blocks

The 14” x 14” x 14” blocks contain a variety of reinforcements in attempt to understand how different reinforcements will effect ASR expansion. The blocks contain either no reinforcement, reinforcement in one horizontal direction with #3 or #4 bars, reinforcement in both horizontal directions with either #3 or #4 bars, or reinforcement in both horizontal directions with a combination of #3 and #4 bars. A visualization of this can be seen in Figure 3.10.

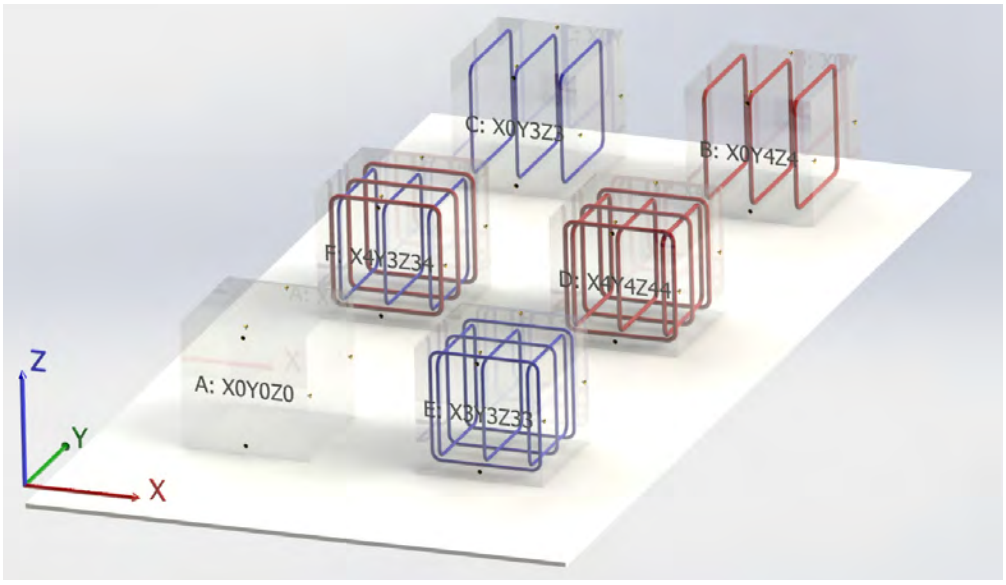

Figure 3.10: 14” × 14” × 14” blocks with various reinforcement

As with the shear specimens, certain blocks are outfitted with temperature sensors and strain gauges. Blocks are stored in both the fog room and the lab to study the effects of temperature on ASR expansion.

Table 5.2 details the block's batch, ID, rebar, temperature sensor (if any), location, and strain gauge (if any).

Location of DEMEC points (for expansion measurements) and the reference lines (for crack index determination) are shown in Fig. 3.11.

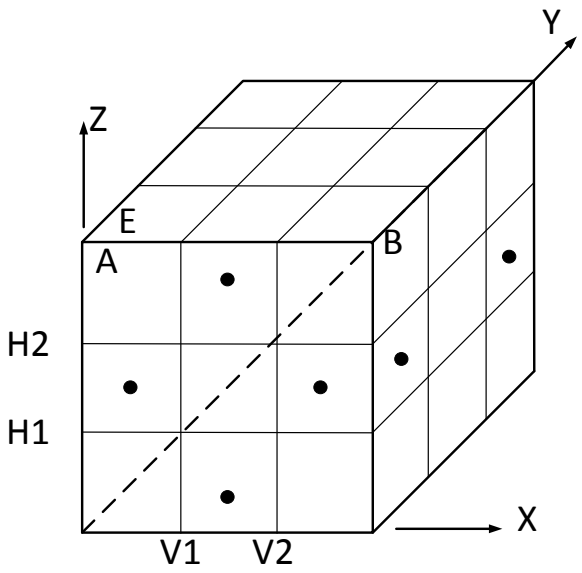

Figure 3.11: 14" × 14" × 14" blocks DEMEC locations and reference lines for crack index measurements

Table 3.4: 14 x 14 x 14 inch Blocks

B: Blocks 14x14x14 inches														
Bat.	**ID**	**Label**	**Rebars**	**Temp.**	**FR**	**SG**								
				ID	**LAB**	**X**	**Y**	**Z(UP)**	**A**	**B**	**C**	**D**	**E**	**F**
1	5	D:X4Y4Z44	D	6	FR	2	3	4				1		
2	1	A:X0Y0Z0	A	5					1					
	2	A:X0Y0Z0	A	6	Lab				1					
	3	B:X0Y4Z4	B		FR			1		1				
	4	B:X0Y4Z4	B		Lab					1				
2	6	A:X0Y0Z0	A	7	FR				1					
	7	A:X0Y0Z0	A	8	Lab				1					
	8	C:X0Y3Z3	C		FR			5			1			
	9	C:X0Y3Z3	C		Lab						1			
	10	E:X3Y3Z33	E*						1					
3	11	A:X0Y0Z0	A	9	FR				1					
	12	A:X0Y0Z0	A	10	Lab				1					
	13	F:X4Y3Z34	F		FR	6	7	8						1
	14	F:X4Y3Z34	F		Lab									1
	15	E:X3Y3Z33	E*										1	
					Sum				7	2	2	1	1	2
** Notes: Spec. 10 may be an A, and Spec. 15 may be a D;*														

3.4.3 Prisms

The 6”×6”×14” (referred to as P14) and 4”×4”×16” prisms (referred to as P16) are located in both the fog room and lab. Unreinforced prisms are considered to give the “true” expansion of the concrete at any given time. Additionally, they are used to determine the temperature and reinforcement effects on the concrete’s expansion. As with the other specimens, there is a combination of reinforced and unreinforced prisms, and some are outfitted with temperature sensors and strain gauges. Table 3.5 shows a full overview of all P14 specimens.

Table 3.5: Large Prisms: 6 x 6 x 14 inch (5 bars)

Batch	ID	Reactive	Temp	Rebar	Strain Gauge	Loc.
1	1	Yes				FR
	2		11	Y	11	
	3					LAB
	4					
2	5	Yes				FR
	6			Y	12	
	7					LAB
	8		12			
3	9	Yes	13			FR
	10			Y	13	
	11					LAB
	12					

Table 3.6: Small Prisms: 4 x 4 x 16 inch (4 bars)

Batch	ID	Reactive	Temp	Rebar	Strain Guage	Loc.
1	1	Yes				FR
	2		14	Y	14	
	3					LAB
	4		15			
2	5	Yes				FR
	6			Y	15	
	7					LAB
	8					
3	9	Yes	16			FR
	10			Y	16	
	11					LAB
	12					

To see how the rebar had moved once the prisms had been cast, the ends of two prisms (one of each side) was chiseled away to expose the rebar. It was observed that there had been some downward movement in the rebar due to vibrating the concrete. Below is a schematic of the potential final locations the rebar, Figure 3.12. The black circles represent the idealized location of the rebar and the darker blue areas are the potential final areas of rebar location.

3.4.4 Wedge Splitting Test Specimens

The wedge splitting tests (WST) specimens are used to determine the fracture energy of the concrete. Dimensions of the WST specimens in Figure 3.13 are 200×200×100mm with a 30×60mm notch cut out of the top. Expansion of WST specimens is not trackedbut specimens are stored in both the lab and fog room. An inventory of the wedge splitting test specimens is shown in Table 3.7.

3.4.5 Cylinders

Twelve 4×8” cylinders and three 6×12” cylinders of each mix were cast at the same time as all other specimens. Cylinders are used for compression tests to determine concrete’s compressive strength and for Brazilian tests to quantify tensile strength. Cylinders will also be used for petrographic analysis to examine

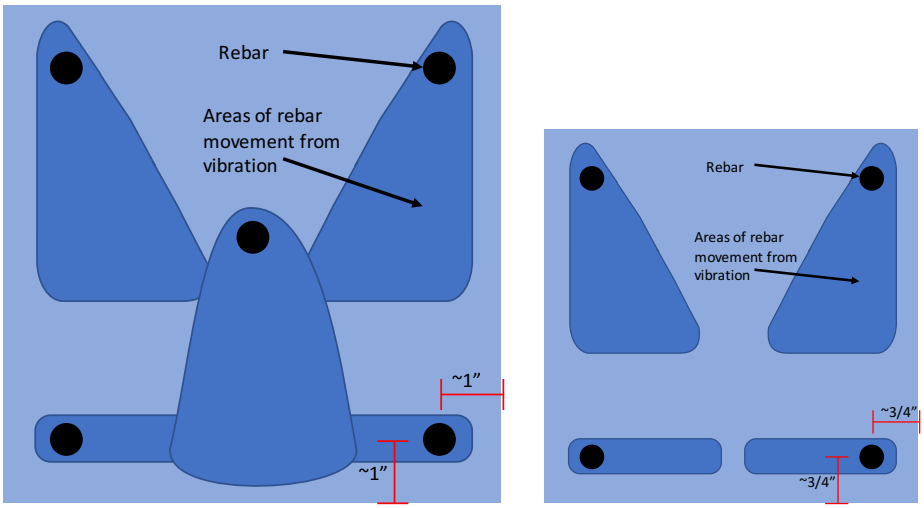

(a) P14 (b) P16

Figure 3.12: Potential final areas of rebar locations

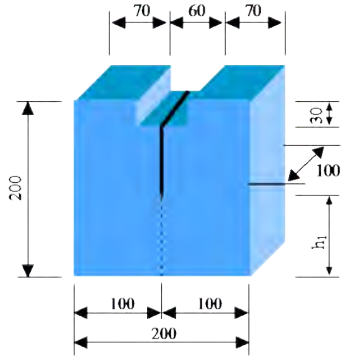

Figure 3.13: Dimensions of wedge splitting test specimen

Table 3.7: Wedge Splitting Test Specimens

Bat.	ID	Reac.	Loc
1	1	Yes	FR
	2	Yes	FR
	3	Yes	LAB
2	4	Yes	FR
	5	Yes	
	6	Yes	LAB
3	7	Yes	FR
	8	Yes	
	9	Yes	LAB
4		No	
		No	
		No	

ASR on a microscopic level. Half of the small cylinders have already been broken to determine the 7 and 28 compressive strength in the concrete.

3.5 Fog Room

As mentioned previously, the fog room in CU Boulder's structures lab is being utilized to store and cure a majority of the specimens. Using the room's integrated heaters and humidifier, the room is kept at a constant temperature of 100°F and 95% relative humidity. Sensors are placed inside the room to monitor and log the temperature and humidity of the room.

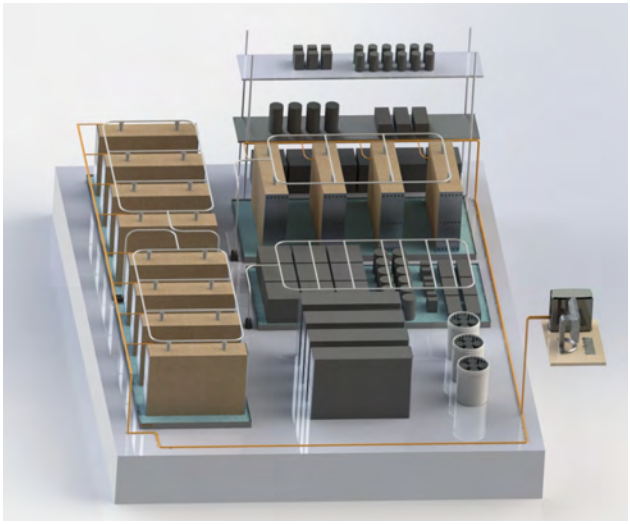

Figure 3.14: Installation of reactive and non-reactive shear specimens, blocks, prisms, and cylinders in the fog room

Initially, the fog room was not properly operational to provide the conditions needed for this research. Facilities management installed a new humidifier and upgraded the heat system by utilizing steam that is available in the building that will provide heat year round. The heat was not operational before the specimens were installed in the fog room. To provide heat during installation, oil-filled electric space heaters, shown in Figure 3.15, were used in the fog room to keep the room as close to 100°F as possible. Ultimately five space heaters were used to provide the target temperature.

Figure 3.15: Electric space heater used to heat the fog room during heat installation

The size and orientation of the pans hold specimens and sodium hydroxide had to be thoughtfully oriented in the fog room so that all specimens would fit and each shear specimen can be brought in using a forklift. Initial measurements of the fog room were used to develop a plan that was confirmed by Solidworks drawings,

Figure 3.14.

The specimens were brought in the fog room using a forklift with a spreader bar that lifts two straps wrapped under the bottom of the sample, Figure 3.16. Specimens are placed in the pans on small concrete blocks for strap removal and to ensure the bottom is exposed to sodium hydroxide. A "first in, last out" plan was implemented when placing specimens in the fog room to minimize the amount of moving samples around when removing them for testing. However, this will be somewhat controlled by the expansion levels of each specimen at the time of testing. The forklift was also used to place the blocks into the pans. Once in the pans, the blocks could be slid by hand to their proper location. All smaller specimens were carried into the room by hand.

Figure 3.16: Placing shear specimen in fog room with forklift

3.5.1 Leaching

It has been will documented by Lindgård et al. (2010) that without proper wetted wrappings, alkalis can leach from the surface of the concrete which will slow the rate of expansion. Additionally, the wrappings must be wetted with a solution that has the same alkalinity as the internal pore solution. Wetting with water alone can actually promote more leaching than unwrapped specimens by drawing alkalinity out of the concrete.

As mentioned previously, one of the ultimate goals of this research is to create ASR expansion in concrete samples as quickly as possible. To do this, steps to prevent leaching of the specimens are taken in one of two ways depending on specimen size and storage. First, small specimens such as prisms, cylinders, wedge splitting tests, and blocks in the lab are submerged in plastic containers filled with 1.0M NaOH. Prisms, cylinders, and wedge splitting test samples are submerged in the fog room. Second, large reactive specimens and blocks in the fog room are wrapped with burlap and wetted with 1.0M NaOH. Even though large volume specimens leach alkalinity at a slower rate, every effort is taken to prevent leaching through the use of wrapping specimens in burlap and frequently wetting with NaOH through the use of a unique sprinkler system.

3.5.2 Sprinkler System

To prevent leaching of alkalinity from the concrete, shear specimens and blocks in the fog room are wrapped in burlap and wetted with a 1M aqueous sodium hydroxide (NaOH) solution. All the samples (except the cylinders, prisms, and wedge splitting test specimens) are placed in the 96" x 48" x 3" steel pans containing the sodium hydroxide which is pumped to the top of the concrete, Fig. 3.17.

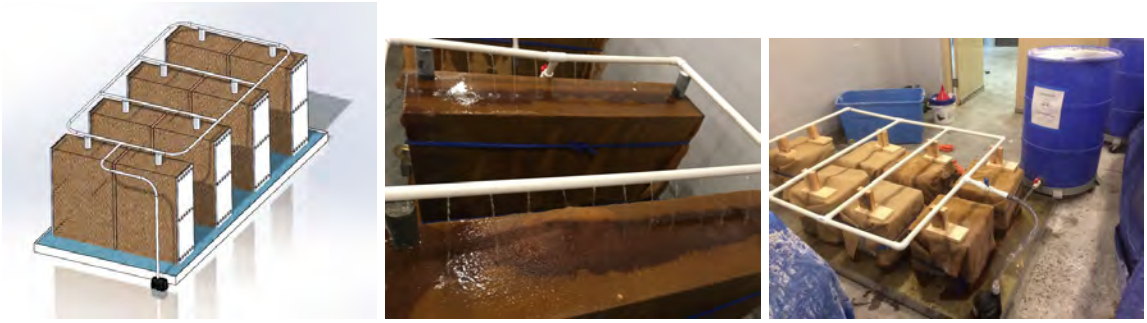

(a) Shear specimens in pans with sprinkler system

(b) Sprinkler system wetting the burlap wrapped shear specimen

(c) Sprinkler system installed over blocks and filling pan with NaOH solution

Figure 3.17: Sprinkler system for the specimens

Initially, salt water fish tank pumps were used to pump sodium hydroxide through the PVC system. These pumps were unreliable in providing a continual flow of solution. Additionally, there was a significant loss of solution due to splashing off of the specimens and out of the pans. To mitigate these problems, sump pumps shown in Figure 3.18 are utilized and prove to be much more reliable. However, since sump pumps are not designed to run continuously, they are connected a timer that turns the pumps on every 1.5 hours for three minutes. This is a sufficient amount of time to keep the burlap wet. To prevent splashing, the samples and sprinkler systems are cover in a tarp with the edges tucked into the pans.

Figure 3.18: Sump pumps used to power sprinkler system

The NaOH solution is carried through PVC pipe, which is not reactive with sodium hydroxide, where it is sprayed across the top of the specimen through holes drilled into the pipe. To provide constant pressure

at each spray point, the piping system is constructed in a loop across the samples using PVC tees and 90^o elbows. Each specimen will have multiple spray points across its top face to ensure sufficient wetting. Solution flows down the sides of the specimen, saturating the burlap and holding liquid against the surface preventing leaching on all sides of the specimen. Excess liquid is collected in the steel pans where the process is repeated. The cylinders, prisms, and wedge splitting test specimens are submerged in plastic tubs and buckets containing sodium hydroxide, Fig. 3.19.

Figure 3.19: Prisms, cylinders, and wedge splitting test specimens stored in plastic bins in fog room

The non-reactive shear specimens and cylinders are not wetted with sodium hydroxide or wrapped in burlap. They are stored in the fog room at the same ambient temperature and humidity as the reactive samples.

3.6 NaOH Solution Preparation

To prevent alkali from leeching out of the concrete and have a consistent ASR reaction throughout the specimen, the pH of the NaOH solution in the pan should match the internal pH of the concrete pore water. Katayama (2017) states that concentration of the pore water in concrete is dependent on the water-to-cement ratio and provides Equation 3.1to estimate the internal molarity.

$$\left[HO^{-}\right] = 0.339 \times \frac{Na_2O(\%)}{w/c} + 0.022 \tag{3.1}$$

Using target values of 1.6% Na_2O and water-to-cement ratio of 0.53, the concentration of NaOH solution is 1.045 mol/L. This value is rounded to 1.0 mol/L as the target concentration to prevent alkalinity leeching which has a pH of 14.

To maintain such a high pH on the surface of the specimens, four baths of a sodium hydroxide (NaOH) solution are prepared. Each pan can hold up to 50 gallons of the solution. The NaOH solution is prepared in a 55-gallon drum on a cart for mobility. To produce a 1M solution, 40 grams of solid NaOH is needed per liter of water for a total of 16.69 lb (7.57 kg) of solid NaOH for 50 gallons (189.3 liters) of solution. The volume of water is determined by taring the scale for the weight of the barrel and weighing out a certain

quantity of water. Knowing that water weighs 8.34 lb/gallon, the volume can be easily calculated from its weight, Figure 3.20.

NaOH is added to the drum slowly and the solution stirred continually until all the solid has dissolved. The solution is added to the pans by opening a ball valve installed at the bottom of the drum or by hand with a bucket to fill the pans and tubs that are not easily accessible. After the pans are filled, any excess sodium hydroxide is stored in the barrel in the fog room. Due to evaporation, the pans will occasionally be refilled using the excess NaOH solution as needed.

Over the course of the curing process, the pH of the NaOH solution gradually decreases due to a carbonation reaction or excess water dripping from the ceiling into the pans due to the high humidity in the fog room. To prevent water dripping into the pans, the specimens are covered with plastic which also prevents water splashing out of the pan while during wetting. To keep the pH at the target value, the pH is monitored with a digital pH meter and high molarity solution is added to bring the entire solution to the target pH.

Figure 3.20: Weighing water and NaOH for NaOH solution preparation and mixing NaOH Solution

3.7 Lab Floor

A number of specimens are stored on the lab room floor to study the effects of ASR at room temperature, Figure 3.21(a). The specimens are stored in tubs that are filled with 1M sodium hydroxide. Two blocks per tub are stored in 4 of the 5 tubs, Figure 3.21(b). The fifth tub is filled with the prisms and wedge splitting test specimens. Each tub is fitted with a lid for safety and to prevent solution evaporation. The reactive cylinders are stored in buckets filled with sodium hydroxide solution with a tight fitting lid. The non-reactive cylinders are stored on floor without a container, Figure 3.21(c).

(a) Blocks and prisms stored in lab (b) Plastic containers storing blocks and prisms (c) Cylinders in lab

Figure 3.21: Specimens stored in the laboratory at room temperature

4 Monitoring

4.1 Introduction

During the curing process, it is important to monitor the specimen expansion to ensure that the experiment is progressing as planned. Multiple tools, instruments, and sensors are used to monitor and understand the expansion of concrete specimens. Datum discs and a strain gauge are used to monitor the expansion of the concrete. Figure 4.1 shows an overview of the sensor configuration used to collect other useful data about the specimen and fog room.

The instrumentation includes a laptop computer to log expansion measurements and to collect information from the specimen temperature sensors embedded in certain specimens and ambient room sensor. A National Instruments DAQ is utilized to collect strain measurements from strain gauges adhered to the specimen rebar. Finally, a handheld pH probe is used to monitor the pH of the sodium hydroxide. All of these measurement tools and sensors work in concert to provide a full picture of the factors affecting the concrete expansion and the progress of the expansion. This section discusses in detail each of these tools to provide a complete picture of the data collection and specimen monitoring.

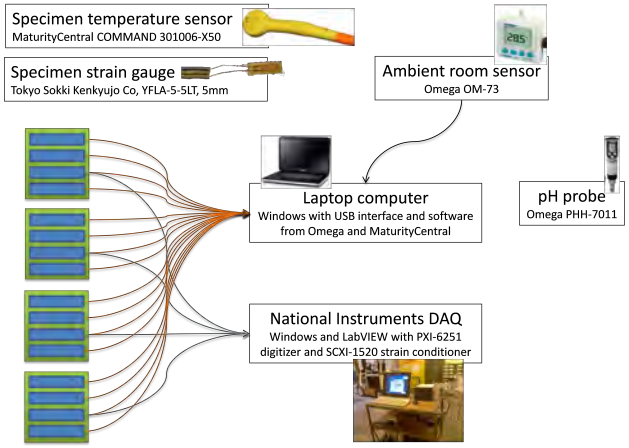

Figure 4.1: Instrumentation overview for fog room specimens

4.2 Expansion Measurements

To track the expansion of the concrete, the distance between two specific points on the concrete surface must be measured to see how far they are moving in relation to one another. With a ceramic epoxy, datum

discs are adhered on the top and sides of the shear specimens and 14" blocks and in the axial direction of the prisms, Figure 4.2(a). Using a low-thermal deformability measuring bar, datum discs are placed on the concrete surface approximately 300mm apart. A DEMEC mechanical strain gauge is used to document the expansion by measuring the change in distance between each disc, Figure 4.2(b).

(a) Datum disc attached with brushable ceramic epoxy

(b) Measuring bar and DEMEC gauge

Figure 4.2: Expansion measurements device

On the shear specimens, eight discs are applied to the surface to accommodate six measurements. A schematic of these these locations are shown in Figure 4.3. Two are placed longitudinally on top of the specimen to track the longitudinal expansion and two more at a diagonal to monitor the transverse expansion. Four more discs are placed in a square on the side of the specimen to provide two additional longitudinal and two vertical measurements.

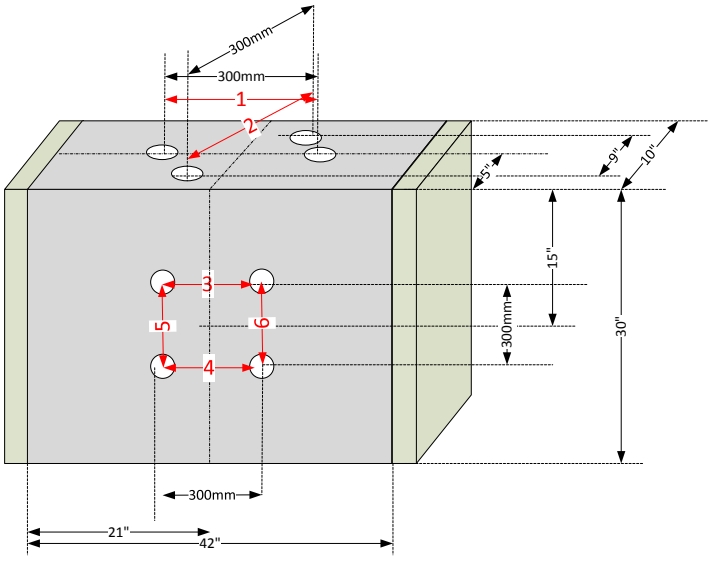

Figure 4.3: Locations of datum disks and order of measurements

For the blocks, six discs are used to measure the three orthogonal directions, two horizontal and one vertical. The vertical direction is considered the Z axis while the two horizontal directions are the X and Y

axes.

Approximately once a month (often more frequently), the location of the discs is measured to see how far they have moved. For a period of 24 hours before these measurements are taken, the temperature and humidity of the fog room is lowered to ambient conditions to provide comfort for those taking the measurements. One person will place each end of the DEMEC in each of the discs while a second person records the data on the laptop computer. The device includes a serial cable that connects to a computer via USB so that measurements are automatically logged into an Excel spreadsheet to reduce error in reading and recording. A baseline measurement was taken for each set of discs which will serve as the starting "zero" since it cannot be assumed that each disc is placed exactly 300mm apart.

The datum discs were initially placed using the adhesive that came with the DEMEC device. After being exposed to the sodium hydroxide solution, the adhesive corroded and the discs could easily be removed from the concrete surface. To replace the discs onto the specimens, a ceramic epoxy was used. This epoxy provides excellent corrosion resistance as well as resistance to high heat and humidity. The epoxy is the red substance around the disc in Figure 4.2(a).

At the time of expansion measurements, additional measurements are also taken or collected. Strain measurements, discussed in Section 4.6, are taken, internal specimen temperature data and fog room temperature and humidity data is download, pans and tubs are refilled with sodium hydroxide (if necessary), and general maintenance to the fog room is completed.

4.3 Crack Index Measurements

Crack index measurements were computed for all specimens (except shear) 500 days after casting.

Crack measurements were recorded through a 20x measuring microscope with a resolution of 0.005" or 0.1 mm, Fig. 4.4.

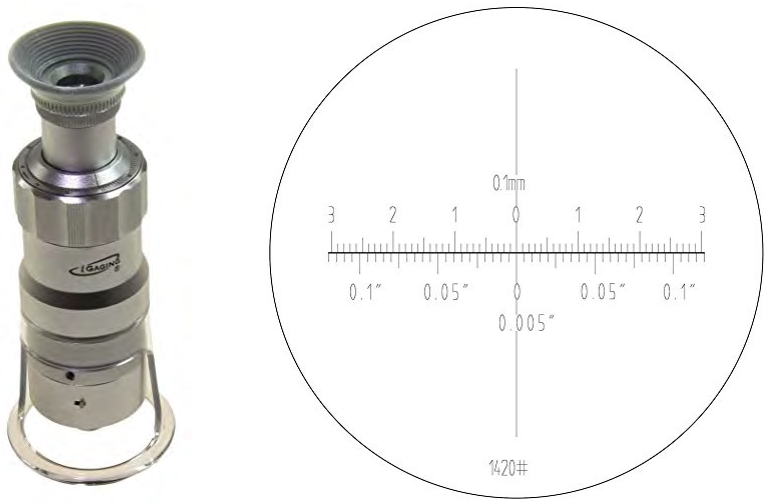

Figure 4.4: Measuring microscope for crack index determination

4.4 Internal Specimen Sensors and Data Logging

The temperature inside of the specimens is measured using embedded temperature sensors and computer software. Each sensor is a self-contained, battery-powered data acquisition device that takes temperature measurements every hour and records them to internal memory with a time stamp. Each sensor operates independently which means that the sensors continuously records data starting with the concrete pouring. When measurements are taken, the laptop computer running the software is connected to each sensor to download the record of measurements for storage. To date, 5 temperature sensors have stopped working due to unknown reasons. While they provide an incomplete record of the internal temperature, the data that was collected is still useful.

(a) Internal temperature probe being cast into concrete specimens

(b) Laptop computer connected to temperature probe (orange wire) via USB and alligator clips

Figure 4.5: Internal temperature measurement

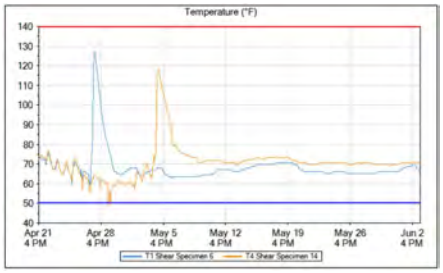

Figure 4.6: Sample graph from software logging data over time

Internal humidity sensors were not used to track the moisture content of the concrete since internal moisture directly influences ASR expansion. This experiment required sensors that could be embedded into the specimens and automatically track humidity conditions to be downloaded at a future point. Humidity sensors must be installed after casting and is a labor intensive process. Additionally, humidity sensor outputs have to be manually tracked which would not serve the long timeline of this project that requires a lot of data to get a full picture of the internal moisture content. Finally, and most importantly, since the specimens are either wetted or submerged it is expected that the internal humidity would be close to %100.

4.4.1 Internal Specimen Temperature Data

Two separate trends of temperature can be seen on Fig. 4.7; the specimens located the fog room and the specimens in the lab. The fog room temperature is consistently higher than the lab. Spikes down in the temperatures correspond to when the heat is shut off in the fog room to take expansion measurements.

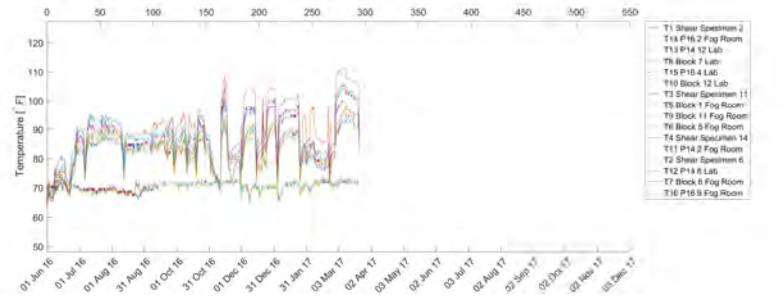

Figure 4.7: Variation of all temperatures

These average internal temperature measurements are used to compare the specimen temperature to the rate of expansion. Results of this comparison are seen in Section 8.4.3

4.5 Fogg Room Temperature and Relative Humidity

The room's temperature and humidity will be controlled by electronic control systems that add heat from the building's regular heating system and adds humidity from a dedicated humidifier. A data logger was installed within the fog room to measure the ambient temperature and relative humidity every 30 minutes to verify that the room's temperature and humidity are being kept within the desired limits for the proper curing of the specimens. The logger is connected to the computer and the data is downloaded and stored in an Excel spreadsheet. Similar to the internal temperature, MATLAB code has been written to analyze the data. Each data point for both internal and external temperature and external humidity is time stamped so data from separate sensors can be directly compared.

Unfortunately, the sensor is not waterproof and eventually the water dripping from the ceiling due to the high humidity in the fog room shorted out the sensor. Obtaining a sensor that was waterproof or probe style sensor that connected to the data logger proved to be beyond the available budget of the project. An outdoor thermometer and humidity sensor was installed in the fog room to ensure the temperature and humidity was in the acceptable range.

4.5.1 Temperature and Relative Data

The graph in Fig. 4.9 shows the temperature (blue) and the relative humidity (orange) of the fog room. Spikes down in temperature correspond to when the heat is shut off in the fog room to take expansion measurements.

At the beginning of December 2016, the saturated environment of the fog room caused the temperature and humidity data collection device to malfunction and stop collecting data. In its place, a thermometer and humidity gauge has been placed in the fog room to be read manually when data is collected. Periodically, the fog room temperature and humidity is checked and manually logged. Because of this, jumps can be seen in the graph between each temperature and humidity data points

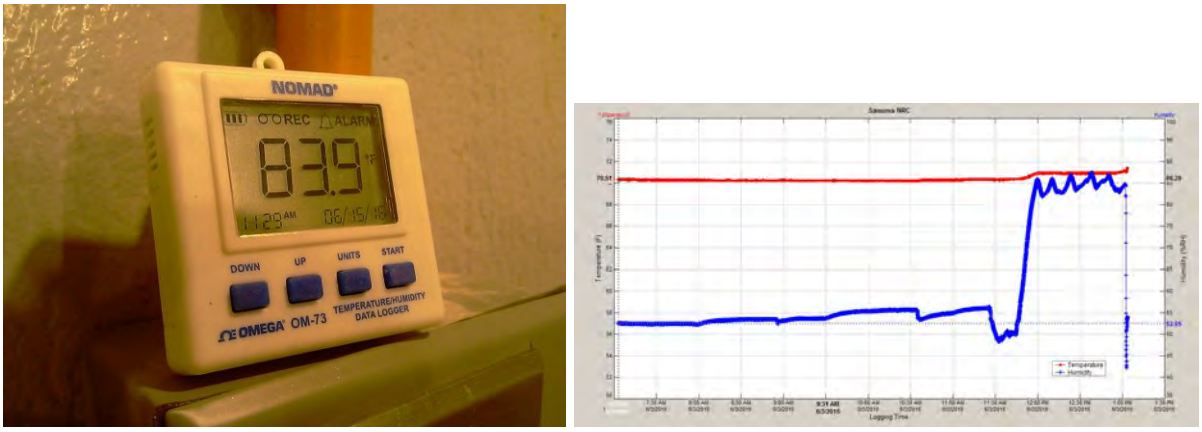

(a) Temperature and humidity data logger installed in fog room

(b) Sample graph of logged temperature (red) and humidity (blue)

Figure 4.8: Fog room temperature & relative humidity data logger and sample graph

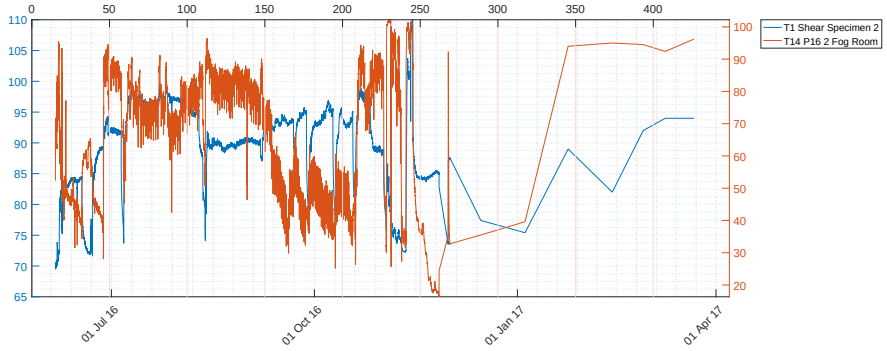

Figure 4.9: Temperature and relative humidity variation

4.6 Strain Gauges

Strain gauges are bonded to rebar segments inside of select shear specimens, 14" cubes, and prisms to investigate the strain introduced because of ASR expansion. Strain gauges are produced by Tokyo Sokki Kenkyuio Co. Ltd. and the model number is YFLA-5-5LT. The gauge length is 5 mm, gauge factor is 2.11± 2%, and gauge resistance is 119.5 ± 0.5 ohms. The gauges themselves do not have any internal circuitry or data acquisition and therefore require an external system for taking measurements. Measurements can only be taken while connected to the external system, which is done when expansion measurements are taken. A National Instruments computer utilizing a PXI-6251 digitizer and a SCXI-1520 strain conditioning module will make the strain measurements, Figure 4.10. Those measurements are displayed on the screen and recorded by hand into a separate file. Similar to the datum disc measurements, initial baseline strain measurements were taken to compare the subsequent measurements to.

4.6.1 Strain Data

Strain Data

Generally, an increase in strain can be seen as expansion progresses, Figure 4.11. Jumps in data can be contributed to the sensitivity in the connection between the gauge and the measurement device that

(a) Monitoring computer

(b) Alligator clips connected to strain guage wires

Figure 4.10: Data acquisition system for strain gauges

make acquiring data points difficult. Additional, over the course of the curing process, multiple gauges have stopped working making it impossible to collect additional strain data.

4.7 pH Measurements

4.7.1 Handheld pH Probe

A handheld pH probe is used to test the concentration of the NaOH solution. Before each set of pH measurements are taken, the probe is calibrated per the manufacturer's specifications. Measurement of pH in each of the of the pans will allow action to be taken as necessary to increase or decrease the pH of the baths by manual means (i.e. addition of NaOH solution to raise pH or addition of water to lower it).

Over the course of the experiment, the sodium hydroxide was found to decrease in pH. This occurs by either diffusion of carbonic acid from the atmosphere that neutralizes the strong base, dilution through the addition of water that drips from the ceiling into the pans from high humidity in the room, or a combination of time. To combat this, the pH is periodically checked with the handheld probe. If the pH has decreased, a concentrated batch of NaOH is added to bring the pH back to the target level. However, it is multiple months before any significan dilution of the solution is observed. The process of determining the volume and molarity of the concentrated solution to be added is outlined in Section 4.7.3.

4.7.2 Titration

Titration is also utilized as a method to determine the concentration of the sodium hydroxide solution. First, 10 mL of sodium hydroxide is measured in a graduated cylinder and added to the Erlenmeyer flask. 4 drops of the indicator are added to the flask, giving the liquid a purple color. Next, the pipet is filled with a commercially available 10% v/v HCl solution and an initial reading is taken. The HCl is slowly added to the Erlenmeyer flask while being continually swirled until the solution just turns clear. A final HCl reading is taken. Using the volume of NaOH and HCl and the known concentration of HCl (1.165 mol/L), the following equation is used to calculate the molarity of sodium hydroxide.

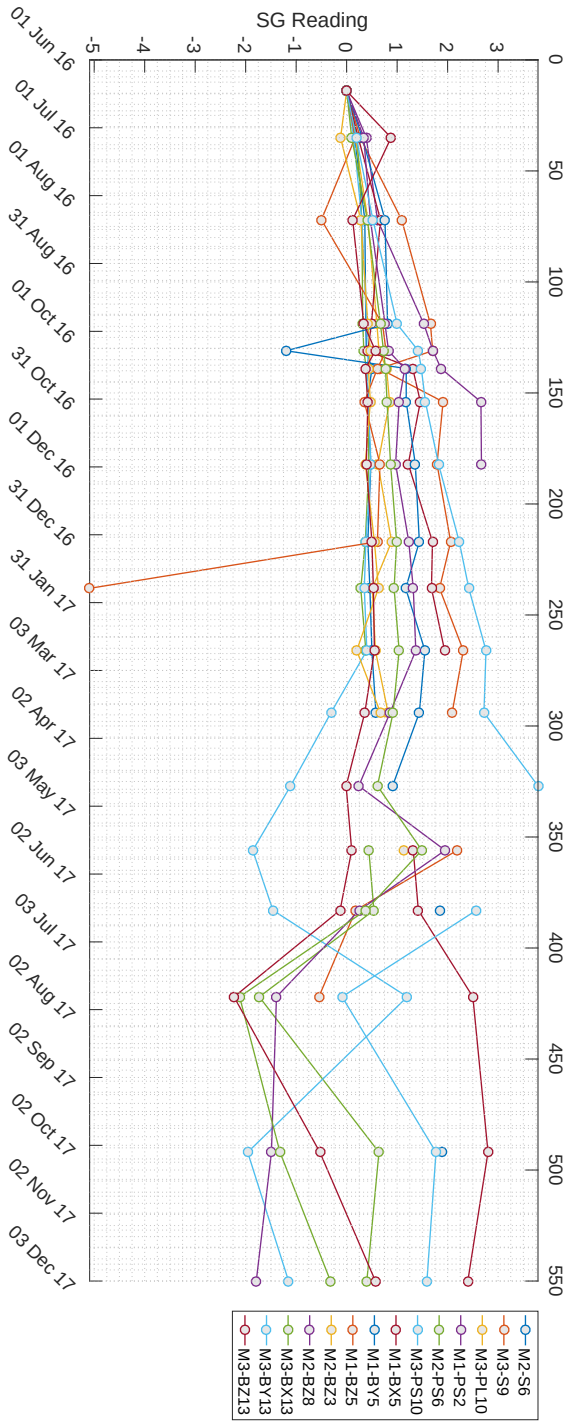

Figure 4.11: Variation of all strain gauges

$$M_{\mathrm{NaOH}} = \frac{M_{\mathrm{HCl}} \times \left(V_{\mathrm{HCl}}^{\mathrm{final}} - V_{\mathrm{HCl}}^{\mathrm{initial}}\right)}{V_{\mathrm{NaOH}}} \tag{4.1}$$

Titration of a clear solution (before it is added to the pans) has been very successful in determining a

Figure 4.12: Handheld pH probe

molarity of the solution that matches the expected values. However, the solution that is taken from the pans is brown in color due to leeching of the burlap into the solution. Since the equivalence point is determined by color of the solution, this provides a challenge to determine accurate results. Therefore, titration is used to confirm the molarity of a new batch of NaOH but when checking the solution in the pans, the handheld pH meter is utilized.

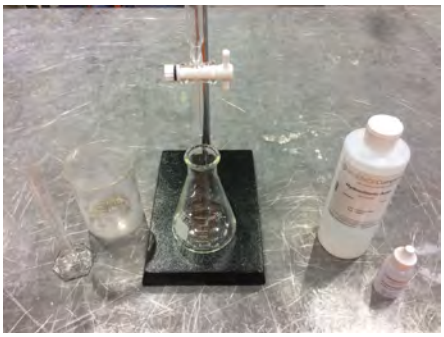

Figure 4.13: Titration Equipment

4.7.3 pH Adjustment Calculations

Below is a sample calculation for determining the molarity of the solution based on the pH measured using the pH probe. The spreadsheet estimates the current volume of the pan by measuring the depth at each corner of the pan and determining the volume from the average depth and subtracting out the volume being taken by the specimens. Warnings have been built in to inform the user if the amount of solution added to the pan will cause an overflow. At the beginning of the experiment, it was unclear if the pH would increase over time due to evaporation of water and leaving excess NaOH or decrease. Now that the curing process is close to complete, the NaOH always decreased. It was never observed the pH of NaOH increased.

$$\text{Measured } pH = 13.8$$

$$\text{Molarity} = 10^{-(14-pH)} = 0.631 \ \frac{\text{mol}}{\text{liter}}$$

The target molarity is 1M (with a corresponding pH of 14). The volume and the mass of NaOH that must be added to bring the solution in the pan up to 1M can be calculated. To do this, Equation 4.2 is used.

$$M_{pan}\, V_{pan} + M_{add}\, V_{add} = 1M\, (V_{pan} + V_{add}) \tag{4.2}$$

Rearranging the equation and converting the added molarity to an added mass by multiplying it by the molecular weight of NaOH (40 gram/mol), Equation 4.3 is used in the spreadsheet.

$$m_{add} = \frac{1M\, (V_{pan} + V_{add}) - M_{pan}\, V_{pan}}{V_{add}} \left(40 \ \frac{\text{gram}}{\text{mol}}\right) \tag{4.3}$$

In the example, assume the volume in the pan is determined to be 94 liters and a volume of 40 liters is to be added to the solution. Below gives the mass of NaOH that to be added to keep the solution at 1M.

$$m_{add} = \frac{1M\, (94 \text{ liter} + 40 \text{ liter}) - \left(0.631 \ \frac{\text{mol}}{\text{liter}}\right)\, (94 \text{ liter})}{40 \text{ liter}} \left(40 \ \frac{\text{gram}}{\text{mol}}\right) = 74.7 \ g \ \text{ of } \ \text{NaOH}$$

If the pH of the solution in the pan is greater than 14, the solution can be diluted using Equation 4.4.

$$V_{add} = \frac{V_{pan}\, (M_{pan} - 1M)}{1M} \tag{4.4}$$

For the example, assume the pH is measured to be 14.2 (which corresponds to a molarity of 1.585 M) and volume in the pan is again 94 liters. The volume of water that is added to the pan to bring the molarity back to the desired level is

$$V_{add} = \frac{94 \text{ liter}\, (1.585M - 1M)}{1M} = 54.99 \text{ liter}$$

4.8 Safety

Due to the high concentration of the NaOH solution, safety is of the upmost importance during the curing process. Before entering the fog room, a person must at minimum wear splash proof goggles. Additional safety equipment included shin height rubber boots, chemical resistant rubber gloves, and a vapor respirator in Figure 4.14. While taking measurements, all pumps are unplugged to ensure that no splashing occurs. Additionally, an MSDS report for a sodium hydroxide solution is posted on the door of the fog room to provide all relevant safety information and first aid measures. Finally, a sign-in sheet is posted on the door to track who has come in and out of the fog room as well as when and how long they were in there. This, along with keeping the room locked when not in use, controls who has access to the room.

Figure 4.14: Safety equipment: goggles, vapor respirator, rubber boots, and rubber gloves

4.9 Complications

There are have been a number of complications that have delayed the progress of this experiment. Fortunately, each of these are independent of each other so the delays are not compounded. A summary of these complications are presented in the Table 4.1.

At the beginning of this experiment, the fog room did not have the capabilities required to properly cure the specimens. Facilities management committed to installing a new humidifier to supply humidity to the room and reconnect the heat to the university's heating source. While this work was initially completed, the installation did not work as promised.

First, after many delays connecting heat to the fog room, it was discovered that the heat was supplied by the hot water in the building. In an effort to save energy during the summer, the university turns the hot water off in the building. Thus, heat is unavailable to the fog room during this time. To provide heat to the fog room, the heat would have to be turned on in the entire wing of the building. Unfortunately, this was not discovered until after the work was essentially completed. To provide the proper heat for the experiment, up to five 1500-watt oil-filled electric space heaters were placed on the floor of the fog room, keeping the room at 96^{o}F. During this time, the facilities management worked to connect the heat to the steam pipes near the structures lab to provide heat for the fog room in the future year-round. This was completed in January of 2017 and is currently providing sufficient heat to the fog room.

Next, the humidifier proved to only be working intermittently after it was installed. It is believed that it was a refurbished humidifier that never worked at its complete capacity. Additionally, once the space heaters were installed, the humidifier proved to not have enough capacity to supply 95% relative humidity at high temperatures. A new humidifier with twice the capacity had to be ordered and installed. The installation was completed in November 2016 and successfully supplied the required relative humidity.

Once the new humidifiers were installed, the combination of temperature and humidity proved to exceed the dew point and moisture coated all exposed surfaces. The data logger mentioned in 4.5 proved to not be waterproof and shorted out in December 2016. Probe style temperature and humidity sensors with independent continuous data loggers proved to be too expensive for the project budget. Therefore, the an outdoor thermometer and humidity gauge was installed into the fog room to provide manual identification of the fog room conditions. Additionally, the heater and humidifier provided their own sensors that displayed

the fog room conditions. These sensors are sufficient to prove that the ambient conditions of the fog room are sufficient to properly cure the specimens.

Table 4.1: RH and T during initial installation phase

Date	Temp (°F)	RH (%)	Comments
29-May-16		-	Specimens Installed in Fog Room
7-Jun-16	85	-	2 Heaters, Humidifier working intermittently
22-Jun-16	90	-	3rd heater installed, Humidifier working intermittently
28-Jun-16	90	88	Humidifier Working
8-Jul-16	93	75	4th heater installed
23-Sep-16	96	60	5th Heater Installed, Humidifier less effective due to high heat
10-Nov-16	96	95	New Humidifier Installed
8-Dec-16	96	95	Data collection of temperature and humidity stops working
30-Jan-17	90	95	Heater installed. Heat differential between ceiling and specimen level
26-Feb-17	100	95	Fan installed to circulate heat

Finally, as mentioned previously in Section 4.2, the datum discs have proved difficult to keep adhered to the concrete due to the highly caustic sodium hydroxide and extreme ambient conditions of the room. After all the discs had been placed initially they became unattached from the concrete surface and had to be replaced using a brushable ceramic epoxy that has excellent chemical, temperature, and humidity resistance. Fortunately, this was discovered before the initial measurements were taken. However, this brushable ceramic epoxy had a high viscosity and was it was difficult to place them on vertical surfaces of the shear specimens and blocks that had already been installed in the fog room. After a few months, some of the epoxy began to become unattached from the surfaces again. A ceramic epoxy with a much lower viscosity was used to successfully and permanently reattach the discs that came off and reinforced the ones that had not yet detached. Corrections had to be applied to the data that had already collected so they became in agreement with the future measurements. A summary of these corrections is shown in Section 6.1.3.

4.10 Data Flow

To handle the large amount of data collected during this experiment, processes were created to automatically generate graphs so progress could be tracked after each set of measurements were collected. The flow of data from laboratory to report is illustrated by Fig. 4.15:

1. **Data gathering** Two steps
    1. Manually recorded data includes:
        (a) (147) expansions readings with the DEMEC and entered in a spreadsheet.
        (b) (16) strain gauge readings entered in the same spreadsheet.
    2. Electronically downloaded data and stored in spreadsheets:
        (a) Fog room temperature and relative humidity.
        (b) (16) specimen internal temperature sensors
2. **p1.m** A matlab code that reads all data from the three spreadsheets and stores them in a binary file `from-p1.mat`.
3. **p2.m** A matlab code that reads data `from-p1.mat` and create a data structure stored in `from-p2.mat` to facilitate subsequent referencing.

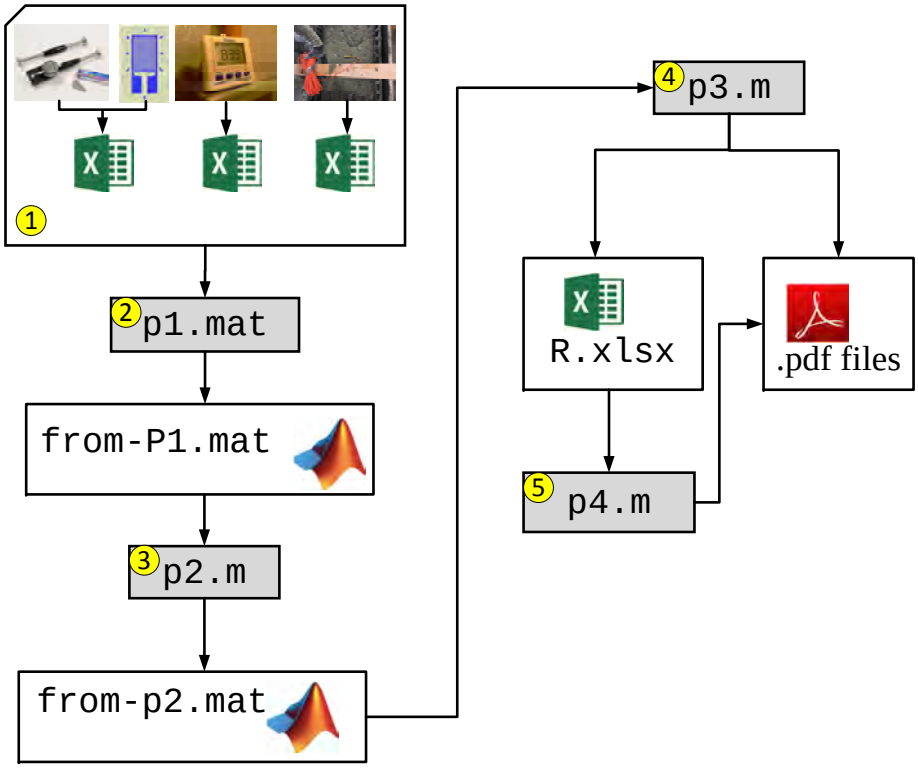

Figure 4.15: Data flow from laboratory to report

4. **p3.m** A matlab code that reads the binary file `from-p2.mat` and
   1. Stores selected data (for each set of reading) in and excel file `R.xlsx`.
   2. Generates selected plots.
5. **p4.m** An interactive program that allows the user to plot any pair or multiple sets of data stored in `R.xlsx`.

4.10.1 Saved data sets

The following data sets are computed and then saved by `p3.m` into `R.xlsx`

1. Average expansion of prisms, categorized by size, reinforcement, and location
2. Average expansion of shear specimens, categorized by measurement direction and reinforcement.
3. Average expansion of blocks categorized by measurement direction, reinforcement group, and location.
4. Average volumetric expansion of blocks by reinforcement group.
5. Average percentage volumetric expansion of blocks by reinforcement group and measurement direction.
6. Average temperature between measurement dates of each specimen outfitted with internal temperature sensor.

4.10.2 Plotted results

The following plots (as `.pdf`) files are generated by `p3.m`

1. All internal specimen temperatures over time in a line graph.
2. Fog room temperature and humidity over time in a line graph.
3. Average expansion of each prism type (separated by size, reinforced or unreinforced in fog room or lab) over time in a bar graph.
4. Average block expansion of each reinforcement group in fog room or lab over time in a bar graph.
5. Average block volumetric expansion of each reinforcement group in fog room or lab over time in a bar graph.
6. Expansion of all blocks, separated by direction, over time in a line graph.
7. Expansion of each block in all three directions over time in a line graph.
8. Average expansion of all shear specimens, categorized by measurement direction, for reinforced and unreinforced specimens in a bar graph.
9. Expansion of all shear specimen, separated by direction over time in a line graph.
10. Expansion of each shear specimen with all six directions over time in a line graph.
11. Block expansion of each measurement direction, normalized to the expansion of the X direction and labeled with reinforcement to concrete ratio (rho) of each direction over time in a scatter plot.
12. Strain gauge measurements over time in a line graph.

5 Pictures of Specimens

5.1 April 25, 2017; XX days

5.1.1 Prisms 6x6x14

With reference to Table 3.6, pictures of the 6x6x14 inch prisms are shown in Fig. 5.1.

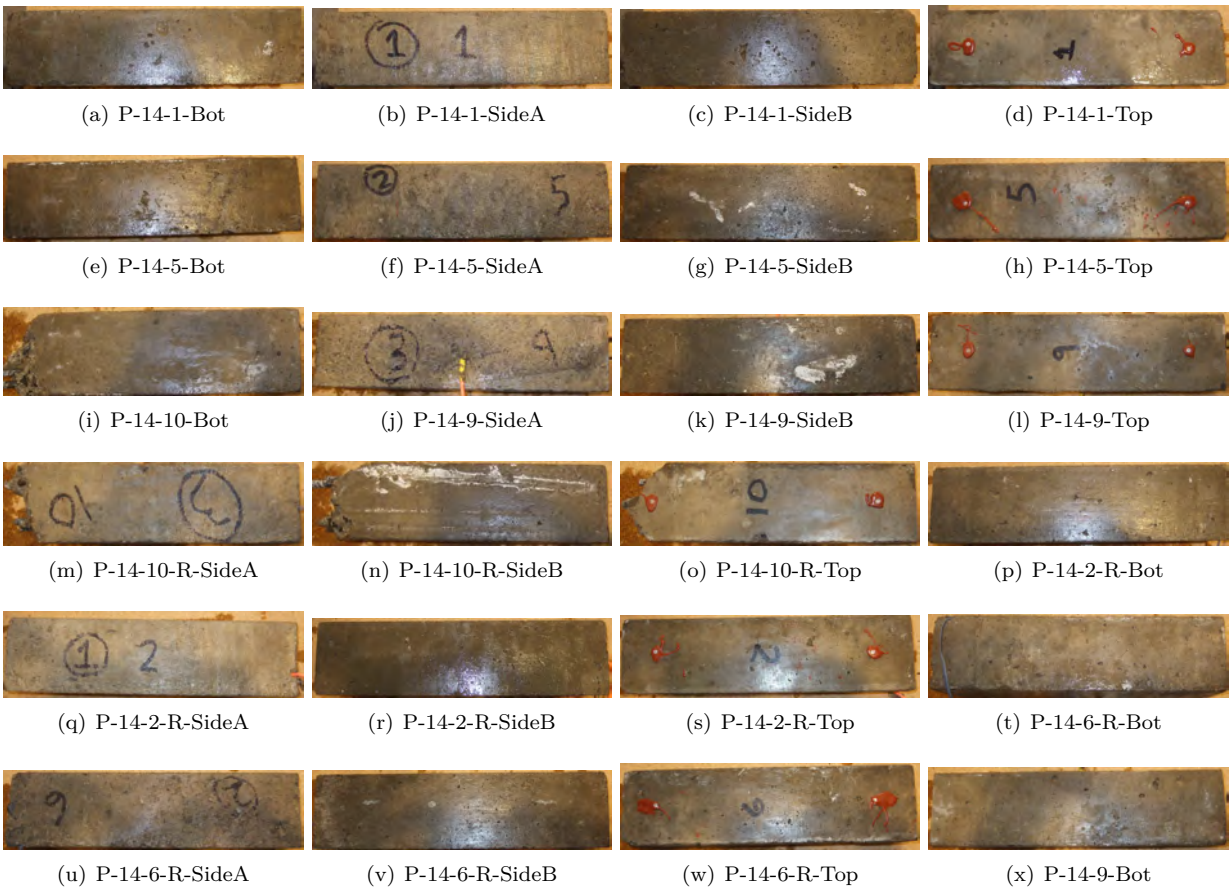

(a) P-14-1-Bot (b) P-14-1-SideA (c) P-14-1-SideB (d) P-14-1-Top

(e) P-14-5-Bot (f) P-14-5-SideA (g) P-14-5-SideB (h) P-14-5-Top

(i) P-14-10-Bot (j) P-14-9-SideA (k) P-14-9-SideB (l) P-14-9-Top

(m) P-14-10-R-SideA (n) P-14-10-R-SideB (o) P-14-10-R-Top (p) P-14-2-R-Bot

(q) P-14-2-R-SideA (r) P-14-2-R-SideB (s) P-14-2-R-Top (t) P-14-6-R-Bot

(u) P-14-6-R-SideA (v) P-14-6-R-SideB (w) P-14-6-R-Top (x) P-14-9-Bot

Figure 5.1: P14 Prismsin fogg room

5.1.2 Prisms 4x4x16

With reference to Table 3.5, pictures of the 4x4x16 inch prisms are shown in Fig. 5.2.

(a) P-16-1-Bot (b) P-16-1-Side-A (c) P-16-1-Side-B (d) P-16-1-Top

(e) P-16-9-Bot (f) P-16-9-Side-A (g) P-16-9-Side-B (h) P-16-9-Top

(i) P-16-2-R-Bot (j) P-16-2-R-Side-A (k) P-16-2-R-Side-B (l) P-16-2-R-Top

(m) P-16-10-R-Bot (n) P-16-10-R-Side-A (o) P-16-10-R-Side-B (p) P-16-10-R-Top

Figure 5.2: P16 Prisms in fogg room

5.1.3 Shear Specimens

5.1.4 Block

5.2 June 2017; XX days

5.2.1 Prisms 6x6x14

Table 5.1: Shear Specimens

Batch	ID	Reactive	Rebars	Temp. ID	Strain Gauge	Loc.
1	1	Y	Y			FR
	2		Y	1		
	3		Y			
2	4	Y	N			
	5		Y			
	6		Y	2	9	
	7		Y			
	8		N			
3	9	Y	Y		10	
	10		Y	3		
	11		Y			
	12		N			
4	13	No	Y			
	14		Y	4		
	15		N			
	16		N			

Table 5.2: 14 x 14 x 14 inch Blocks

Batch	ID	Reactive?	Rebar ID	Temp. ID	FR or LAB	Strain Guage X	Y	Z(UP)	A	B	C	D	E	F
1	5		D	6	FR	2	3	4				1		
2	1	Yes	A	5					1					
	2		A		Lab				1					
	3		B		FR			1		1				
	4		B		Lab					1				
2	6	Yes	A	7	FR				1					
	7		A	8	Lab				1					
	8		C		FR			5			1			
	9		C		Lab						1			
	10		E										1	
3	11	Yes	A	9	FR				1					
	12		A	10	Lab				1					
	13		F		FR	6	7	8						1
	14		F		Lab									1
	15		D									1		
					Sum				6	2	2	2	1	2

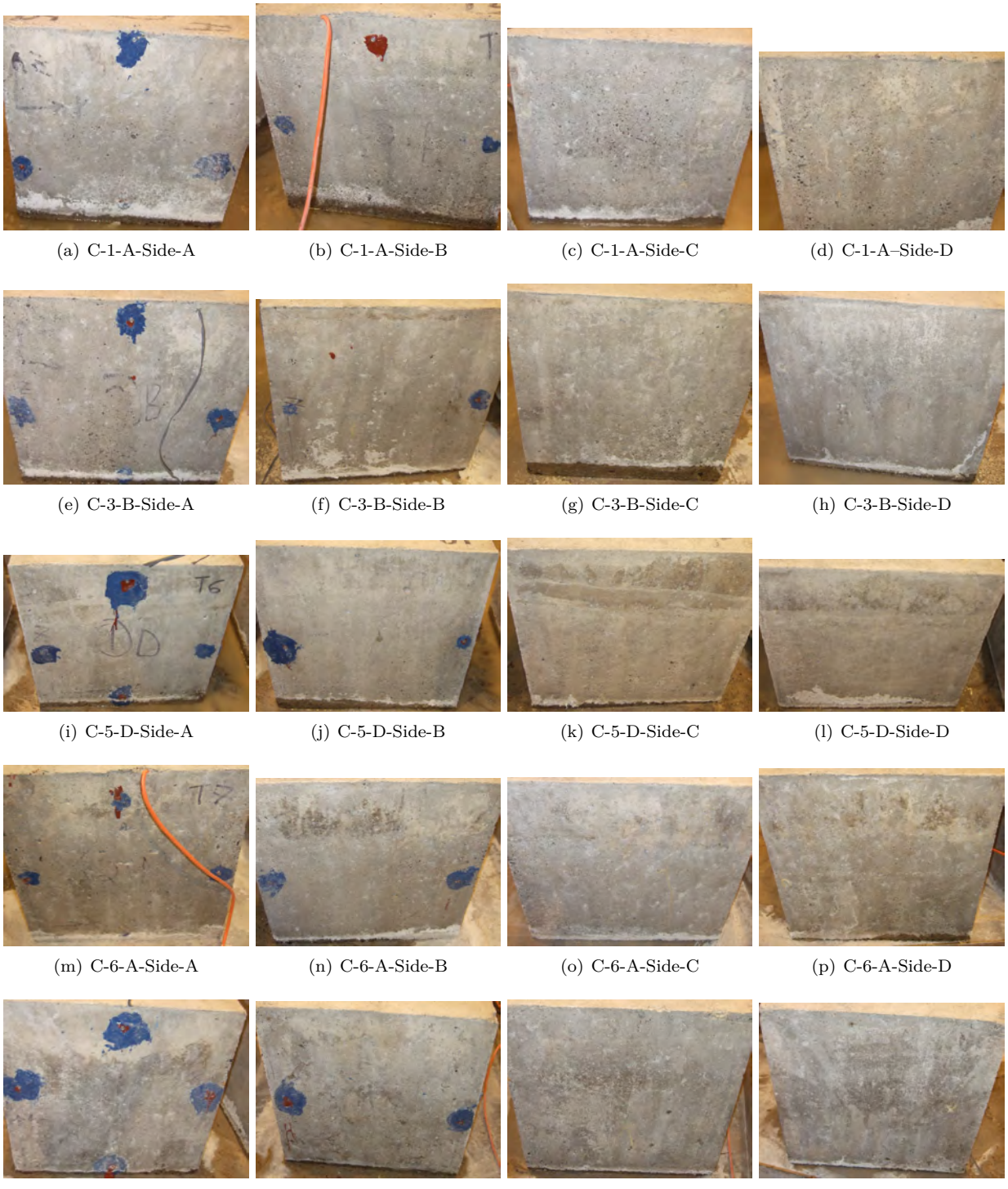

(a) C-1-A-Side-A (b) C-1-A-Side-B (c) C-1-A-Side-C (d) C-1-A–Side-D

(e) C-3-B-Side-A (f) C-3-B-Side-B (g) C-3-B-Side-C (h) C-3-B-Side-D

(i) C-5-D-Side-A (j) C-5-D-Side-B (k) C-5-D-Side-C (l) C-5-D-Side-D

(m) C-6-A-Side-A (n) C-6-A-Side-B (o) C-6-A-Side-C (p) C-6-A-Side-D

(q) C-8-C-Side-A (r) C-8-C-Side-B (s) C-8-C-Side-C (t) C-8-C-Side-D

Figure 5.3: Cubes; Part I

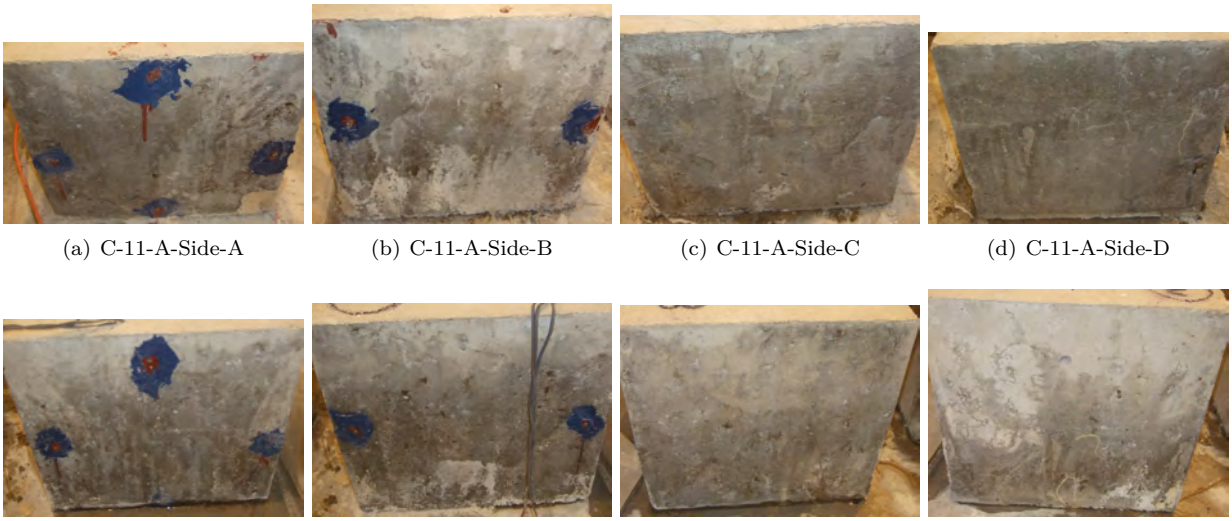

(a) C-11-A-Side-A (b) C-11-A-Side-B (c) C-11-A-Side-C (d) C-11-A-Side-D

(e) C-13-F-Side-A (f) C-13-F-Side-B (g) C-13-F-Side-C (h) C-13-F-Side-D

Figure 5.4: Cubes; Pasrt II

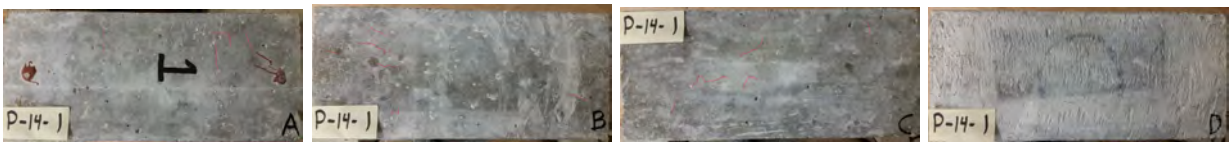

(a) P-14-1-SideA (b) P-14-1-SideB (c) P-14-1-SideC (d) P-14-1-SideD

Figure 5.5: P14-1 Prisms

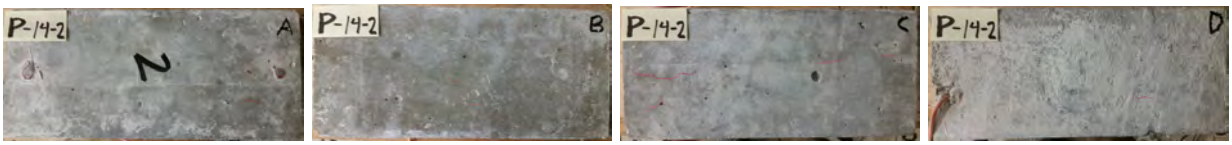

(a) P-14-2-SideA (b) P-14-2-SideB (c) P-14-2-SideC (d) P-14-2-SideD

Figure 5.6: P14-2 Prisms

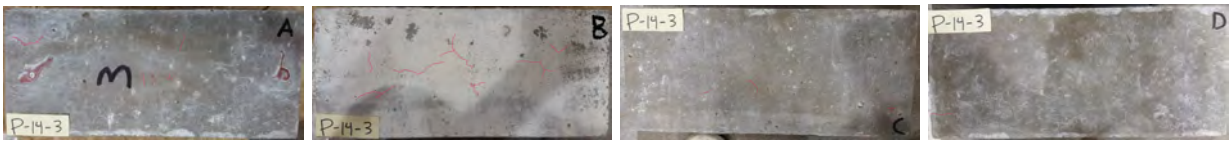

(a) P-14-3-SideA (b) P-14-3-SideB (c) P-14-3-SideC (d) P-14-3-SideD

Figure 5.7: P14-3 Prisms

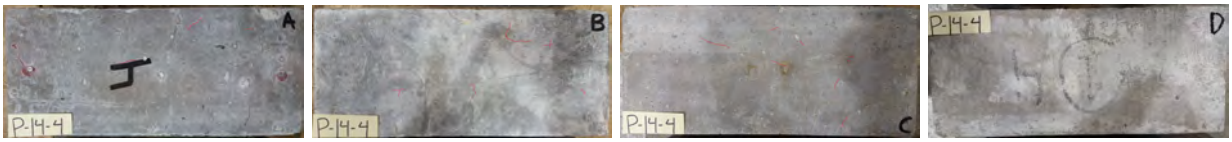

(a) P-14-4-SideA (b) P-14-4-SideB (c) P-14-4-SideC (d) P-14-4-SideD

Figure 5.8: P14-4 Prisms

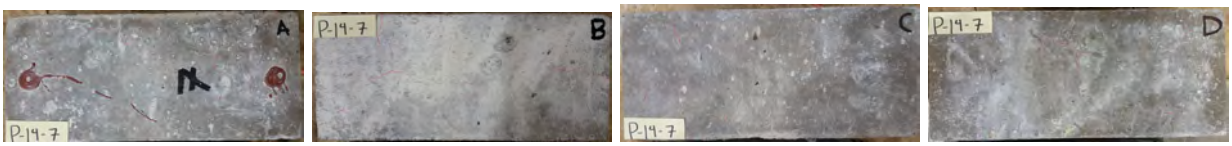

(a) P-14-7-SideA (b) P-14-7-SideB (c) P-14-7-SideC (d) P-14-7-SideD

Figure 5.9: P14-7 Prisms

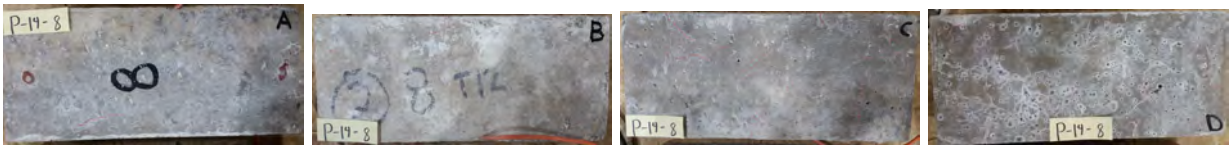

(a) P-14-8-SideA (b) P-14-8-SideB (c) P-14-8-SideC (d) P-14-8-SideD

Figure 5.10: P14-8 Prisms

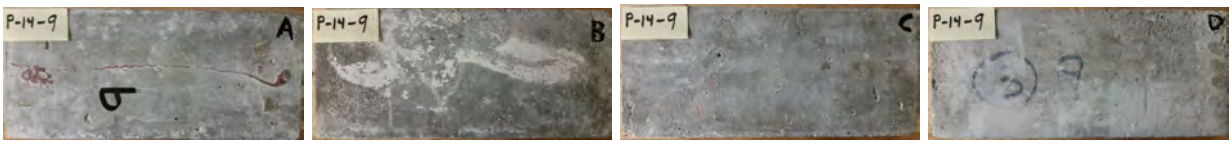

(a) P-14-9-SideA (b) P-14-9-SideB (c) P-14-9-SideC (d) P-14-9-SideD

Figure 5.11: P14-9 Prisms

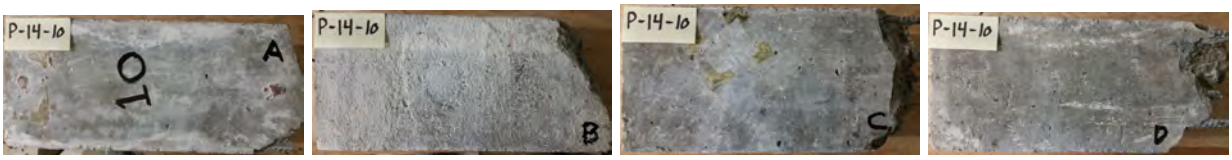

(a) P-14-10-SideA (b) P-14-10-SideB (c) P-14-10-SideC (d) P-14-10-SideD

Figure 5.12: P14-10 Prisms

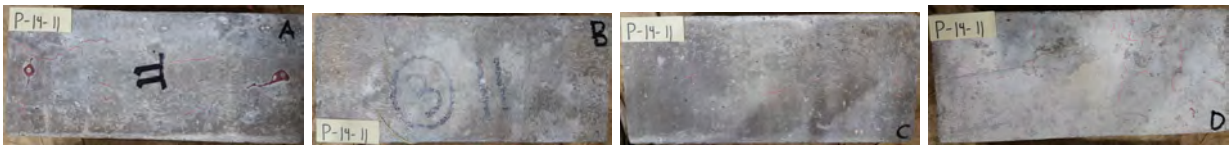

(a) P-14-11-SideA (b) P-14-11-SideB (c) P-14-11-SideC (d) P-14-11-SideD

Figure 5.13: P14-11 Prisms

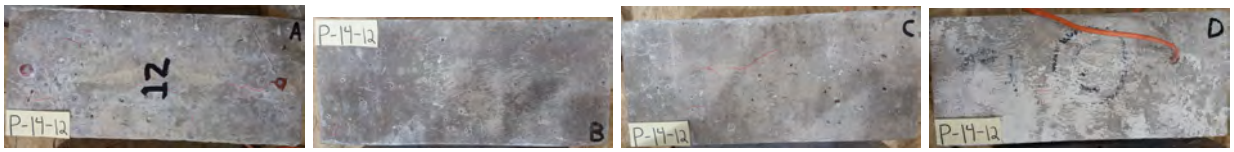

(a) P-14-12-SideA (b) P-14-12-SideB (c) P-14-12-SideC (d) P-14-12-SideD

Figure 5.14: P14-12 Prisms

5.2.2 Prisms 4x4x16

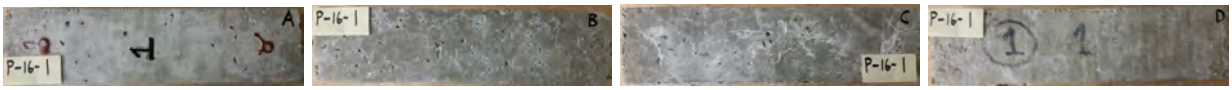

(a) P-16-1-SideA (b) P-16-1-SideB (c) P-16-1-SideC (d) P-16-1-SideD

Figure 5.15: P16-1 Prisms

(a) P-16-2-SideA (b) P-16-2-SideB (c) P-16-2-SideC (d) P-16-2-SideD

Figure 5.16: P16-2 Prisms

(a) P-16-3-SideA (b) P-16-3-SideB (c) P-16-3-SideC (d) P-16-3-SideD

Figure 5.17: P16-3 Prisms

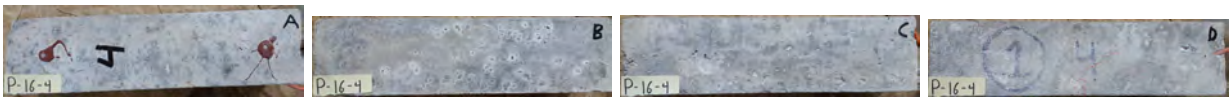

(a) P-16-4-SideA (b) P-16-4-SideB (c) P-16-4-SideC (d) P-16-4-SideD

Figure 5.18: P16-4 Prisms

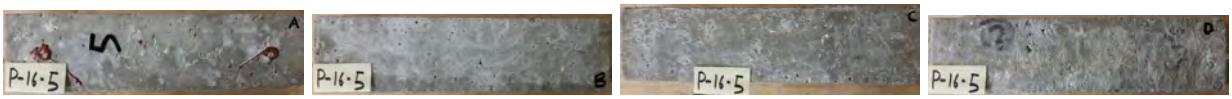

(a) P-16-5-SideA (b) P-16-5-SideB (c) P-16-5-SideC (d) P-16-5-SideD

Figure 5.19: P16-5 Prisms

(a) P-16-6-SideA (b) P-16-6-SideB (c) P-16-6-SideC (d) P-16-6-SideD

Figure 5.20: P16-6 Prisms

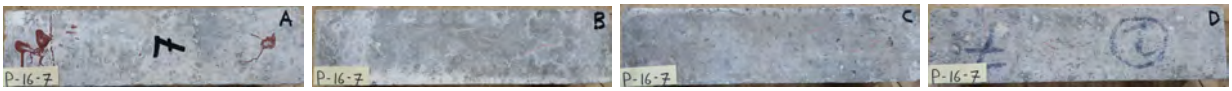

(a) P-16-7-SideA (b) P-16-7-SideB (c) P-16-7-SideC (d) P-16-7-SideD

Figure 5.21: P16-7 Prisms

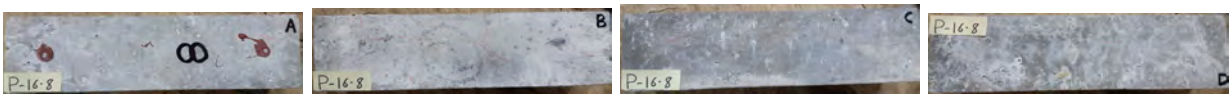

(a) P-16-8-SideA (b) P-16-8-SideB (c) P-16-8-SideC (d) P-16-8-SideD

Figure 5.22: P16-8 Prisms

(a) P-16-9-SideA (b) P-16-9-SideB (c) P-16-9-SideC (d) P-16-9-SideD

Figure 5.23: P16-9 Prisms

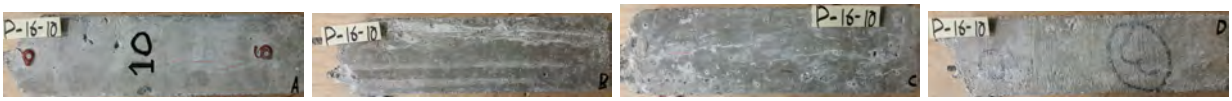

(a) P-16-10-SideA (b) P-16-10-SideB (c) P-16-10-SideC (d) P-16-10-SideD

Figure 5.24: P16-10 Prisms

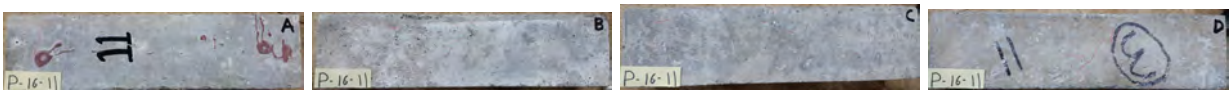

(a) P-16-11-SideA (b) P-16-11-SideB (c) P-16-11-SideC (d) P-16-11-SideD

Figure 5.25: P16-11 Prisms

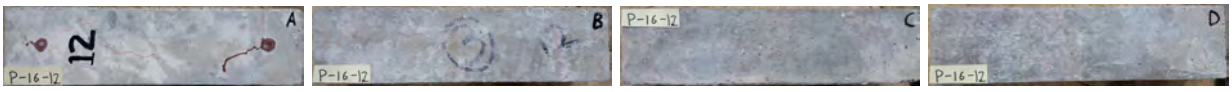

(a) P-16-12-SideA (b) P-16-12-SideB (c) P-16-12-SideC (d) P-16-12-SideD

Figure 5.26: P16-12 Prisms

5.2.3 Shear Specimens

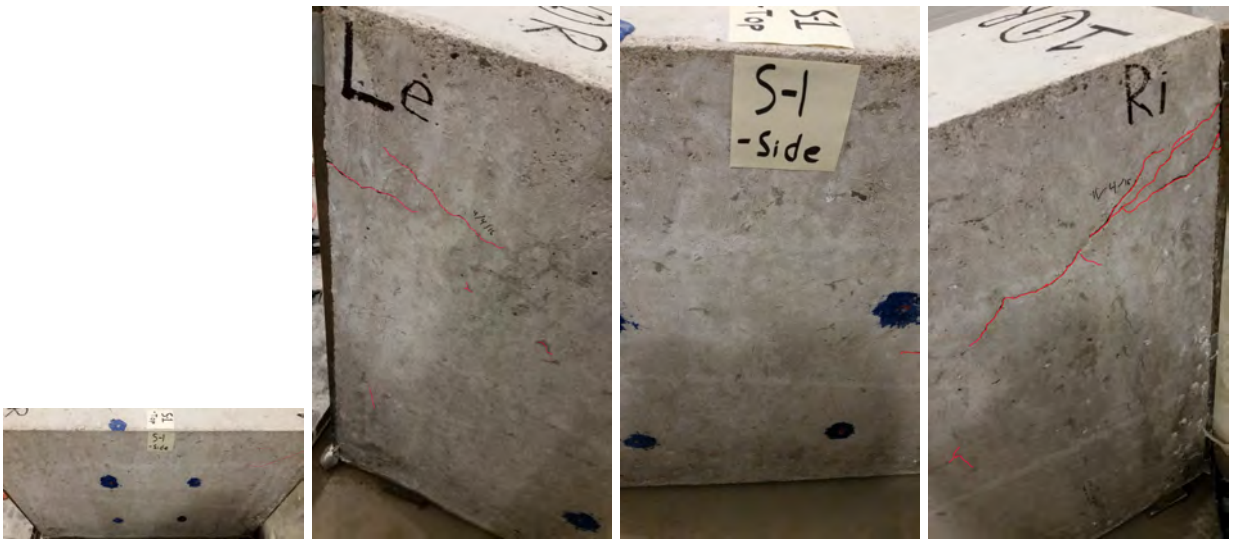

(a) S-1-Side (b) S-1-SideLe (c) S-1-SideM (d) S-1-SideRi

(e) S-1-Top (f) S-1-TopA (g) S-1-TopB (h) S-1-TopC

Figure 5.27: S1

(a) S-2-Side

(b) S-2-SideLe

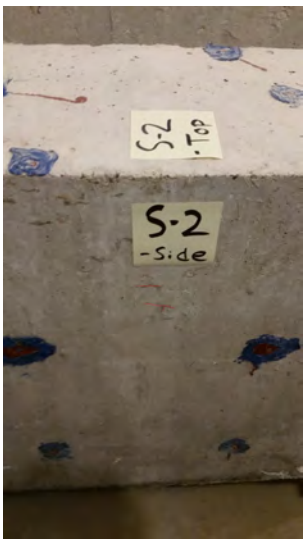

(c) S-2-SideM

(d) S-2-SideRi

(e) S-2-Top

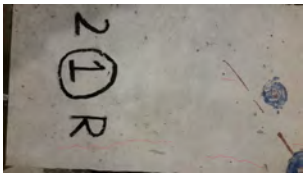

(f) S-2-TopA

(g) S-2-TopB

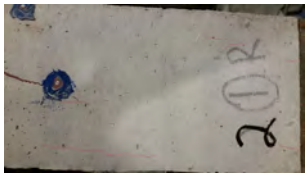

(h) S-2-TopC

Figure 5.28: S2

(a) S-3-Side

(b) S-3-SideLe

(c) S-3-SideLeBot

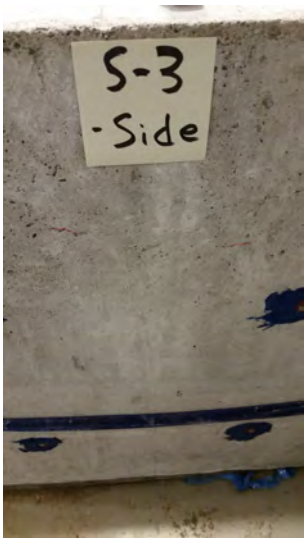

(d) S-3-SideM

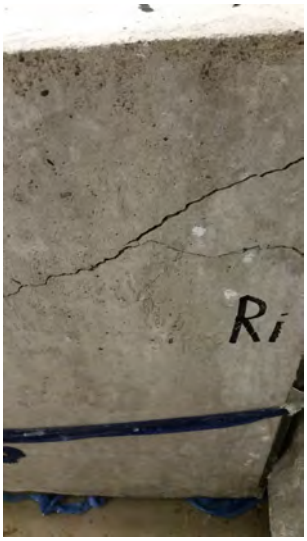

(e) S-3-SideRi

(f) S-3-Top

(g) S-3-TopA

(h) S-3-TopB

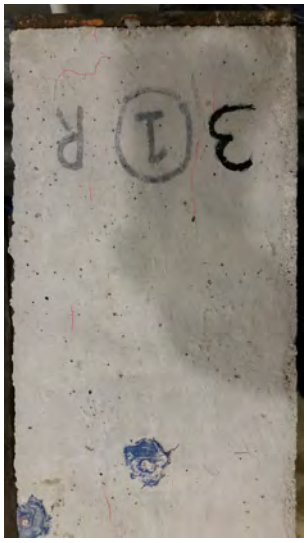

(i) S-3-TopC

Figure 5.29: S3

(a) S-4-Side (b) S-4-SideLe (c) S-4-SideM (d) S-4-SideRi

(e) S-4-Top (f) S-4-TopA (g) S-4-TopB (h) S-4-TopC

Figure 5.30: S4

(a) S-5-Side

(b) S-5-SideLe

(c) S-5-SideM

(d) S-5-SideRi

(e) S-5-Top

(f) S-5-TopA

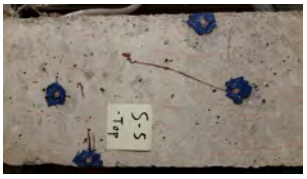

(g) S-5-TopB

(h) S-5-TopC

Figure 5.31: S5

(a) S-6-Side

(b) S-6-SideLe

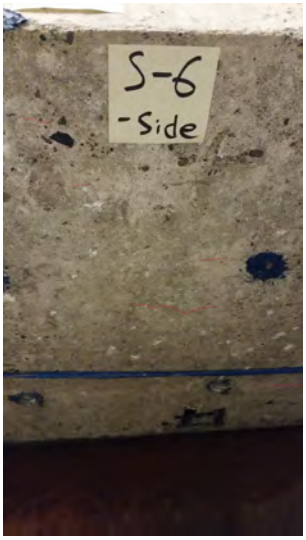

(c) S-6-SideM

(d) S-6-SideRi

(e) S-6-Top

(f) S-6-TopA

(g) S-6-TopB

(h) S-6-TopC

Figure 5.32: S6

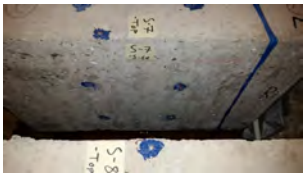

(a) S-7-Side

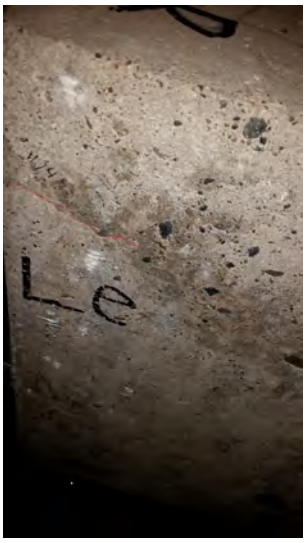

(b) S-7-SideLe

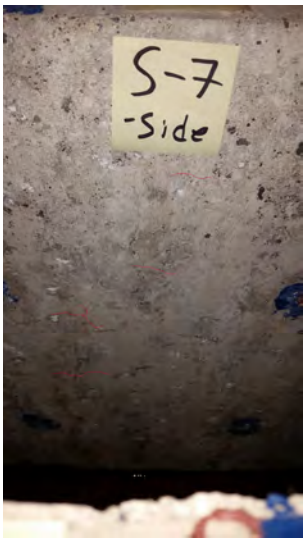

(c) S-7-SideM

(d) S-7-SideRi

(e) S-7-Top

(f) S-7-TopA

(g) S-7-TopB

(h) S-7-TopC

Figure 5.33: S7

(a) S-8-SIDE

(b) S-8-SideLe

(c) S-8-SideLeBot

(d) S-8-SideM

(e) S-8-SideMBot

(f) S-8-SideRi

(g) S-8-SideRiBot

(h) S-8-Top

(i) S-8-TopA

(j) S-8-TopB

(k) S-8-TopC

Figure 5.34: S8

(a) S-9-Side

(b) S-9-SideLe

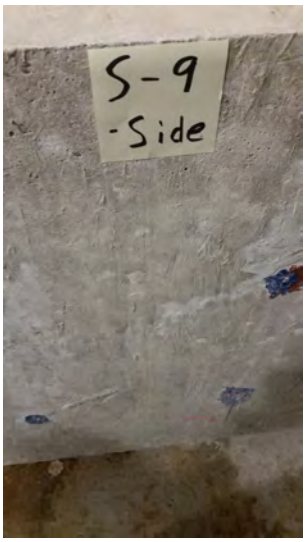

(c) S-9-SideM

(d) S-9-SideRi

(e) S-9-Top

(f) S-9-TopA

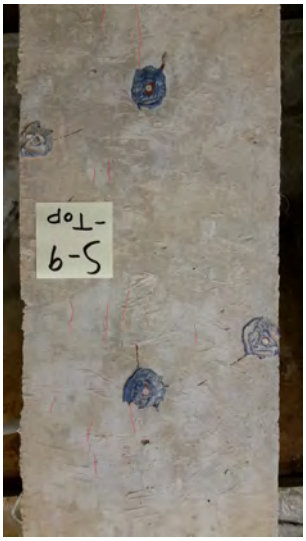

(g) S-9-TopB

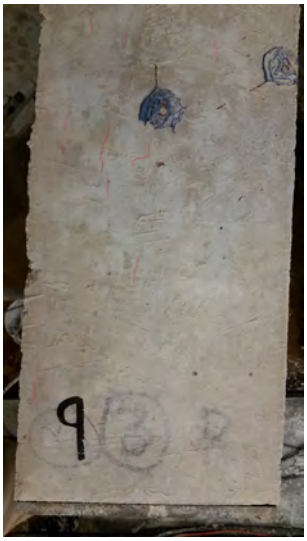

(h) S-9-TopC

Figure 5.35: S9

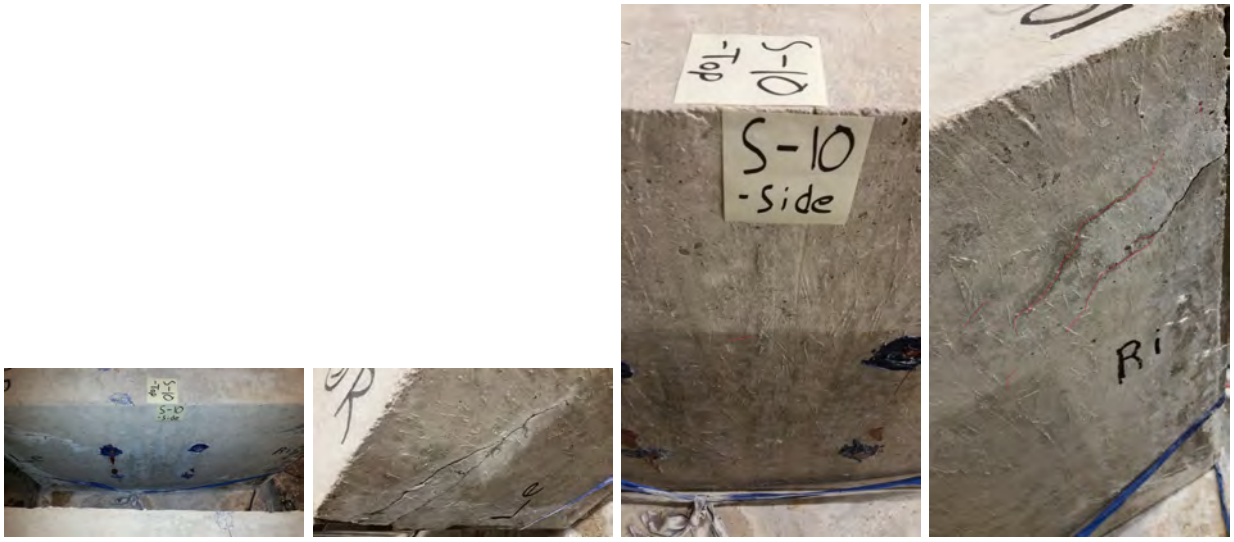

(a) S-10-Side (b) S-10-SideLe (c) S-10-SideM (d) S-10-SideRi

(e) S-10-Top (f) S-10-TopA (g) S-10-TopB (h) S-10-TopC

Figure 5.36: S10

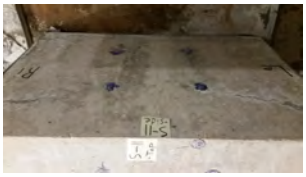

(a) S-11-Side

(b) S-11-SideLe

(c) S-11-SideLeBot

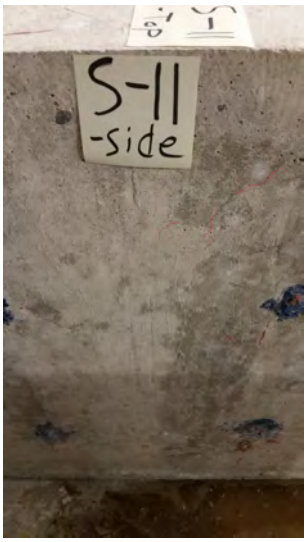

(d) S-11-SideM

(e) S-11-SideRi

(f) S-11-Top

(g) S-11-TopA

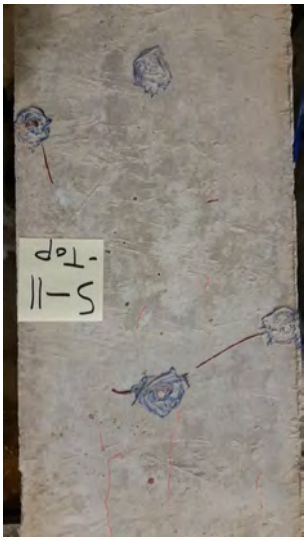

(h) S-11-TopB

(i) S-11-TopC

Figure 5.37: S11

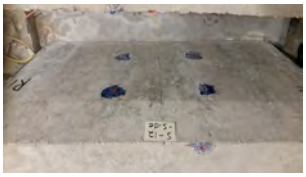

(a) S-12-Side

(b) S-12-SideLe

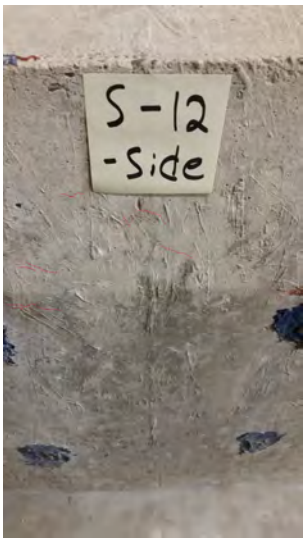

(c) S-12-SideM

(d) S-12-SideRi

(e) S-12-Top

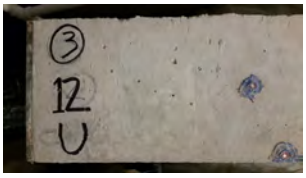

(f) S-12-TopA

(g) S-12-TopB

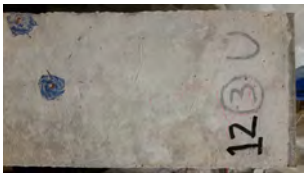

(h) S-12-TopC

Figure 5.38: S12

(a) S-13-Side

(b) S-13-Top

Figure 5.39: S13

(a) S-14-Side

(b) S-14-Top

Figure 5.40: S14

(a) S-15-Side (b) S-15-Top

Figure 5.41: S15

(a) S-16-Side (b) S-16-Top

Figure 5.42: S16

5.2.4 Block

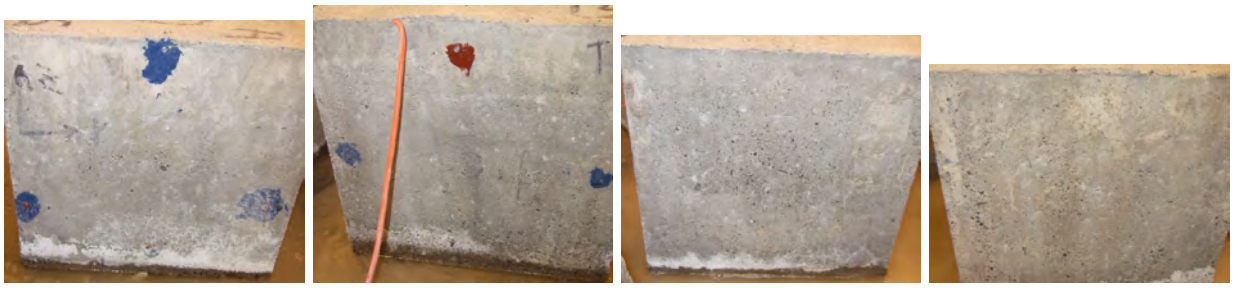

(a) C-14-1-SideA (b) C-14-1-SideB (c) C-14-1-SideC (d) C-14-1-SideD

Figure 5.43: C-1

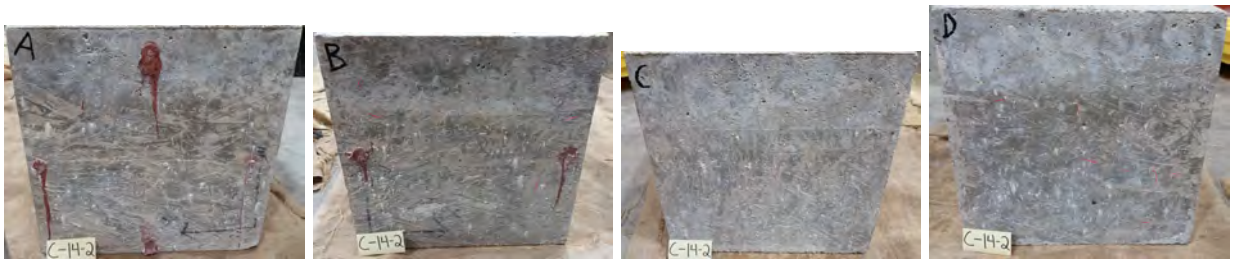

(a) C-14-2-SideA (b) C-14-2-SideB (c) C-14-2-SideC (d) C-14-2-SideD

(e) C-14-2-Top

Figure 5.44: C-2

(a) C-14-3-SideA (b) C-14-3-SideC (c) C-14-3-SideD

Figure 5.45: C-3

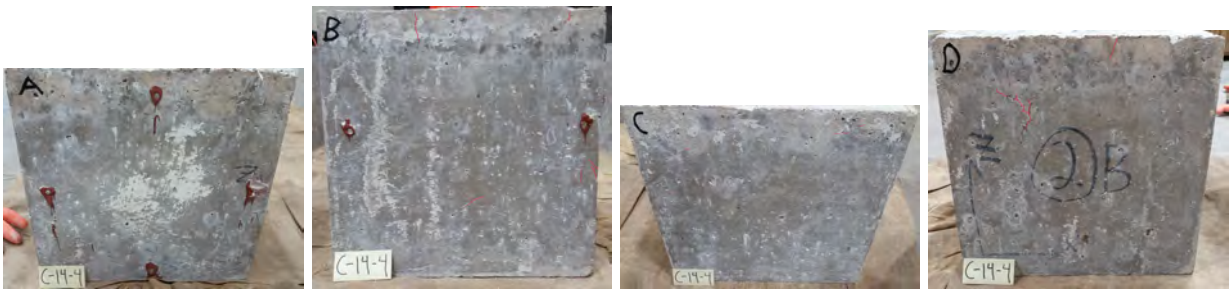

(a) C-14-4-SideA (b) C-14-4-SideB (c) C-14-4-SideC (d) C-14-4-SideD

(e) C-14-4-Top

Figure 5.46: C-4

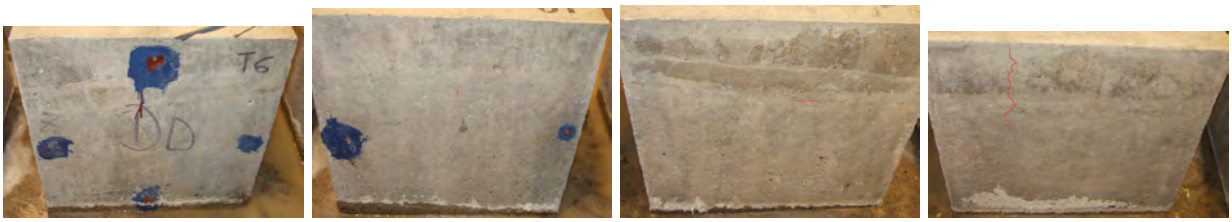

(a) C-14-5-SideA (b) C-14-5-SideB (c) C-14-5-SideC (d) C-14-5-SideD

Figure 5.47: C-5

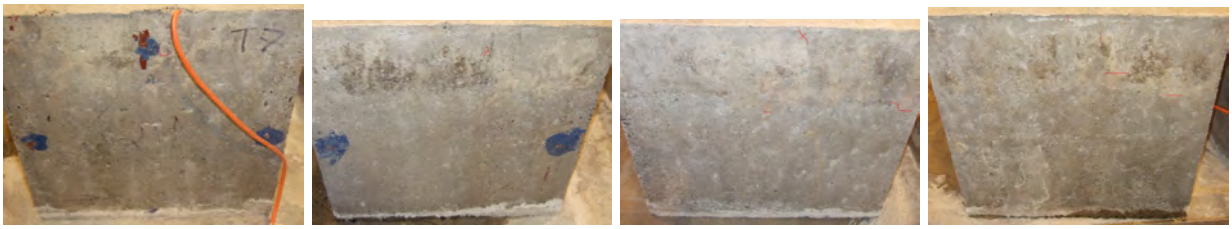

(a) C-14-6-SideA (b) C-14-6-SideB (c) C-14-6-SideC (d) C-14-6-SideD

Figure 5.48: C-6

(a) C-14-7-SideA (b) C-14-7-SideB (c) C-14-7-SideC (d) C-14-7-SideD

(e) C-14-7-Top

Figure 5.49: C-7

(a) C-14-8-SideA (b) C-14-8-SideB (c) C-14-8-SideC (d) C-14-8-SideD

Figure 5.50: C-8

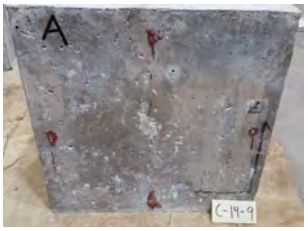

(a) C-14-9-SideA

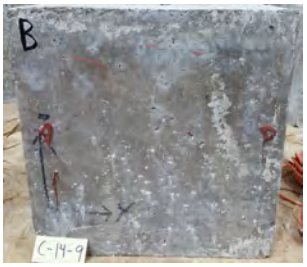

(b) C-14-9-SideB

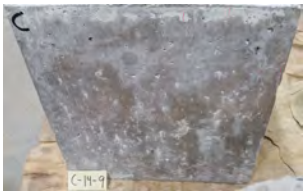

(c) C-14-9-SideC

(d) C-14-9-SideD

(e) C-14-9-Top

Figure 5.51: C-9

(a) C-14-10-SideA.jpg

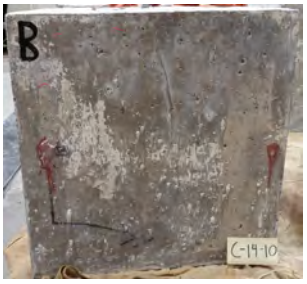

(b) C-14-10-SideB

(c) C-14-10-SideC

(d) C-14-10-SideD

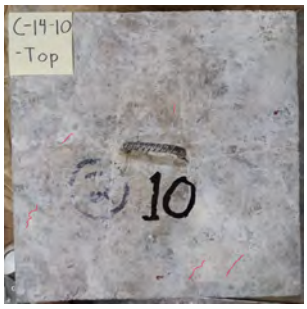

(e) C-14-10-Top

Figure 5.52: C-10

(a) C-14-11-SideA (b) C-14-11-SideC (c) C-14-11-SideD

Figure 5.53: C-11

(a) C-14-12-SideA (b) C-14-12-SideB (c) C-14-12-SideC (d) C-14-12-SideD

(e) C-14-12-Top

Figure 5.54: C-12

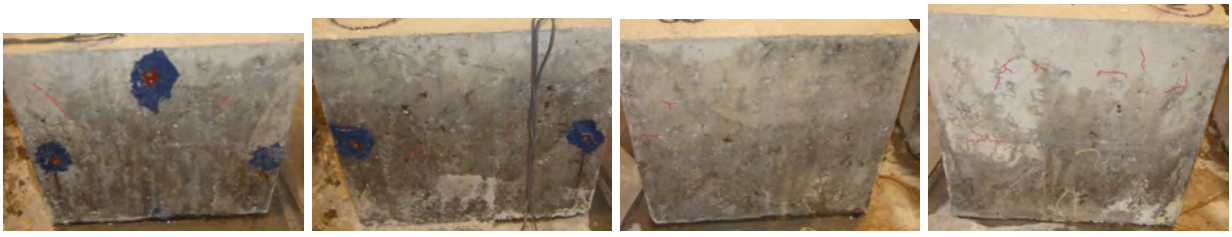

(a) C-14-13-SideA (b) C-14-13-SideB (c) C-14-13-SideC (d) C-14-13-SideD

Figure 5.55: C-13

(a) C-14-14-SideA

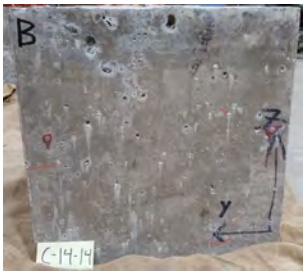

(b) C-14-14-SideB

(c) C-14-14-SideC

(d) C-14-14-SideD

(e) C-14-14-Top

Figure 5.56: C-14

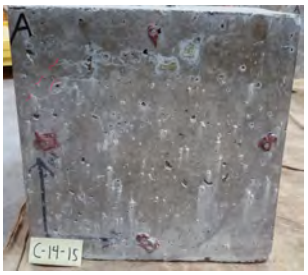

(a) C-14-15-SideA

(b) C-14-15-SideB

(c) C-14-15-SideC

(d) C-14-15-SideD

(e) C-14-15-Top

Figure 5.57: C-15

6 Expansion Measurements

6.1 Introduction

In a literature search of the effects of reinforcement and environmental effects on ASR expansion, a number of predictions are made so they can be compared to the results.

First, it is predicted that the reinforced specimens will expand less than their unreinforced counterparts. Furthermore, the specimens with greater concrete to reinforcement ratio will have less expansion. The rebar embedded in the concrete absorbs the strain created by the expansive ASR gel and the concrete itself will have less expansion. Therefore, the more rebar present to absorb strain, the less the concrete will expand.

Additionally, it has been shown that high heat and humidity promote and accelerate the production of ASR. It is predicted that the blocks and prisms stored in the hot and humid conditions of the fog room will have greater expansion than those stored at ambient conditions in the lab.

Since all specimens are created with the same concrete mix, all specimens theoretically should have the same volumetric expansion. It is recognized that experimental results are not perfect so expansion will not be exactly the same. However, volumetric expansions should be at least be comparable to one another. Comparing the sum of expansions in each orthogonal direction, it is expected the volumetric expansion should be similar, regardless of shape or size of the specimen.

Finally, since higher temperatures correspond to greater expansion it is expected that higher temperatures will produce a faster rate of expansion between measurements. Since over the course of this project the heat in the fog room has been variable due to the simultaneous installation of a new heating system, a variety of average temperature ranges are available to make this comparison.

6.1.1 Measurements

During the course of the experiment, efficient methods were developed to monitor the progress of the expansion of the shear specimens, blocks, and prisms in the fog room and lab to ensure that they were expanding properly and at a sufficient rate. A MATLAB code was developed to automatically import, process, and plot the expansion of the raw data. This section discusses this process of monitoring the specimen expansion.

Originally it was intended to simply monitor the expansion of selected specimens to assess degree of expansion and then decide when the shear specimens should be tested. However, as the program progressed it was decided to instrument a multitude of specimens, Table 6.1.

To facilitate reading of the plots in this chapter, the following convention was systematically adopted:

——— Inside the fog room

– – – In the laboratory (room temperature)

-		Expansion		Other	
Specimen Type	Number	Reading/specimen	Total	Temperature	Strains
Reactive Shear Specimens	12	6	72	3	2
Non Reactive shear Specimens	4	2	8	1	-
$6 \times 6 \times 14$ inch prisms	10	1	10	3	3
$4 \times 4 \times 16$ inch prisms	12	1	12	3	3
$14 \times 14 \times 14$ inch Blocks	15	3	45	6	8
Total	55	-	147	16	16

Table 6.1: Total number of data readings

Color Red	Batch 1 (reactive)
Color Green	Batch 2 (reactive)
Color Blue	Batch 3 (reactive)
Color black	Batch 4 (non reactive)
O	With reinforcement
X	No reinforcement

6.1.2 Expansion Calculation

Raw data collected with the DEMEC device in the lab measures the distance between two datum discs. The DEMEC is zeroed to 11.811 inches (300 mm) and the output to the spread sheet is the length above or below the zero. Expansion at any point is calculated using Equation 6.1 where L_0 is the initial measurement and L_n is the measurement at any given point in time in inches.

$$\varepsilon = \frac{L_o - L_n}{L_o + 11.811} \times 100\% \tag{6.1}$$

6.1.3 Data Corrections

Occasionally, alterations must be applied to the data to correct for inconsistencies in the data. There are two reasons that that the data would need to be corrected:

- Outlying data point with a value significantly greater than or less than general trend line to does not represent that actual expansion due to errors in measurement.
- Datum disc detaches from concrete surface and reattached. The disc is reattached at a "zero" measurement point.

To correct the outlier data point, an average is taken of the data point before and after the outlier to bring it into the general expansion trend line. To correct for a datum disc that has detached, all of the measurements that are taken after the disc is reattached are raised to be in line with the current expansion trend line as shown in Fig. 6.1 using the Equations 6.2 to 6.6.

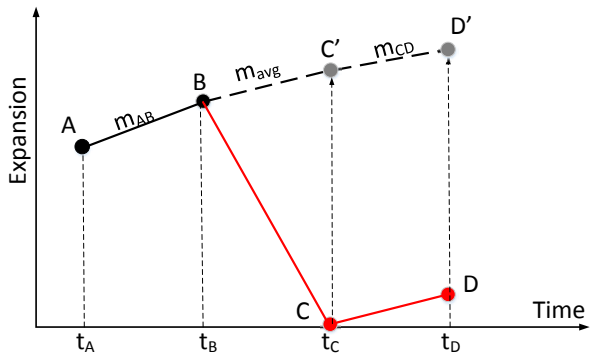

Figure 6.1: Graphical Representation of Data Correction

$$m_{AB} = \frac{B-A}{t_2-t_1} \tag{6.2}$$

$$m_{CD} = \frac{D-C}{t_4-t_3} \tag{6.3}$$

$$m_{avg} = \frac{m_{AB}+m_{CD}}{2} \tag{6.4}$$

$$C' = B + (t_3-t_2)m_{avg} \tag{6.5}$$

$$D' = C' + (t_4-t_3)m_{CD} \tag{6.6}$$

Point C is the first measurement taken after the disc has been reattached at the zero position showing zero expansion. Using the average slope between the two points before the disc detached (A and B) and after it is reattached (C and D), all subsequent measurements are raised so a cohesive expansion curve is formed.

6.2 Averaged Expansions

This section outlines the average plots used during the curing process to ensure that the specimens were expanding as expected. Expansion averages also ensured that the MATLAB code was working properly and allowed identification of any outlying data points that would need to be corrected as a result of an improper reading or datum disc detaching from the specimen. If some of the averages seemed unexpected, the graphs in Section 6.3 would be consulted to determine the specific cause.

6.2.1 Prism Averages

Figure 6.2 shows the average expansion of each prism size, separated reinforced and unreinforced prisms in the fog room and unreinforced prisms. in the lab. There are no reinforced prisms in the lab. The unreinforced prisms in the fog room are considered to show the "true" expansion of the concrete and will serve as guidance about when to take specimens out of the fog room for testing. As can be seen in the graphs, both sizes have reached the target expansion level of 0.5%. The reinforced specimens in the fog room have expanded less than the unreinforced lab specimens. Explanation for this is found in Section 8.3.

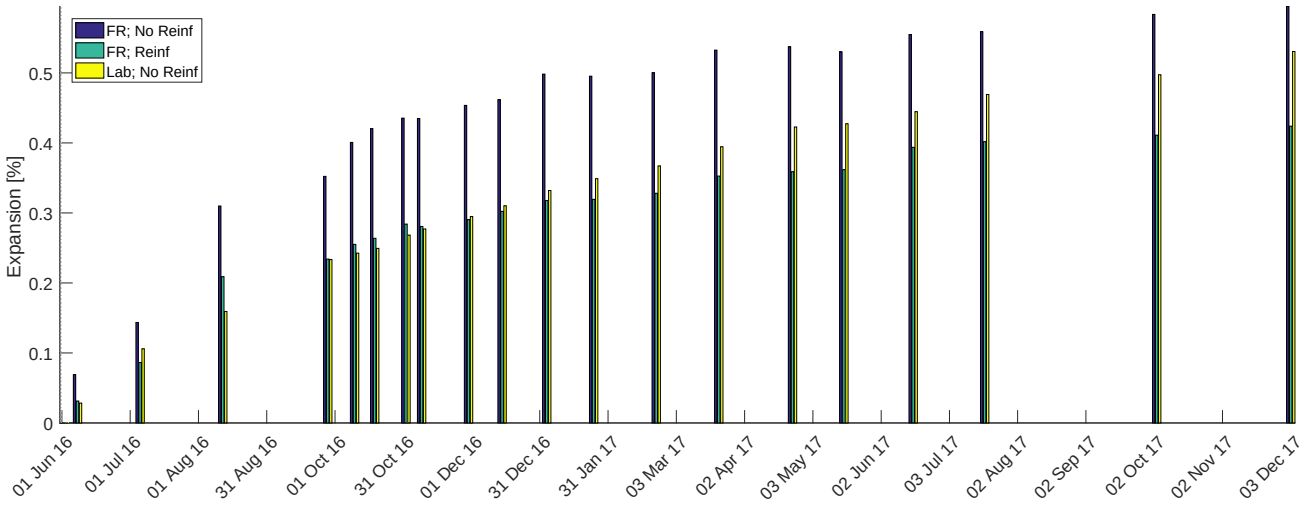

(a) Average 6 × 6 × 14 inch Prisms (P14)

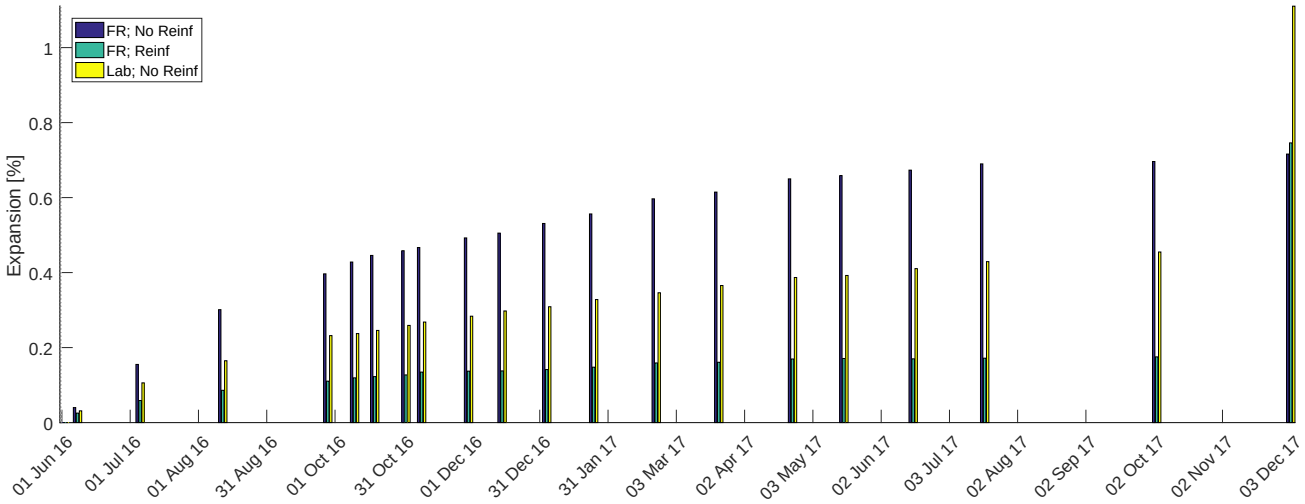

(b) Average 4 × 4 × 16 inch Prisms (P16)

Figure 6.2: Average prism specimen

In these plots it can be seen that the prisms are continually expanded meaning the curing process is proceeding as expected. Additionally, the unreinforced prisms in the fog room have greater expansion that the reinforced prisms in the fog room and the prisms stored in the lab which support the experimental prediction.

6.2.2 Block Averages

Expansion of the block specimens in each are organized by reinforcement type and graphs are separated by measurement direction (X, Y, or Z) and specimen location (Fog Room or Lab). The X and Y axes are horizontal measurements, orthogonal to one another. The Z axis is vertical. The reinforcement groups can list the reinforcement in each direction. For example, F:X4Y3Z34 means that reinforcement F has #4 bars in the X direction, #3 bars in the Y direction, and both #3 and #4 bars in the Z direction. All reinforcement are hoops so any reinforcement that is in either the X or Y direction will also be in the Z direction. If

reinforcement is present in both the X and Y direction, then Z is doubly reinforced. A schematic of this layout is shown in Figure 3.10.

Since all blocks are continually expanding and the results are reasonable, it is generally believed that the results are reliable. However, there are a couple of curious results that will require further analysis. In the X and Z directions, some reinforced blocks have greater expansion than the unreinforced blocks. For the Y direction, unreinforced blocks have greatest expansion but some reinforced blocks have similar expansion.

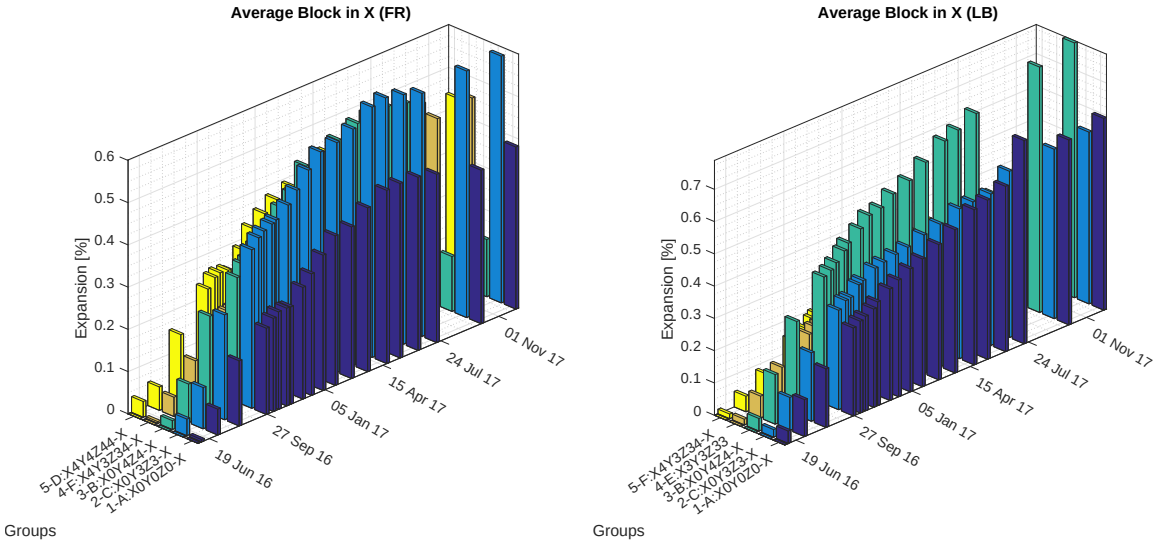

(a) Block Average in X Direction - Fog Room

(b) Block Average in X Direction - Lab

Figure 6.3: Average X direction block specimen response

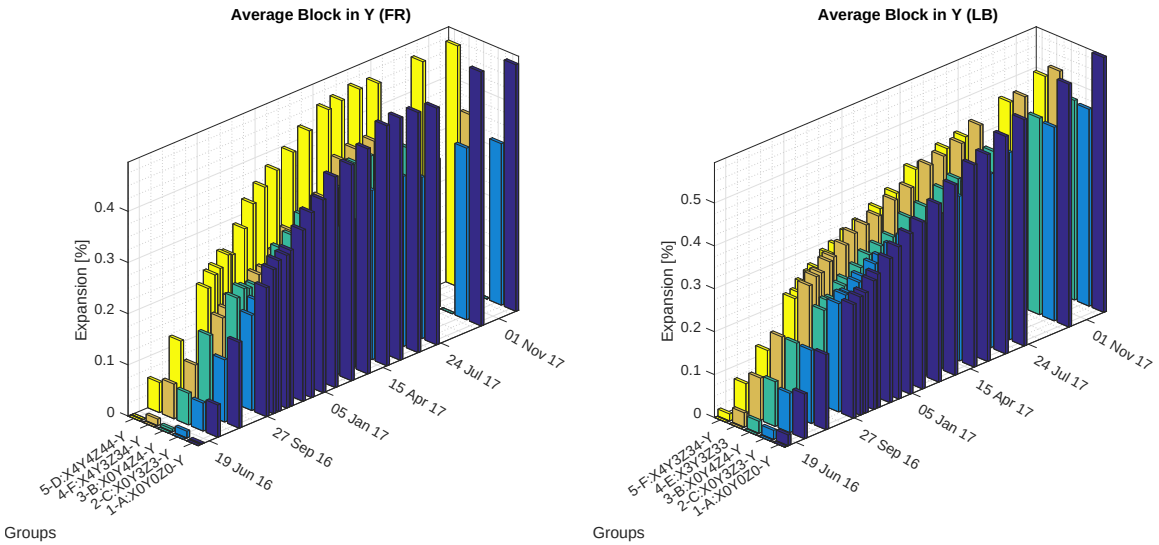

(a) Block Average in Y Direction - Fog Room

(b) Block Average in Y Direction - Lab

Figure 6.4: Average Y direction block specimen response

The volumetric expansion in Figure 6.6 is the sum of the expansion of all three directions. Ideally, all blocks would have identical volumetric expansion. However, the fact that the expansion are all similar to

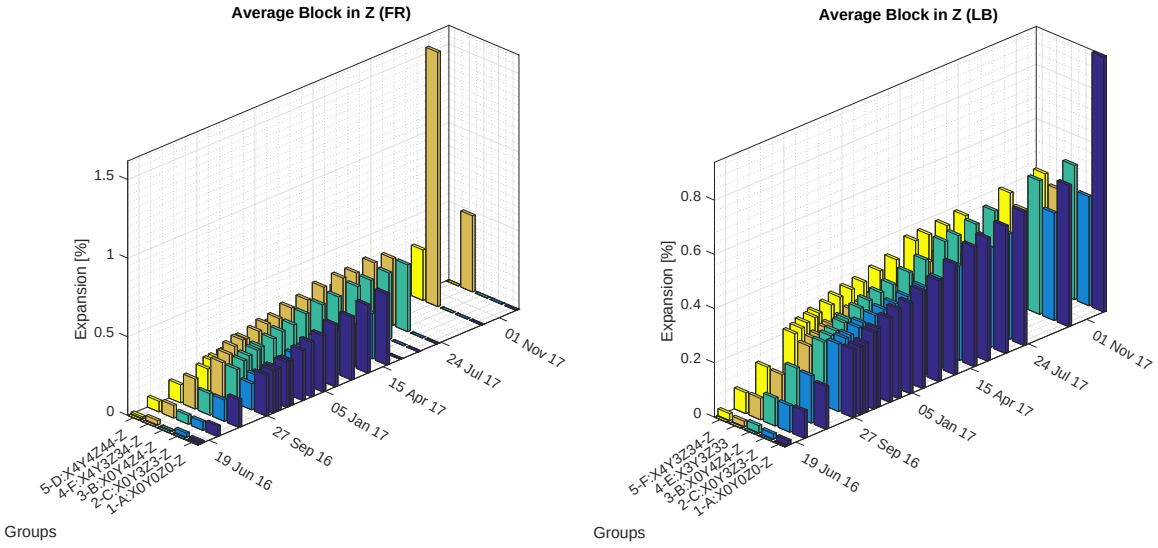

(a) Block Average in Z Direction - Fog Room

(b) Block Average in Z Direction - Lab

Figure 6.5: Average Z direction block specimen response

one another says that the expansion is proceeding normally.

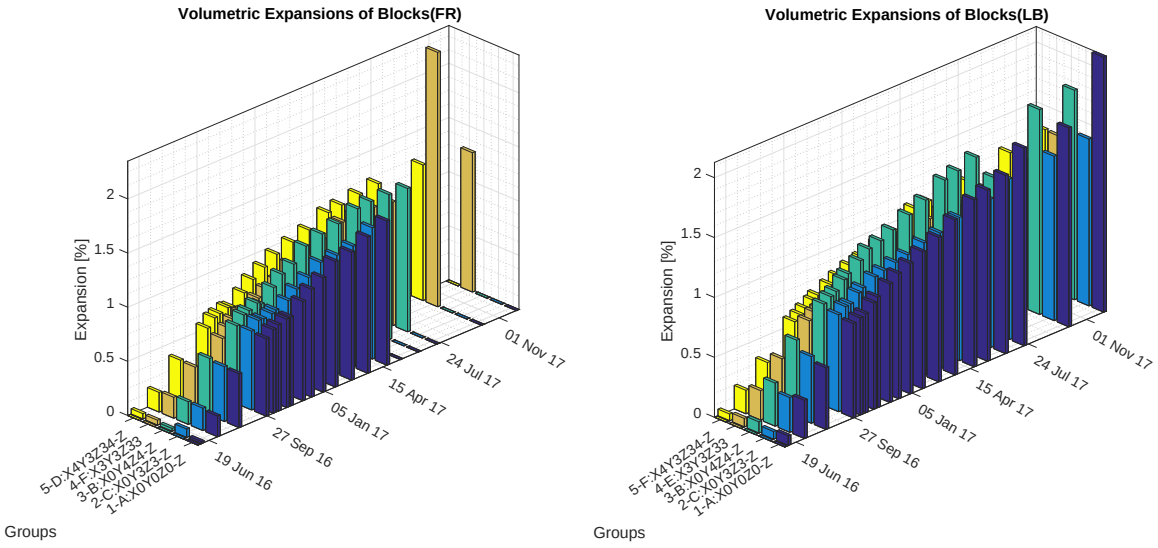

(a) in Fog Room

(b) in Lab

Figure 6.6: Volumetric block expansion

6.2.3 Shear Specimens

Figure 6.7 shows the averages of each measurement direction, with and without reinforcement. Direction 1 is the longitudinal direction on top of the specimen. Direction 2 is the transverse direction. Direction 3 and 4 are longitudinal on the side of the specimen. Direction 5 and 6 are the vertical direction on the side of the specimen.

Averages show that all directions are expanding at about the same rate. For the unreinforced specimens, longitudinal and transverse on the top of the specimen show similar and greatest expansion while the vertical and longitudinal on specimen side show similar expansion. For the reinforced, vertical side and transverse on specimen top show similar and greatest expansion. The longitudinal side has moderate expansion and the longitudinal top has very little expansion due to specimen cracking. While all results may not be exactly what is expected, the fact that the expansion trend is consistent across the entire project time frame says the data is reliable.

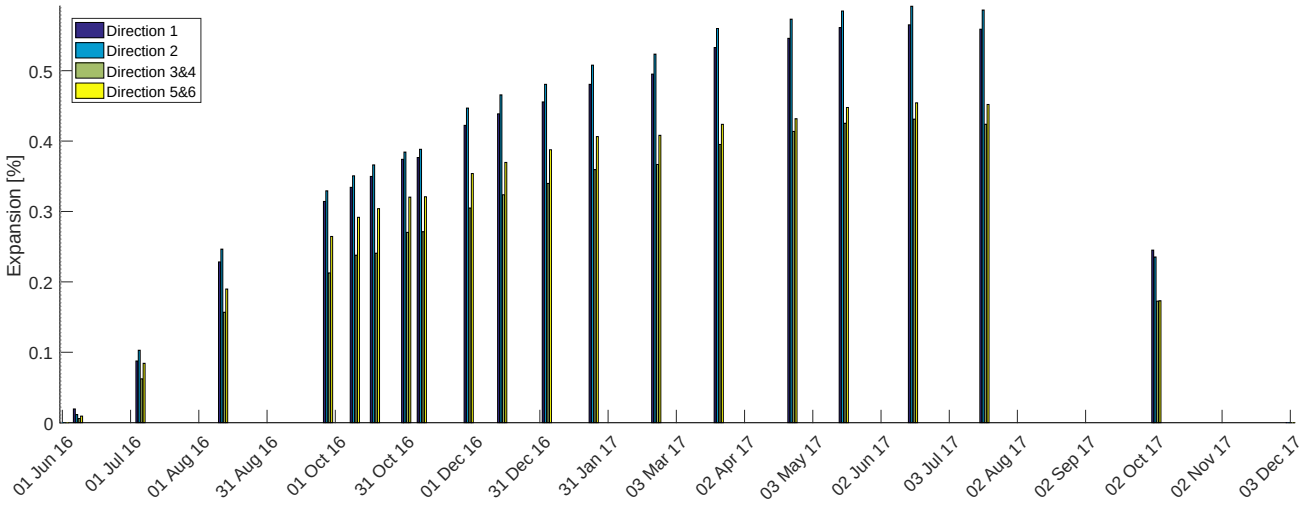

(a) Without Reinforcement

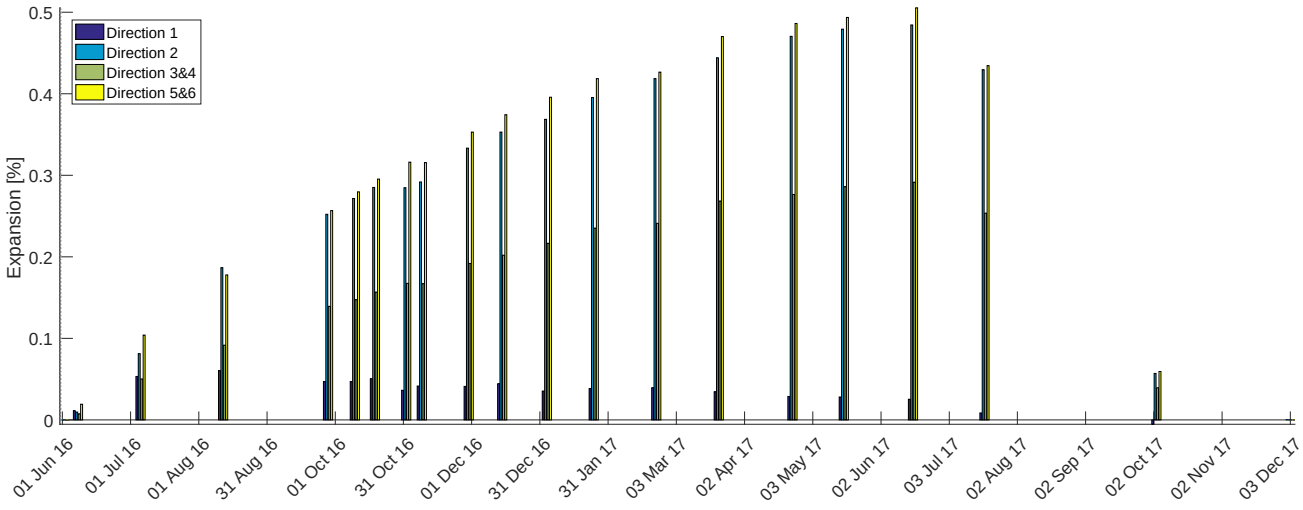

(b) With Reinforcement

Figure 6.7: Average shear specimen

6.3 Individual Specimen Expansions

In addition to the average expansion of the specimens, more detailed plots were created to identify specific trends and problematic data points.

6.3.1 Prism Specimens

Figure 6.8 and 6.9 show the expansion over time of the all the P14 and P16 prisms, respectively. Much information can be found in the legend of these plots.

- "M-1" refers to the batch number.
- "Reb" indicates if the specimen is reinforced or not.
- "1" stands for reinforced while "0" is unreinforced.
- "TG" indicates the temperature gauge ID number
- "SG" is the strain gauge ID number.
- "FR" or "Lab" designates the specimen is located in the fog room or lab

All other inform pertaining to line color, line type, or marker shape corresponds to the convention outlined in section 6.1.1.

While the plots are dense and somewhat difficult to read, general trends can be seen. Non-reinforced prisms are expanding at a greater rate than reinforced prisms and prisms in the fog room are expanding more than the prisms in the lab. Additionally, these plots allowed outliers due to misreading or datum discs detaching could easily be identified and corrected using the process outlined in Section 6.1.3.

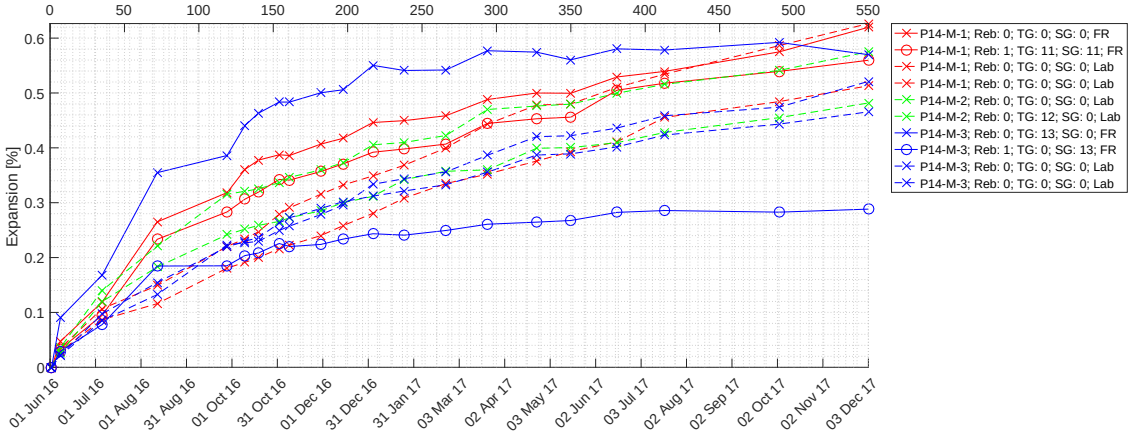

Figure 6.8: $6 \times 6 \times 14$ inch Prisms (P14)

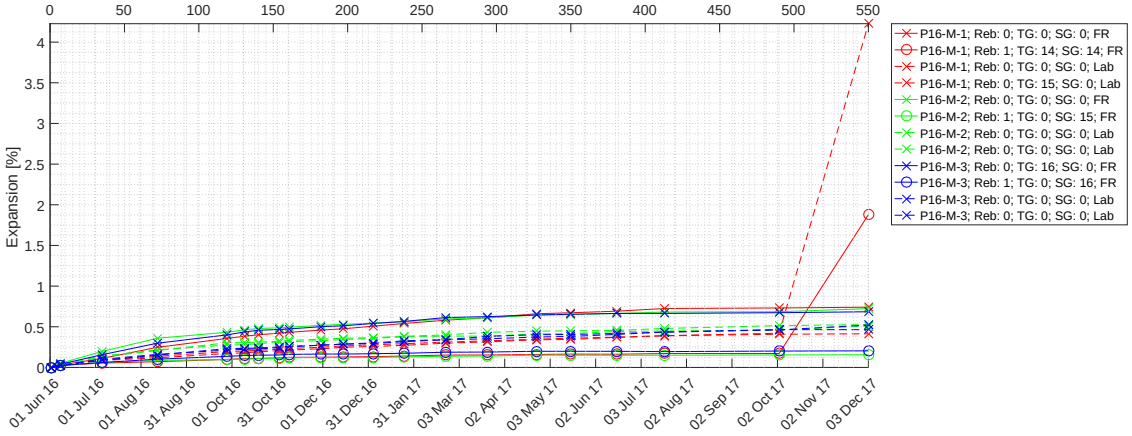

Figure 6.9: $4 \times 4 \times 16$ inch Prisms (P16)

6.3.2 Block Specimens

Figure 6.10 shows the expansion of all blocks, organized by axis. With more specimens, the graph becomes even more dense. Again, these plots ensure continued expansion is achieved and identify the outliers to be corrected. The legend provides the same information as explained in section 6.3.1 which the exception of "Reb". Instead of simply stating if the specimen is reinforced or not, the letter indicates the reinforcement type shown in figure 3.10.

To aggregate the expansion plots even more to see the expansion process on a specimen by specimen basis, the expansion of all three directions of an individual block is plotted. These plots show the effect of the reinforcement in each direction for an individual block. Only a representative sample of the plots are given here. For a complete set of the block expansion plots, see Appendix A.1.

6.3.3 Shear Specimen

As with the blocks, the shear specimens plots in Figure 6.12 are organized by measurement direction. Again, similar the blocks, each individual shear specimen is plotted with all directional measurements on one plot. For a complete set of the shear specimen expansion plots, see Appendix A.2. The plots for the non-reactive specimens may seem random and sporadic compared to the other plots but consulting the axes of these plots show the their expansion is very small compared to the other plots.

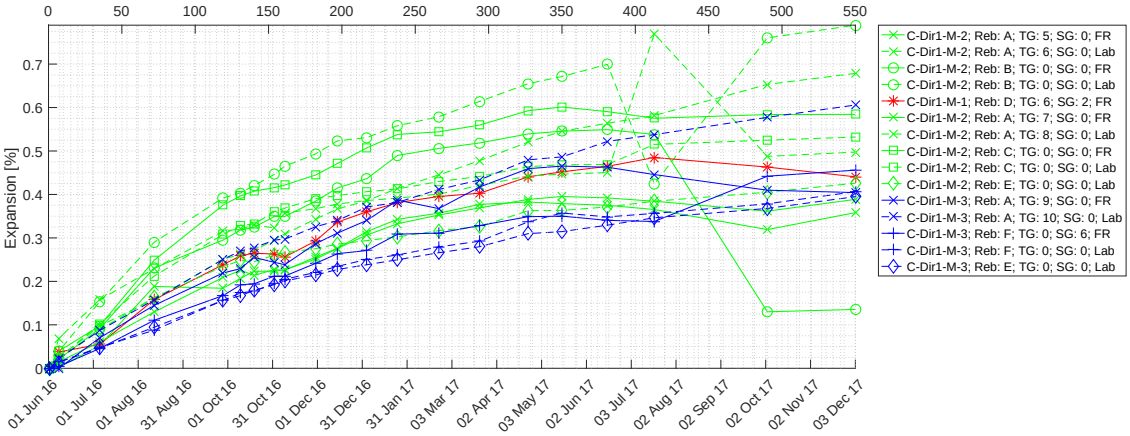

(a) X Direction

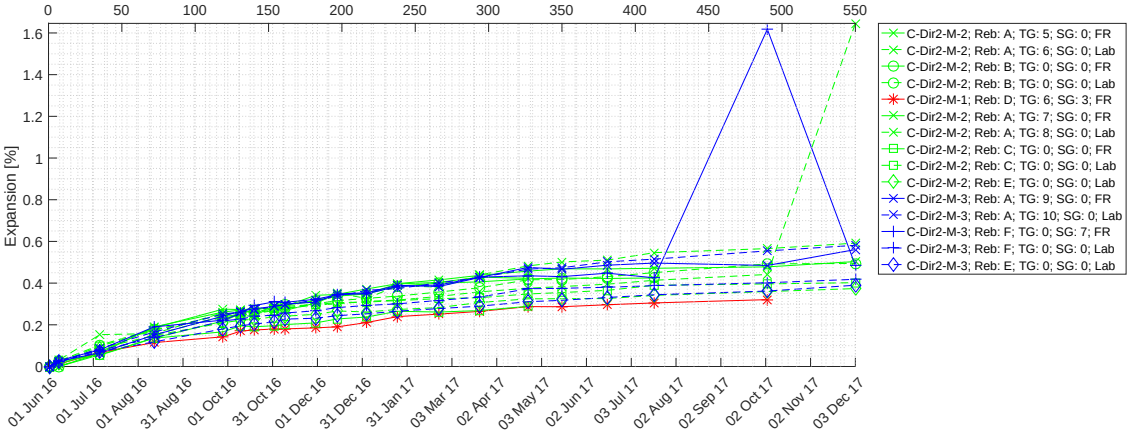

(b) Y Direction

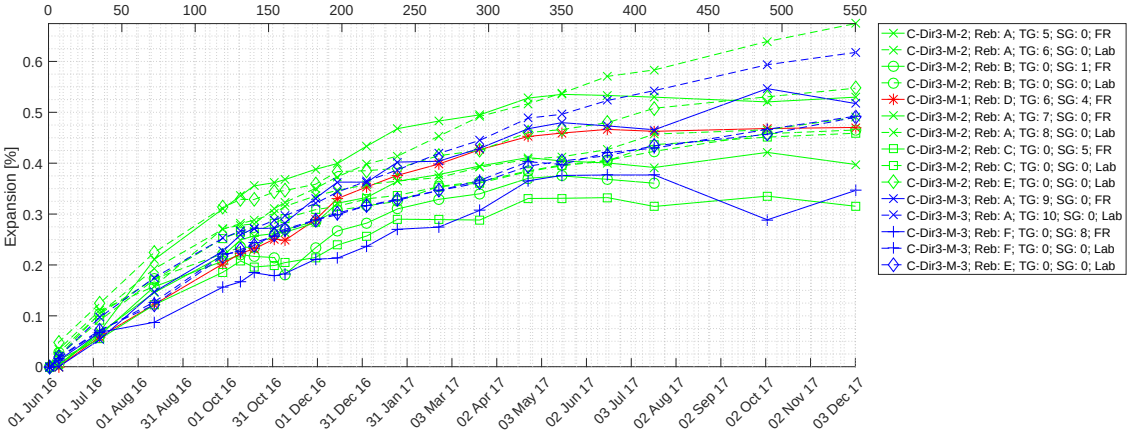

(c) Z Direction

Figure 6.10: Block specimen plotted by axis

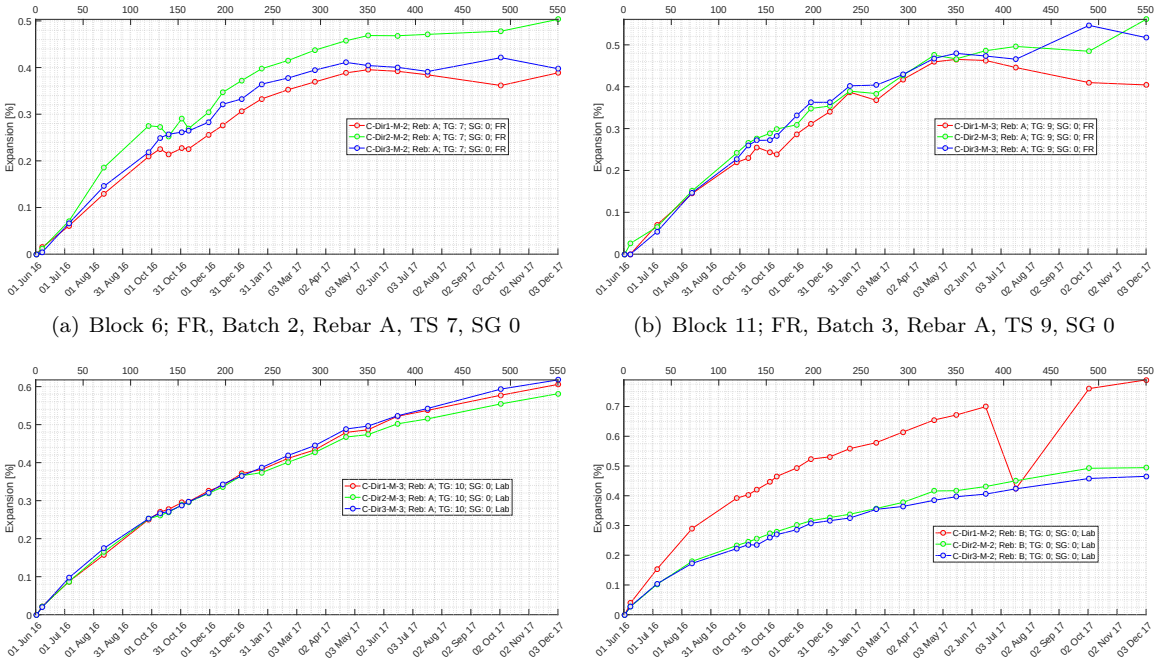

(a) Block 6; FR, Batch 2, Rebar A, TS 7, SG 0

(b) Block 11; FR, Batch 3, Rebar A, TS 9, SG 0

(c) Block 12; Lab, Batch 3, Rebar A, TS 10, SG 0

(d) Block 4; Lab, Batch 2, Rebar B, TS 0, SG 0

Figure 6.11: Individual block specimens

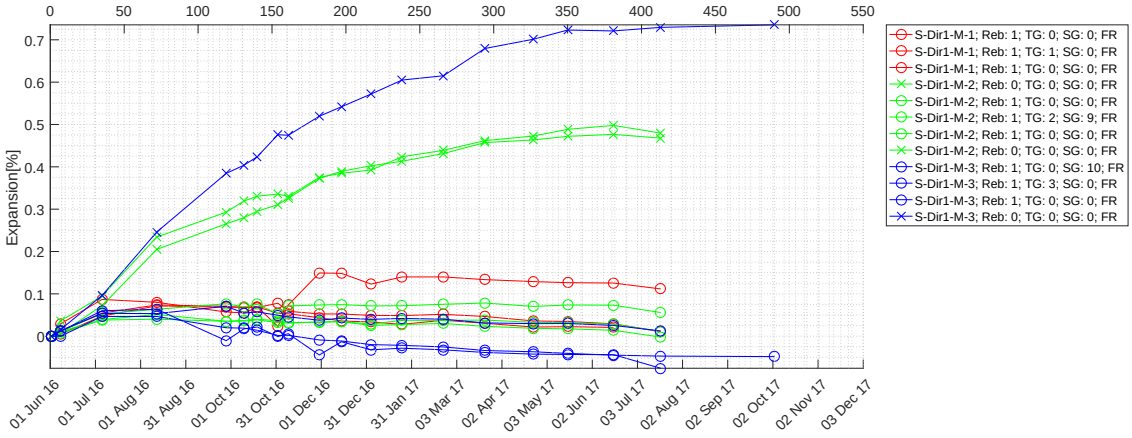

(a) Shear Direction 1

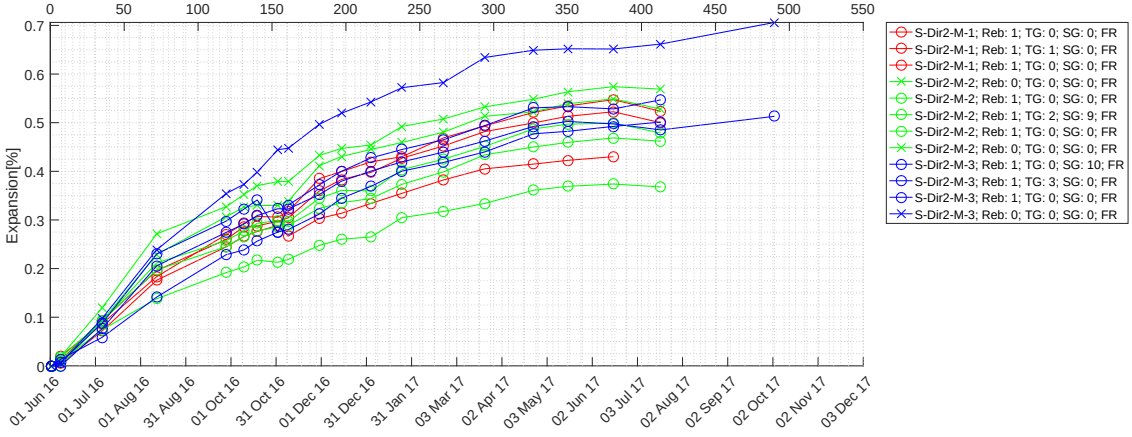

(b) Shear Direction 2

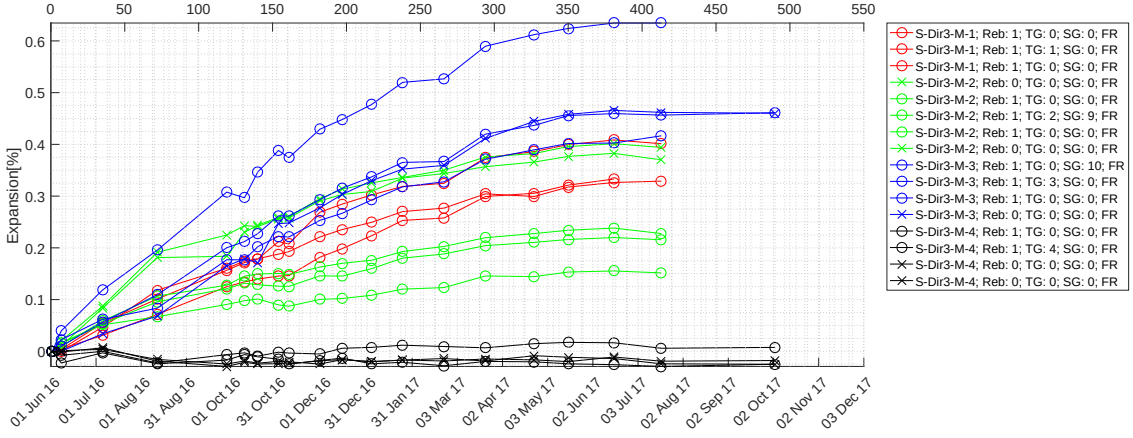

(c) Shear Direction 3

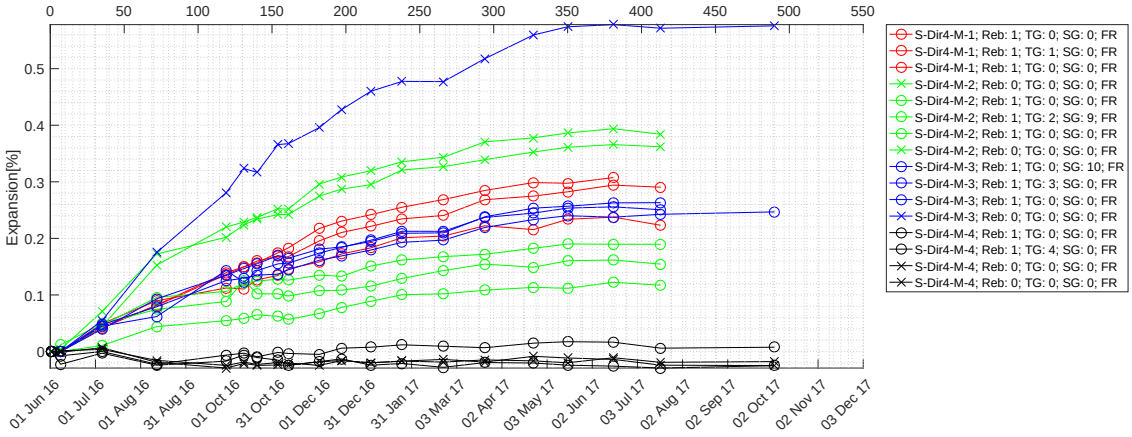

(a) Shear Direction 4

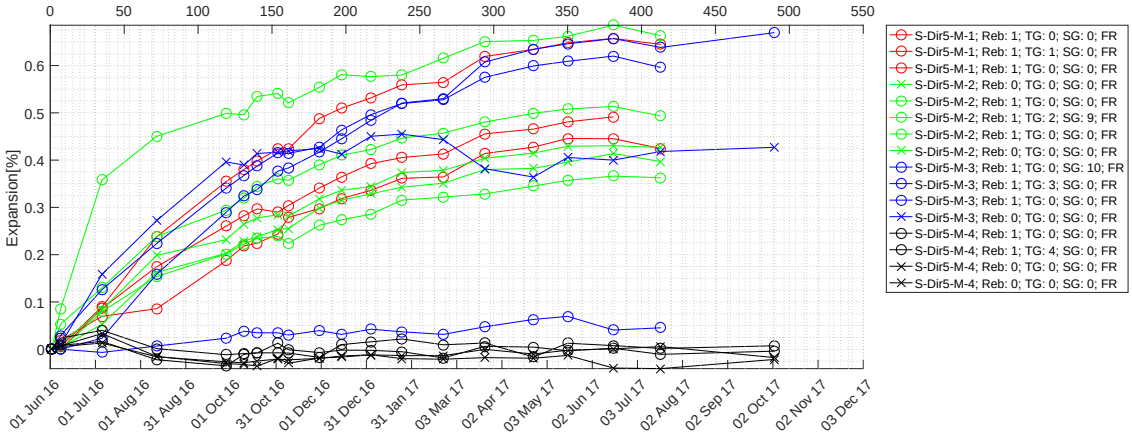

(b) Shear Direction 5

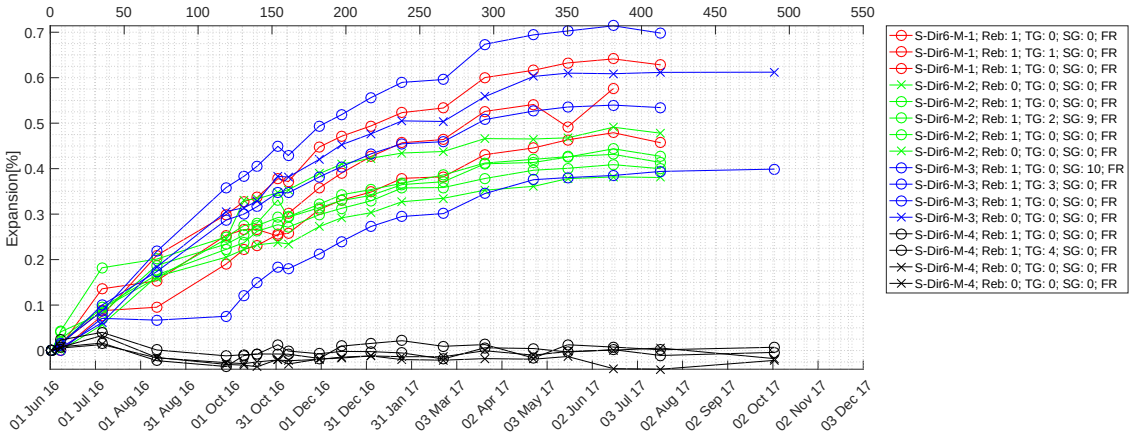

(c) Shear Direction 6

Figure 6.12: Shear specimen; directional response

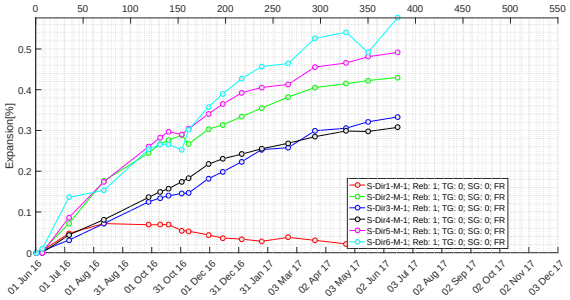

(d) Specimen 1; Reactive, Mix 1, Rebar

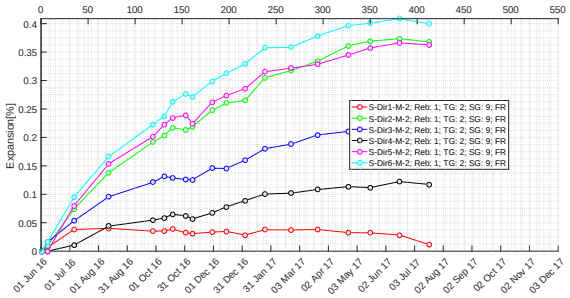

(e) Specimen 6; Reactive, Mix 2, Rebar, TG 2, SG 9

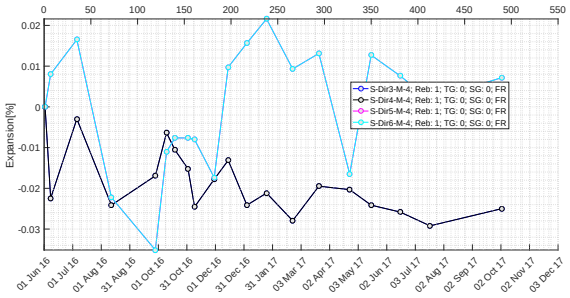

(f) Specimen 13; Non-Reactive, Mix 4, Rebar

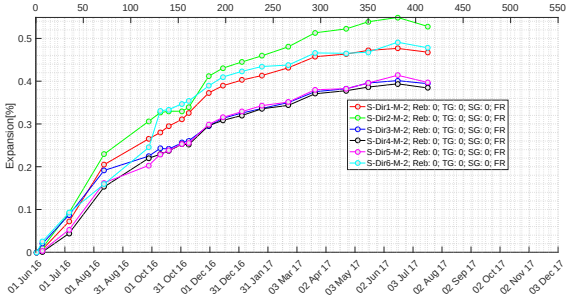

(g) Specimen 4; Reactive, Mix 2, No Rebar

Figure 6.13: Shear specimens

6.4 Data Fitting to Larive's Expansion Equation

Predictive equations for ASR expansion proposed by Larive (1998) and Saouma and Perotti (2006) outlined in Section 2.5 are given using the expansion Equation. Expansion data collected from the unreinforced P14 and P16 prisms in the fog room is compared to the predicted results using the equations to determine if there is a similarity between the two.

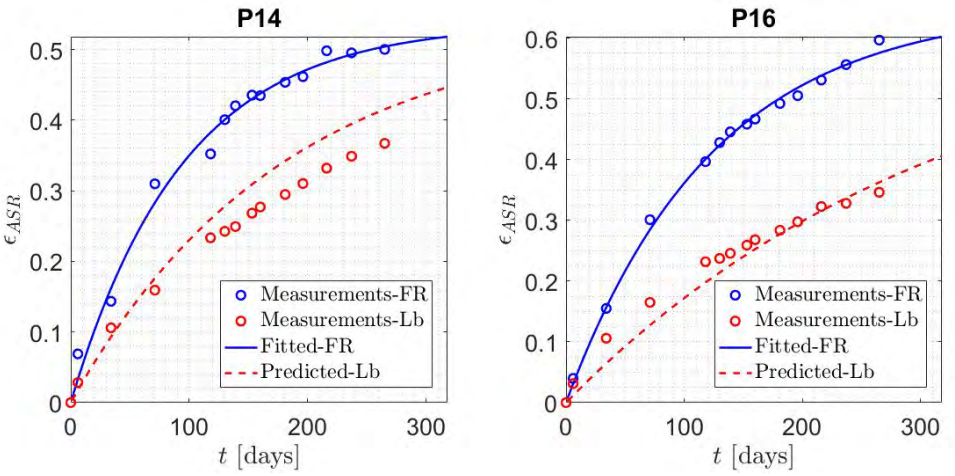

(a) Shear Direction 6

Figure 6.14: Results of fitting predictive equations to expansion data

The process of developing the predictive curves begins with expansion data for the unreinforced P14 and P16 prisms in the fog room fitted using Larive sigmoid equation where the associated τ_l and τ_c values are estimated at the fog room temperature. Next, Equation 2.1 is used to convert the expansion data at the fog room temperature to the lab temperature which accounts for the U_l and U_c effects. An iterative procedure is followed (starting with the universal values) to find the most appropriate U_l and U_c in which the converted (dashed) curve matches with actual lab data. Understanding that a predictive model and actual results will never be exactly the same, the results graphs show that the actual data is relatively close to the predicted. This indicates that the expansion data of the prisms provide further validation to the predictive expansion equations.

This page intentionally left blank.

7 Crack Index Measurements

About 250 crack indexes were recorded on wet specimens 520 days after casting. Only cubes and prisms were targeted, as by then all shear specimens were tested.

14x14x14 blocks, with characteristics shown in Table 5.2 were investigated. Measurements were taken on three orthogonal faces, Fig. 3.11, and on each one two horizontal and two vertical readings were taken, Fig. 7.1.

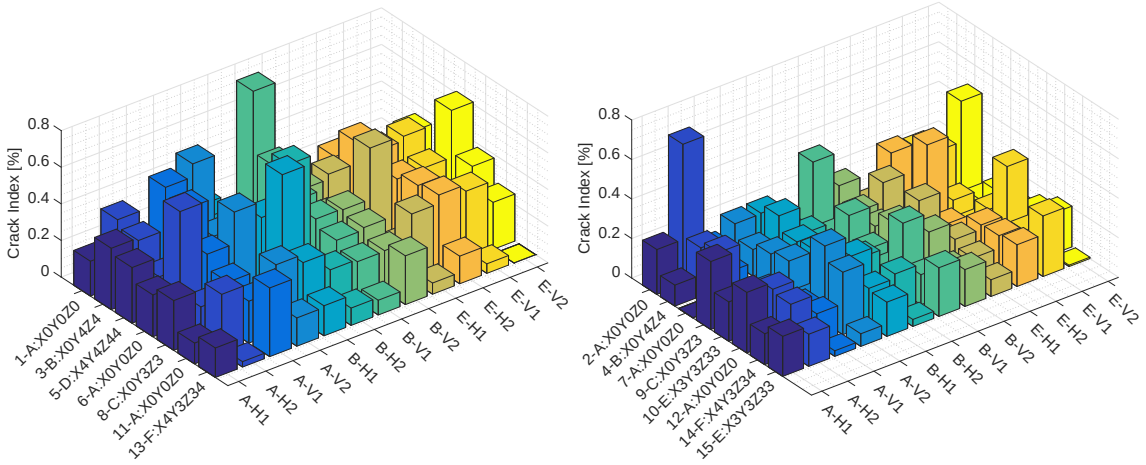

(a) Fogg Room (90°F)

(b) Laboratory Room (70°F)

Figure 7.1: Crack Indexes for Cubes

Likewise, CI readings were taken for the 4x4x16 inch and 6x6x14 inches prisms characterized in Tables 3.5 and 3.6 respectively. For each prisms, three readings were taken, Fig. 7.2 and 7.3.

Whereas a wealth of information is "hidden" in those plots (specially when correlated with the corresponding expansion and reinforcement/temperature information), time and budgetary constrained prevented such an exercise[1].

Suffice it to say that the crack indexes are around 0.5% and seem to correlate well with the expansion measurements.

[1]The entire scope of this report was not part of the proposal.

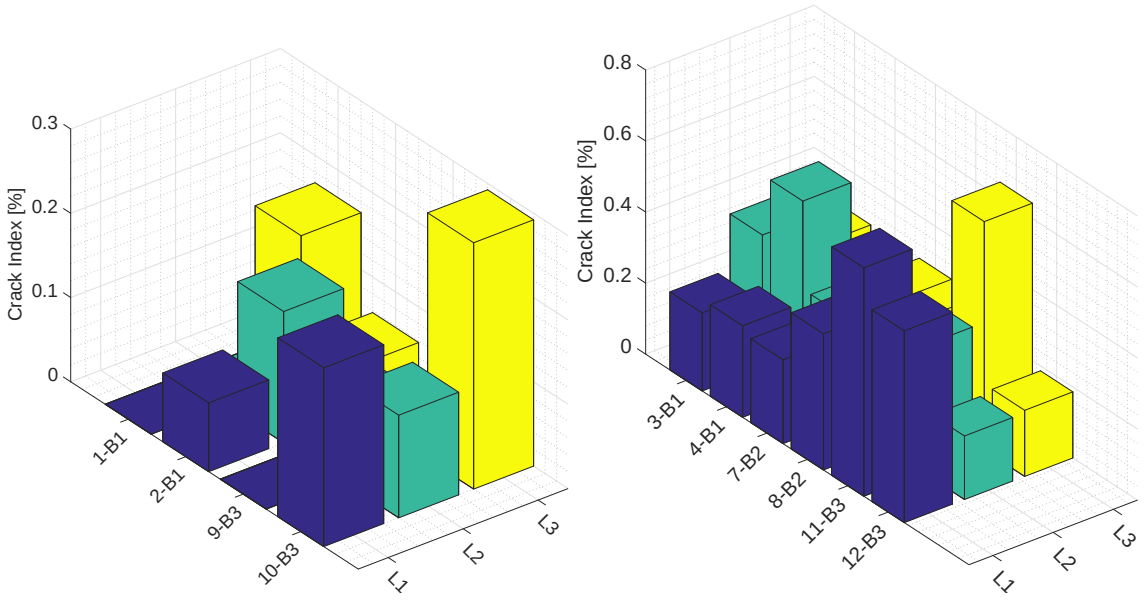

(a) Fogg Room (90°F) (b) Laboratory Room (70°F)

Figure 7.2: Crack Indexes for P14 Prisms (6x6x14 inches)

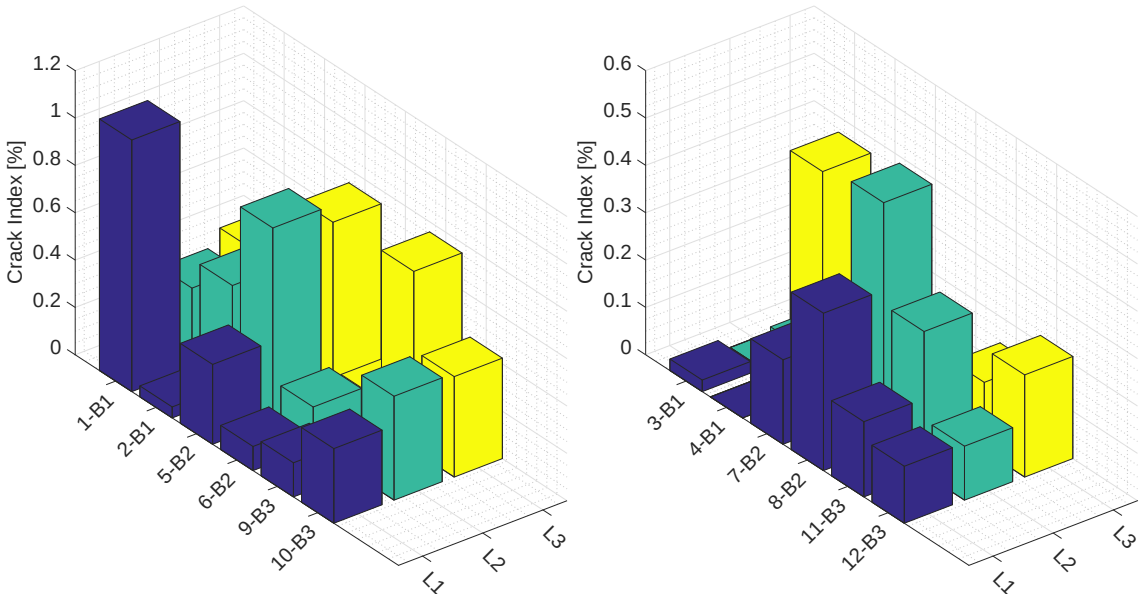

(a) Fogg Room (90°F) (b) Laboratory Room (70°F)

Figure 7.3: Crack Indexes for P16 Prisms (4x4x16 inches)

8 Discussion

needs editing

8.1 Observations July 2017

Close analysis of the pictures, indicate that the Akali-silica reaction has contributed to concrete cracking.

Small cracks are visible on most specimens with the exception of the control specimens in the fog room. In as much as possible, cracks were highlighted in red (by editing the image).

The cracks range from small and acute as seen in the C-14, P-14 and P-16 specimens to spread-out and clear as seen in most of the shear specimens (S-1,S-2, etc.).

Generally, there were expansion increases in almost all direction (all positions) on almost all of the concrete specimen. If there was no expansion in a certain direction, the cause was likely to be the presence of reinforcement resulting in a redirection of the volumetric expansion.

8.2 Prism and Block Comparison

Figure 8.1 is a direct comparison of all unreinforced prisms and blocks in the fog room. Again, since a trend is followed through the experiment, the data is considered reliable.

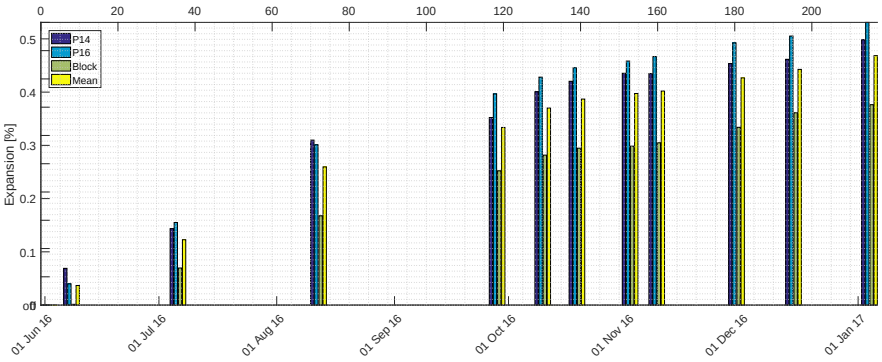

Figure 8.1: Comparison of fog room specimens with no reinforcement

8.3 Reinforcement Effects

To analyze the potential reinforcement effects on ASR expansion, the expansion of an unreinforced specimen (shear, block, or prism) is compared to its reinforced counterpart and plotted. The unreinforced expansion is the independent reference variable and plotted on the x-axis. The reinforced specimen is then considered to be the independent variable and plotted on the y-axis. The graph shows a dotted line along the equation y = x and a line with a linear fit to the data set along with its equation and the y intercept set to zero. A linear fit line will allow a direct comparison to the dependent variable. A line with a slope less than one indicates less expansion than the reference specimen and conversely a slope greater than one indicates greater expansion.

8.3.1 Prisms

Looking at the results of the prism expansion data in Fig. 8.2, there is an obvious correlation between the reinforcement of the prism and resulting expansion. The presence of reinforcement in both prism sizes show expansion inhibition when compared to their unreinforced counterpart. Additionally, there is a trend between the reinforcement ratio and the amount of expansion in each prism size. As the ratio increase, the expansion decreases. From these specimens, it is reasonable to conclude that the presence of the axial reinforcement is stifling the expansion. This does not suggest that the rebar inhibits the reaction occurring in the concrete. Rather the steel rebar absorbs some of the strain that would normally be transferred to the unreinforced concrete.

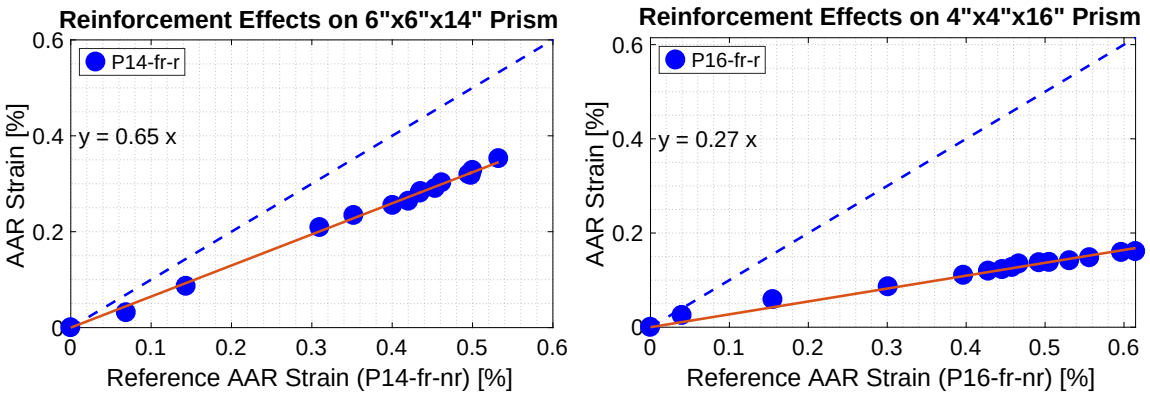

Figure 8.2: Expansion of Prisms in Fog Room

8.3.2 Shear Specimen

Similar to the prisms, Figure 8.3 shows the reinforced shear specimens have less expansion than their unreinforced counterparts. In each of the four directions (longitudinal top, longitudinal side, vertical, and transverse), as the reinforcement ratio increases, the expansion decreases. This again supports the hypothesis outlined at the beginning of the chapter. The measurement that is outside of the trend is in the longitudinal direction on top of the specimen. This is likely due to the cracking observed in the shear specimens as seen in Fig. 8.4

Figures 8.5 and 8.6 show a schematic explaining why this cracking is occurring. The tack weld connecting

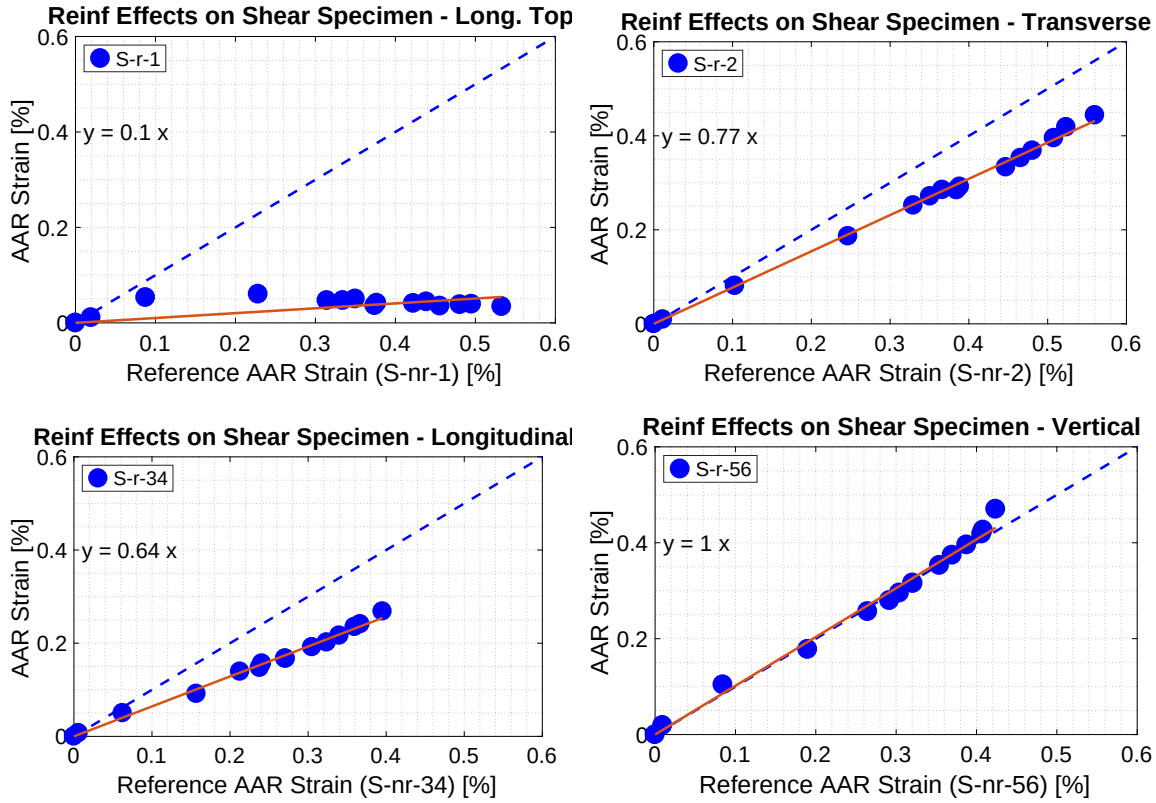

Figure 8.3: Expansion of Shear Specimens in Fog Room

Figure 8.4: Cracking in Shear Specimens

the rebar to steel end plates has become debonded due to tension caused by ASR expansion. A piece of paper is able to be slid between the end plates and the concrete past the point where the reinforcement should be connected to the plate. As the concrete expands longitudinally and presses on the end plates, the rebar is constrained by the concrete forming tension at the weld. Once that weld is broken, the rebar keeps the top portion of concrete in place while the middle of the specimen continues to expand, creating a zone of tension in the specimen. Since this zone is unreinforced, cracking occurs. To further support that the presence of reinforcement is the main contribution to the cracking, the unreinforced specimens show no sign of cracking.

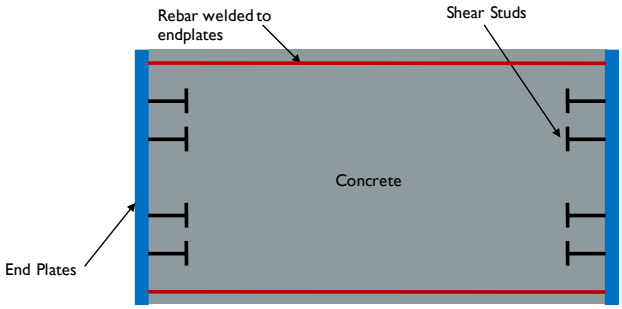

Figure 8.5: Before Expansion

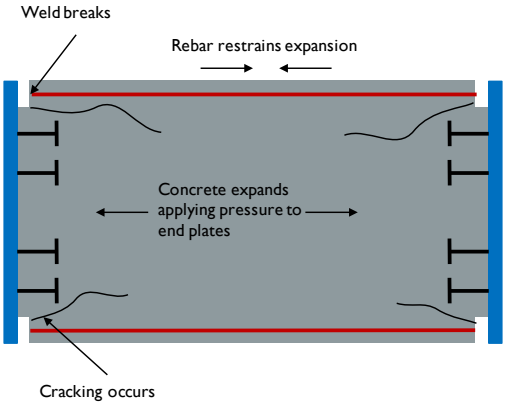

Figure 8.6: After Expansion

8.3.3 Blocks

Most of the blocks in the fog room continue to follow the trend of the reinforced specimens showing less expansion than the unreinforced specimens. However, some of the reinforced directions are showing the same or greater expansion than the unreinforced specimens. This can be seen in the X direction for the F reinforced blocks (Fig. 8.7(a)) or B and F reinforcements for the Z direction (Fig. 8.7(c)). It is more difficult to see that the increase of the reinforcement ratio will decrease the amount of expansion. This can especially be seen in the fog room blocks in the Z Direction. Fig. 8.7(c) shows specimens that are lightly reinforced (B reinforcement) and heavily reinforced (F reinforcement) have similar expansion to the unreinforced blocks. The same graph shows another light and heavy reinforcement specimen (C and D reinforcement, respectively) that have significantly less expansion. It was briefly considered that there may be a contribution by the fact that the Z direction is the direction in which the concrete was poured, but there is not significant evidence from the data that supports this theory.

The results of the blocks in the lab are closer to following the expected trend, though not in every instance. In the X direction (Figure 8.8(a)), the reinforced directions expand less the reference block while the unreinforced directions expand more. The latter is evidence of expansion transfer which will be discussed shortly.

The Y direction (Figure 8.8(b)), shows similar or less expansion than the reference block. For the Y direction, the blocks that are more lightly reinforced (with #3 bars) have greater expansion than those more heavily reinforced (with #4 bars). However, it would be expected that the lightly reinforced blocks would

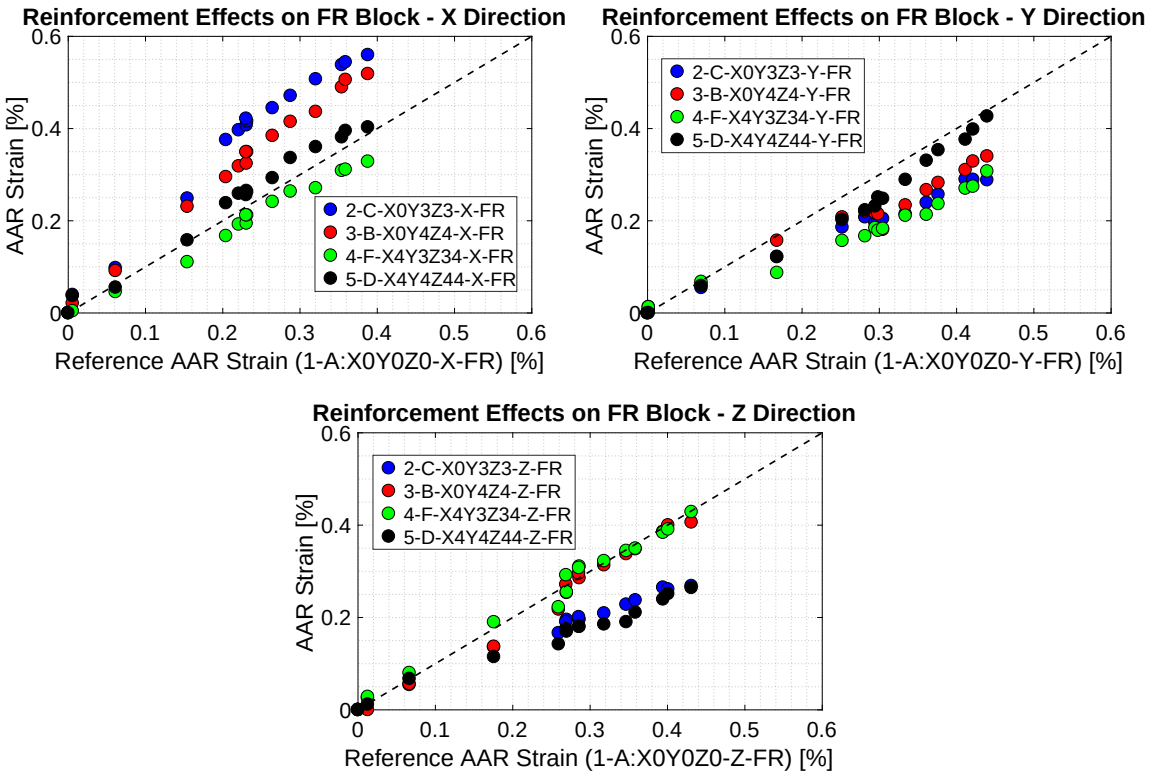

Figure 8.7: Expansion of Blocks in Fog Room

still have less expansion than the unreinforced blocks. Measurements at lower expansion levels have the same expansion as the reference block while greater expansion levels have a separation between the two. This could be that it took time for the concrete to expand enough to engage the rebar. However, there is little evidence of this in other directions of either the fog room or the lab.

The Z direction (Figure 8.8(c)) also has some blocks with similar expansion to the unreinforced reference. Following the hypothesis, it would be expected that all blocks would have less reinforcement than the unreinforced block. However, this does follow the expectation that the blocks with the larger reinforcement ratio are showing less expansion. More results and discussion on the effects of reinforcement ratio are in Section 8.3.4

As mentioned previously both the fog room and lab blocks show signs of "expansion transfer" in the X direction (Fig. 8.7(a) and 8.8(a), respectively) in blocks with biaxial reinforcement (B and C reinforcement). Previous research on the effects of confinement on ASR expansion cite a phenomenon that when concrete with ASR expansion is confined in two direction, then there will be an increase of expansion in the unreinforced direction greater than if there was no confinement at all. The biaxial blocks with greater expansion in the X directions than the unreinforced blocks seem to be following this trend.

8.3.4 Effects of Reinforcement Ratio on Expansion

Previous studies completed by (Musaoglu, Turanli, and Saritas, 2014) show that reinforcement ratios have a distinct effect on expansion. As the reinforcement ratio increases, the expansion decreases. This can be seen in the results of the reinforcement effects on the prisms in Figure 8.2. The reinforcement ratio of P14

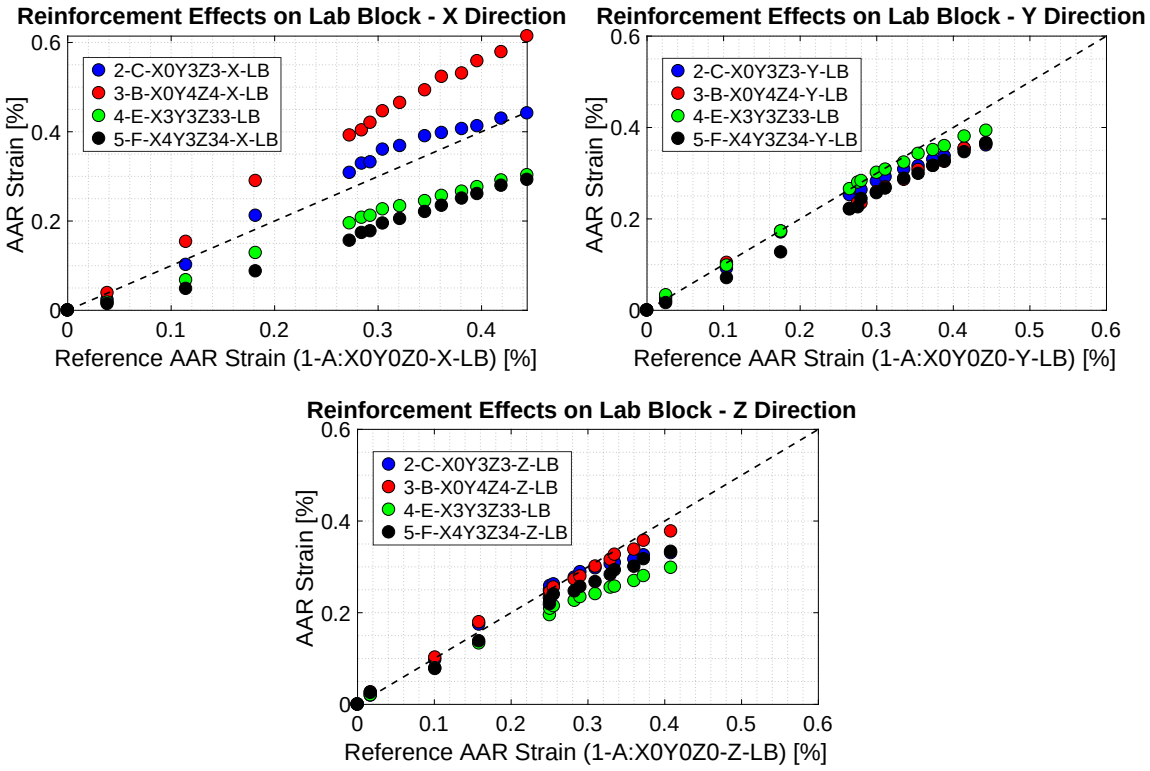

Figure 8.8: Expansion of Blocks in Lab

prisms is 1.53% which has an expansion rate less than P16 which has a reinforcement ratio of 2.75%. These results correlate well with what is expected.

However, the expansion of the blocks do not show the clear correlation between reinforcement ratio and expansion that the prisms do. Figure 8.10 compares the expansion of each direction of each reinforcement type in either the fog room or lab. All expansions are normalized to the x direction. The legend gives the reinforcement ratio (in percent) for each direction.

It would be expected that for reinforcement type A (unreinforced), expansion would be the same for all directions in either the fog room or lab. However, Figure 8.9(a) shows Y and Z expansion is significantly greater than the X in the fog room but Figure 8.9(b) shows the expansion is less in the lab.

Blocks with reinforcement B (Figure 8.9(c) and 8.9(d)) and C (Figure 8.9(e) and 8.9(f)) show expected correlation between the reinforcement ratio and the expansion. These blocks have biaxial reinforcement and the expansion transfer mentioned previously is the reason for good results.

The block with reinforcement D in Figure 8.9(g) also shows good results. Rho in the X and Y direction are equal and are showing similar expansions while the Z direction with greater reinforcement ratio has less expansion. While the two directions do not initially match, as time goes on the expansions match one another.

Block E reinforcement in Figure 8.9(h) show results that do not match predictions. The X and Z directions have matching expansions while having mismatching reinforcement ratios. The Y direction has significantly greater expansion than the other two directions while having the same reinforcement ratio as the X direction.

Blocks containing F reinforcement (Figures 8.10(a) and 8.10(b)) have the most confusing results of all the blocks. In the fog room, the Z direction has the greatest expansion with the greatest reinforcement

ratio while the Y direction has both the least expansion and reinforcement ratio. This is the opposite of what would be expected. Furthermore, the lab block has the directions with both the least and greatest reinforcement ratios have similar expansions.

Many of the results contradict the predictive results. There were many theories as to why this may be. First, it was thought that the pouring direction may play a role in the results. All block specimens were poured in the Z direction. However, there is no indication from the results that the Z direction showing greater or less expansion in all cases. It was thought that the batch from which the concrete came from would play an effect but discussion in Section 8.7 shows that the only substantial differences in batches are in the shear specimens.

Another theory that was proposed is that the outward expansion of the concrete debonded from the reinforcement making the reinforced blocks expand as if they were essentially unreinforced. This debonding would create additional channels for alkali transfer throughout the specimen and expose more surface area of the aggregate which would increase the potential for additional swelling.

Previous research referenced in 2.4 looking at the effects of reinforcement on expansion only look use specimens that have a large length to width ratio. Studies using blocks studying the effects of temperature and only used unreinforced specimens. Since this is a unique study of reinforcement effects on expansion, it could be that the correlation between reinforcement ratios on expansion in three dimensions is complicated and requires the consideration of more factors than simply the reinforcement ratios. Additionally, only 15 blocks were cast with 6 different reinforcement configurations in two different temperature settings. Additionally, half the blocks were wetted while the others were submerged. There may not be enough specimens and too many contributing variables to easily make any definitive conclusions about the reinforcement in these blocks.

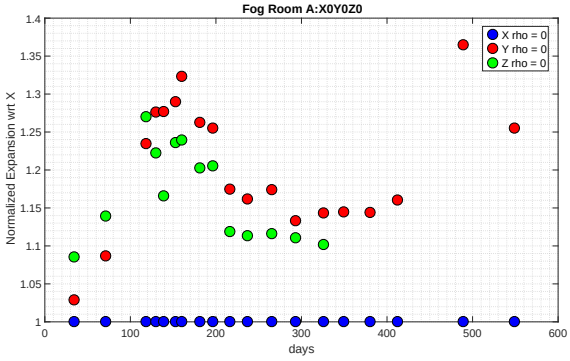

(a) A Reinforcement, Fog Room

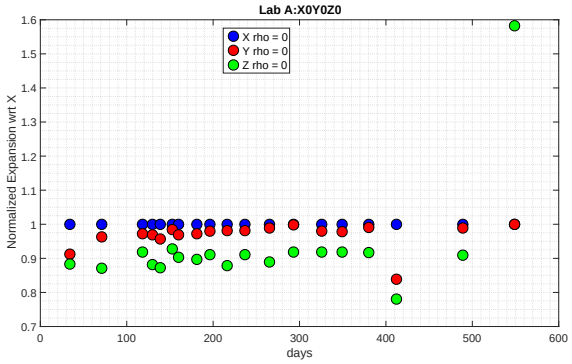

(b) A Reinforcement, Lab

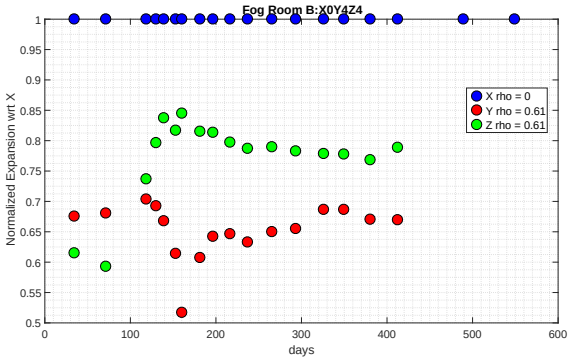

(c) B Reinforcement, Fog Room

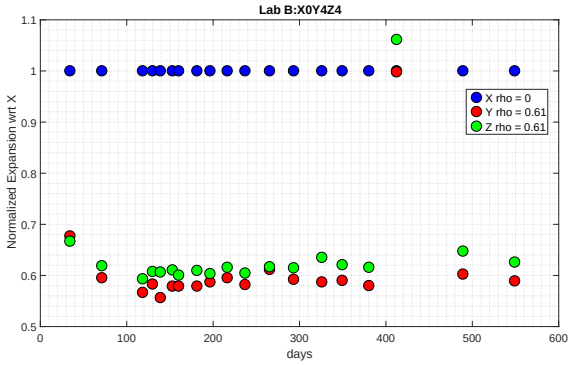

(d) B Reinforcement, Lab

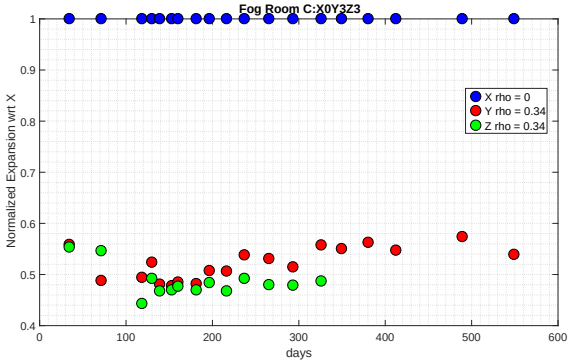

(e) C Reinforcement, Fog Room

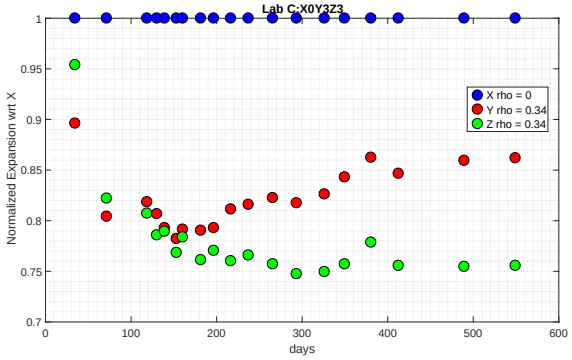

(f) C Reinforcement, Lab

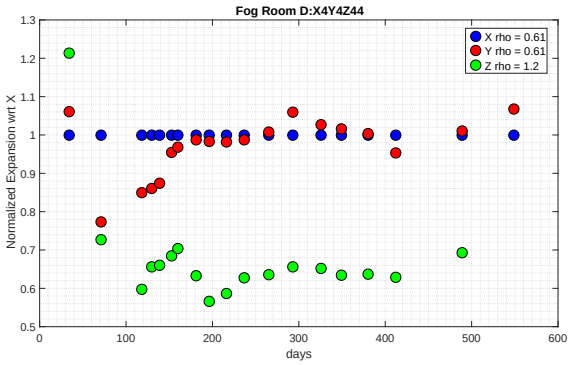

(g) D Reinforcement, Fog Room

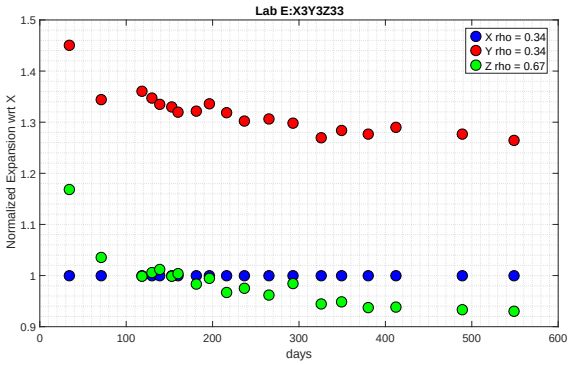

(h) E Reinforcement, Lab

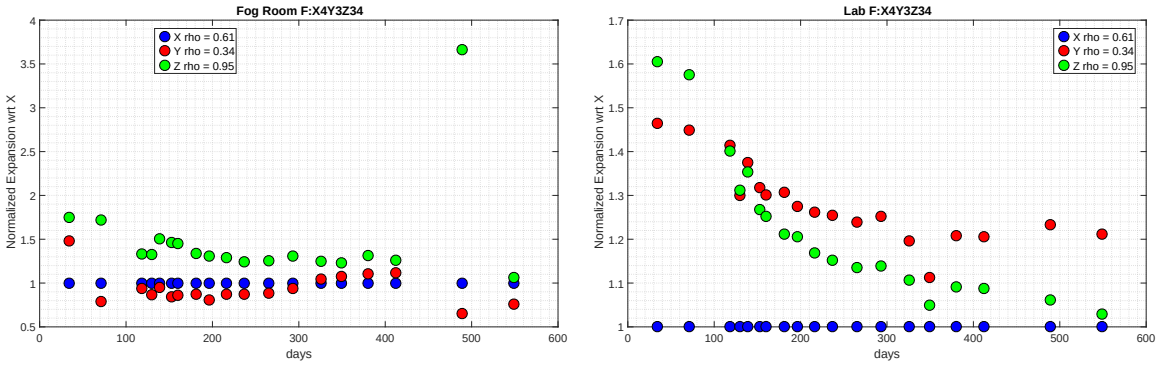

(a) F Reinforcement, Fog Room

(b) F Reinforcement, Lab

Figure 8.10: Steel to Concrete Ratio (Rho) for Blocks

8.4 Temperature Effects

It is hypothesized that greater expansion will be observed In specimens stored at high heat in the fog room than those stored at ambient temperatures in the lab. Lindgård et al. (2012) observes that as temperature increases, the reaction rate accelerates because the solubility of SiO_2 is greater at higher temperatures. This forms a greater amount of gel and produces higher expansion in the concrete.

To determine the effects of temperature on ASR expansion, specimens are compared to their identical counterparts (same size and reinforcement) in the lab. No shear specimens are included in this analysis since there are no shear specimens in the lab. The plots below, measurements from specimens in the fog room are the dependent variable on the x-axis and lab specimen measurements are on the y-axis as the independent variable. As with the reinforcement effects, a linear fit line is applied to the data and a y = x dashed line is plotted. Any linear fit line with a slope less than one shows less expansion in the lab while a line greater indicates greater expansion. Plots are created in such a way that the expected result will fall below the dashed line.

8.4.1 Prisms

Unreinforced prisms of both sizes are showing a definitive decrease of expansion as a results of temperature differences. Figure 8.11 shows lab P14 prisms have about 65% expansion of the fog room prisms. P16 prisms in the lab have an average 58% expansion of the fog room counterparts.

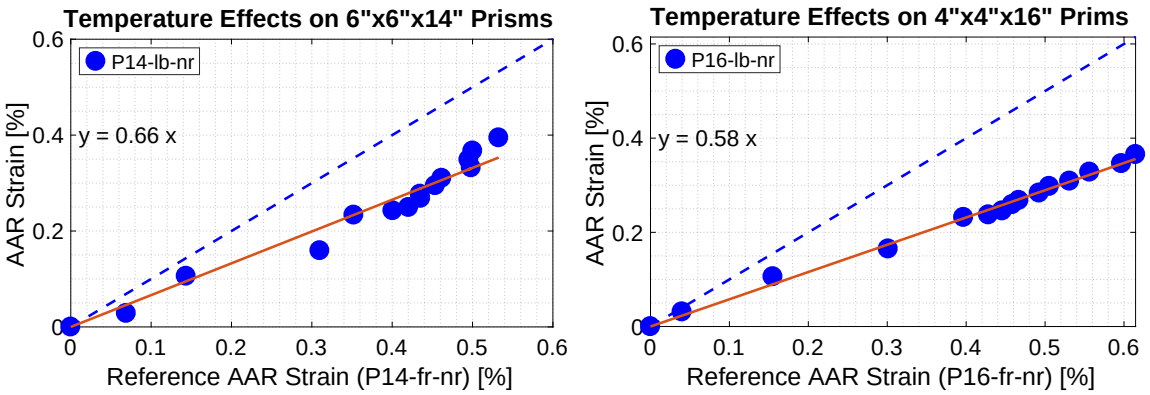

Figure 8.11: Effect of Temperature on Prisms

8.4.2 Blocks

The temperature effects on ASR expansion are not clear in the blocks. Most of the specimens in the lab are showing either similar (within 10%) or greater expansion than their counterparts in the fog room, Figures 8.12 to 8.15. The least expanded blocks show expansion in the lab that is 82% of the fog room block. This is significantly greater than the lab prism with the greatest expansion showing only 65% of the fog room prism.

For the unreinforced blocks, lab blocks have similar (within 5%) or greater expansion than fog room blocks in all three directions. The B reinforcement lab blocks have similar (within 6%) or greater expansion than fog room blocks in all three directions. C reinforcement lab blocks have 30% greater expansion than

fog room blocks in Y & Z Direction while the X Direction expansion in lab is 82% of fog room expansion. Lab blocks with F reinfocement have 30% greater expansion than fog room blocks in Y Direction. X & Z direction expansion in the lab is less than fog room expansion.

There is no discernible trend based on reinforcement ratio or pouring direction that can suggest what would be causing this to occur. It may be caused by the blocks in the lab are submerged in NaOH while the blocks in the fog room are covered in burlap and wetted. Submersion could provide more alkalinity to the blocks and promote greater expansion. Evidence to support this is that the prisms, which are submerged in both the lab and fog room, follow the expected temperature effects.

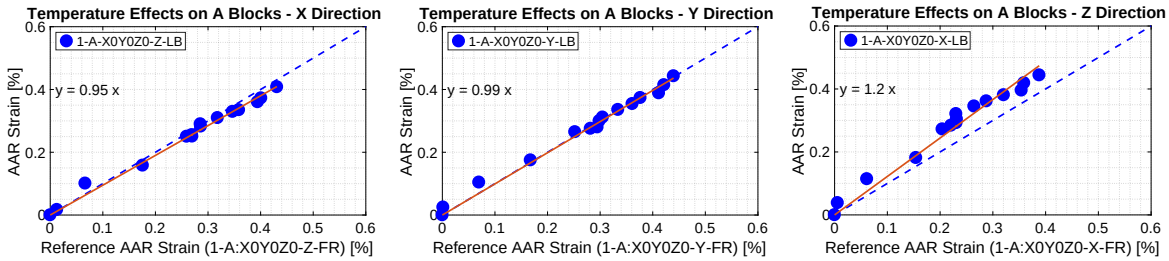

Figure 8.12: Effect of Temperature on Block A

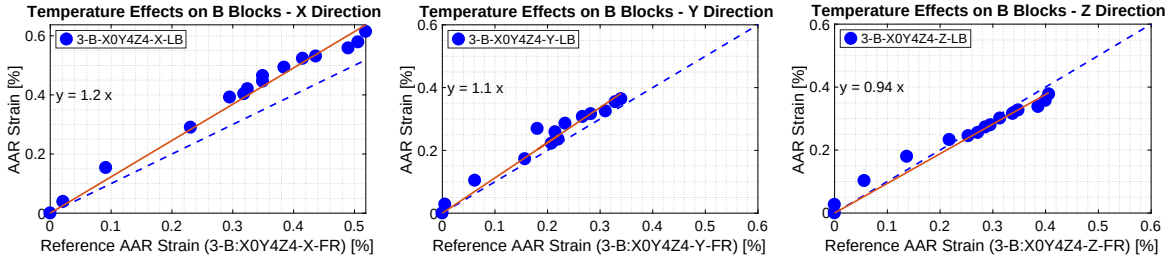

Figure 8.13: Effect of Temperature on Block B

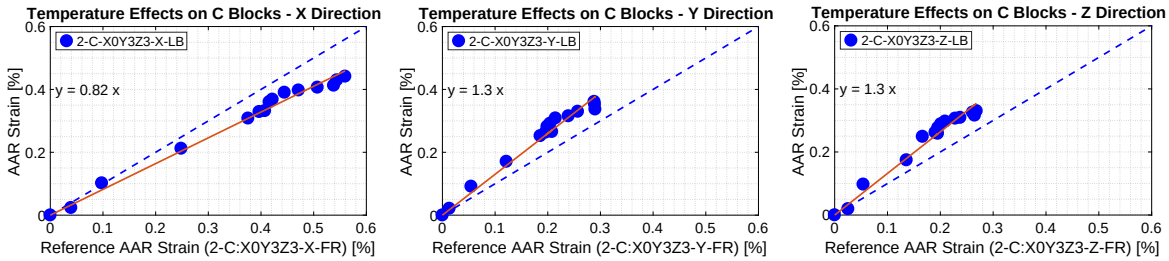

Figure 8.14: Effect of Temperature on Block C

8.4.3 Temperature Effects on Expansion Rate

It was theorized that the temperature of the specimen could be correlated to the rate of expansion in the specimen. Using the internal specimen temperature gauges, average temperatures between data collection dates were calculated. The expansion rate betwwen measurements was calculated by dividing the expansion

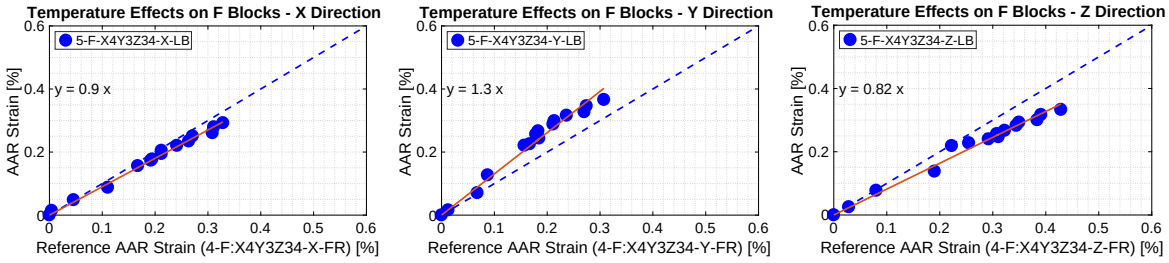

Figure 8.15: Effect of Temperature on Block F

since the last measurements were taken by the time between when the data was taken. The results are show in Figure 8.16.

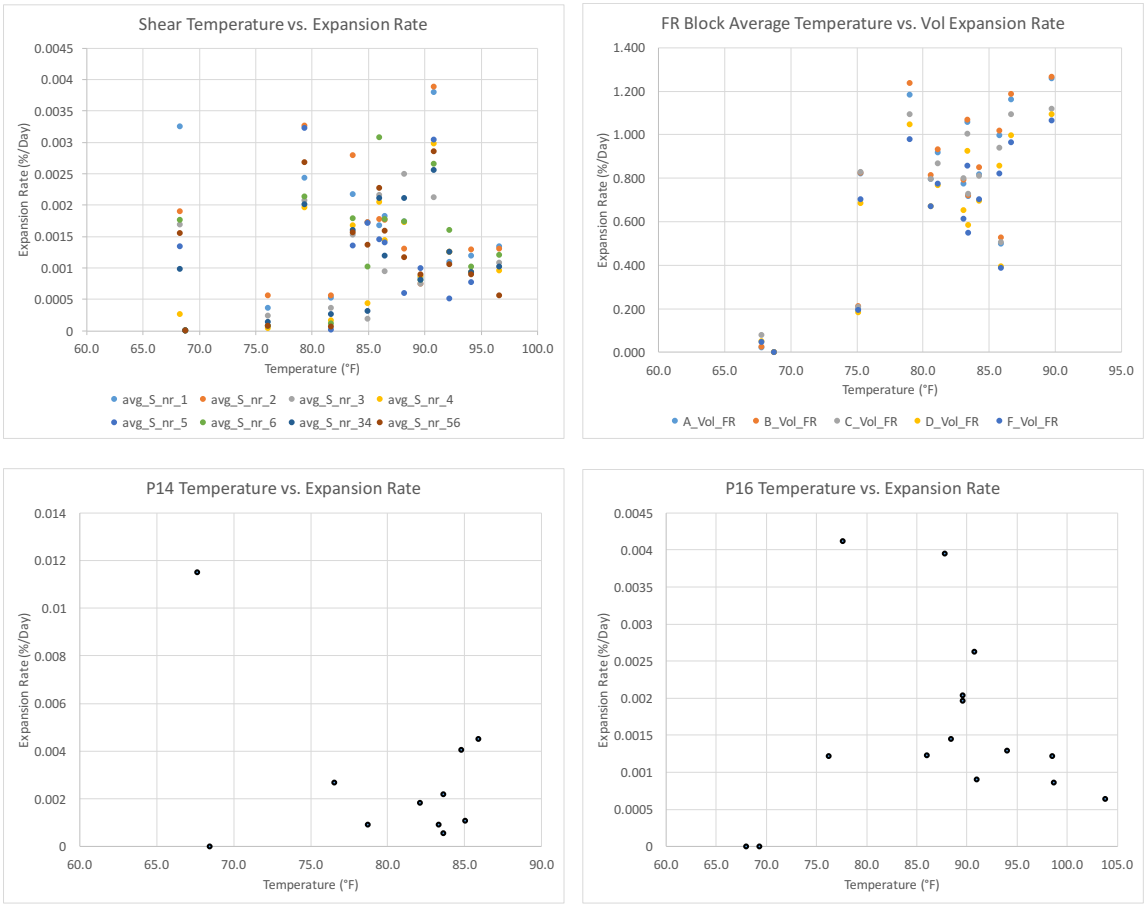

Figure 8.16: Average Temperature verses Expansion Rate

There is not a clear correlation between the expansion rate of percent per day and the internal temperature throughout the specimens. The best representation of the theory is in the volumetric expansion of the blocks. This lack of correlation is surely partially due to the non-linearity of ASR expansion. If expansion occurred linearly over the course of expansion, then a correlation may be seen. Additionally, alkalinity is not applied to the specimen at a constant rate. When spraying the blocks and shear specimens with NaOH, the pH of

the solution decreases over time and occasionally the specimens would dry out for a short period of time due to NaOH splashing or evaporating out of the pans. Due to these additional variables the course of the experiment, analyzing a connection between temperature and expansion rate is an incomplete comparison.

8.5 Volumetric Expansion

It was initially considered that the prisms were essentially expanding axially while the cubes were expanding volumetrically. Comparing the two would verify that all the specimens were expanding at the same volumetric rate. Figure 8.17 shows that the blocks and prisms have similar expansions to one another but the prisms expand significantly less than the blocks. This suggests that the transverse expansion of the prisms cannot be neglected. However, the fact that each specimen expansion is similar to one another confirms that each are expanding at similar volumetric rates.

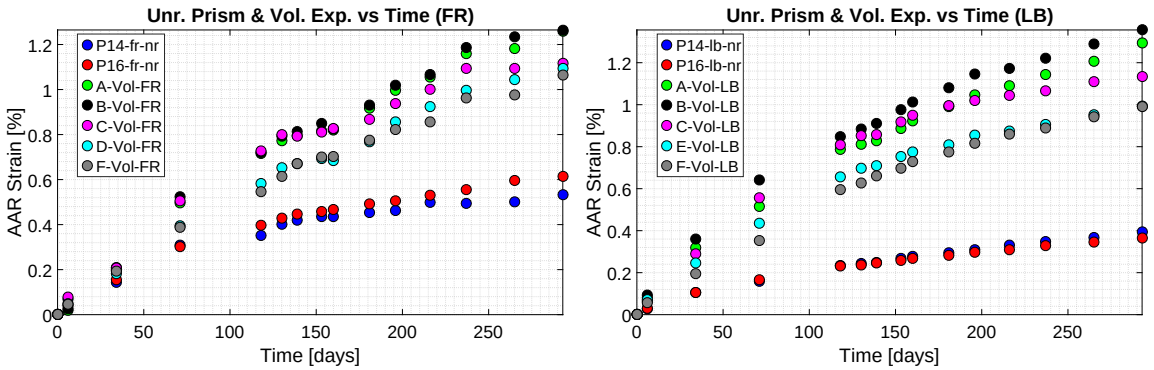

Figure 8.17: Comparison of prism axial expansion and block volumetric expansion for fog room and lab

8.6 Size Effects

To analyze if there is a size effect that contributed to expansion, unreinforced specimens in the fog room and lab where compared to one another in Figure 8.18. To numerically compare specimens of different sizes to one another, the volume to surface area ratio is computed and given in the legend of the plot.

The data suggests that there is no discernible trend showing a relation between size and rate of expansion. In the fog room, block and shear specimens have similar expansion while prisms are showing a greater expansion with a decrease volume to surface area ratio. This would suggest that there is a trend here but when prisms and block are compared in the lab, the trend is not continued. Here, increasing ratios show increased expansion although all three expansions are very similar to one another. The increased prism expansion in the fog room is because the prisms are submerged while the blocks are shear specimens are wrapped and wetted.

8.7 Batch Comparison

It was of interest to see if one batch of concrete was more reactive than the others. Figure 8.19 compares the unreinforced shear specimens, P14 prisms, P16 prisms, and blocks to each other, as the data was available.

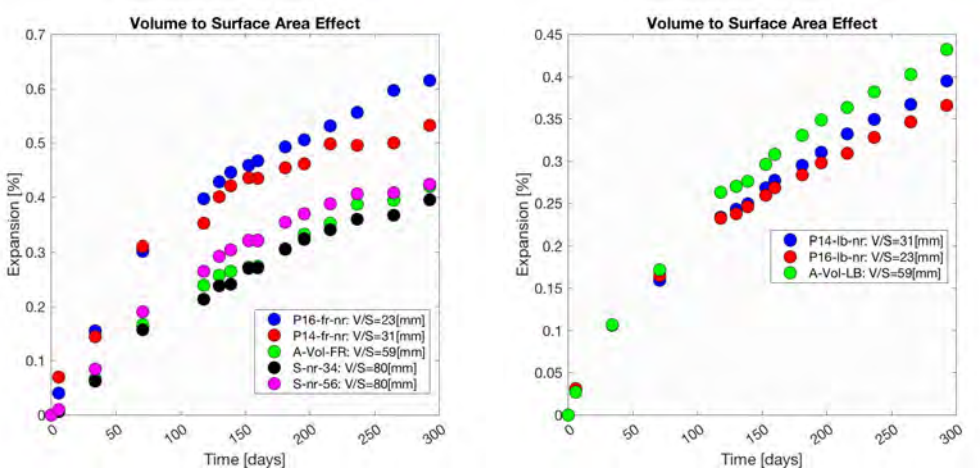

(a) Fog Room (b) Lab

Figure 8.18: Effect of size on specimen expansion in fog room and lab

There is no P14 specimen from Batch 2 and no blocks from batch 1 so that data is not included in those graphs. It is obvious that in the shear specimens and P14, batch 3 is the most expansive. However, P16 and the blocks indicate that batch 2 is slightly more expansive. Considering the batch comparison of the lab specimens in Figure 8.20, there is more evidence that batch 2 is as or more expansive than batch 3.

It was considered that batch 3 shear specimens are more reactive because of way they are stored in the fog room. Specimens of batches 1 and 2 are covered with a plastic tarp that extends to the bottom of the specimen where the batch 3 specimens are covered with plastic to only about halfway down the specimen. This may have inadvertently insulated the specimens in batches 1 and 2 from the exterior heat while batch 3 received more heat and therefore shows more expansion. However, a comparison of the internal temperature of the specimens shows no significant variation in temperature of the specimens.

Another interesting observation when comparing each batch of concrete is that batch 2 is just as expansive (more in some cases) as batches 1 and 3. When mixing batch 2, the slump was extremely low; only 2.25 inches compared to 5.5 and 6.0 inches of batches 1 and 3, respectively. Observing that batch 2 has comparative expansion levels shows that the concrete's slump may not have a substantial effect on ASR expansion.

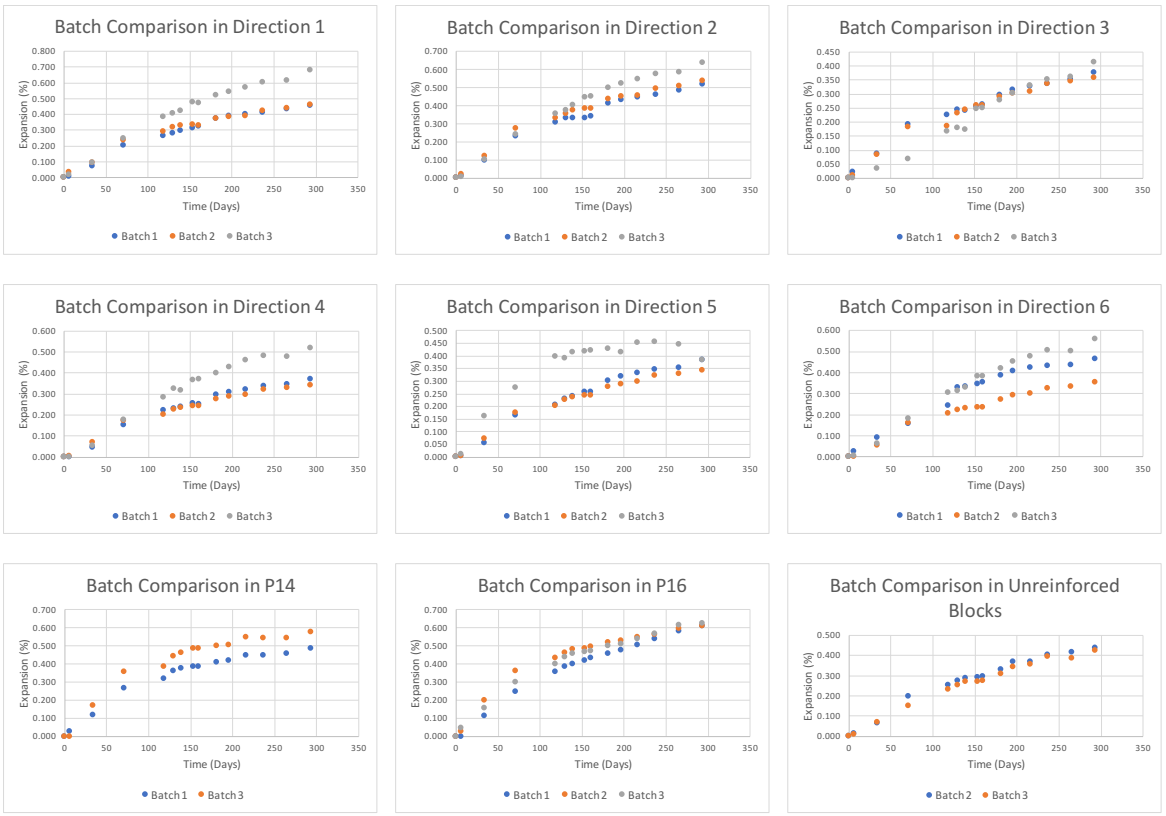

Figure 8.19: Batch Comparison in Fog Room

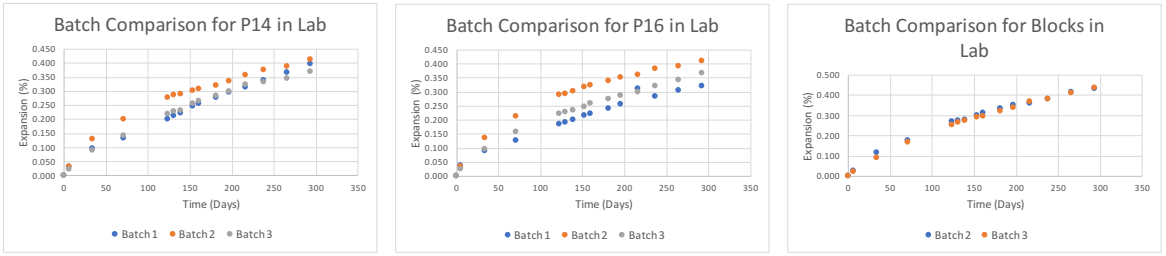

Figure 8.20: Batch Comparison in Fog Room

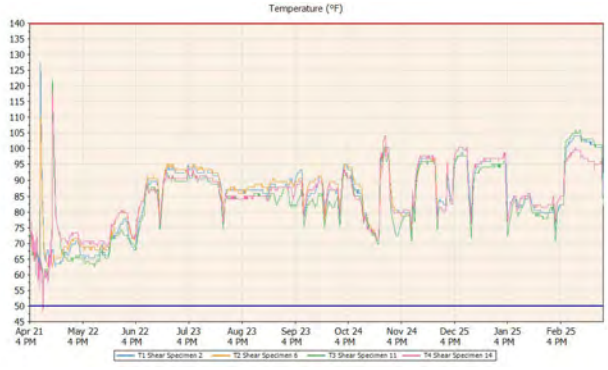

Figure 8.21: Temperature comparison of shear specimens from each batch

This page intentionally left blank.

9 Summary & Conclusion

9.1 Summary

At the conclusion of this research, a number of broad and specific observations and conclusions can be made about the effects of temperature, reinforcement, and size on ASR expansion.

9.1.1 Broad Observations

1. Substantial expansion is observed in all specimens definitively indicating production of ASR.
2. Volumetric expansion for blocks is similar, regardless of reinforcement configuration.
3. No substantial expansion has been observed in the control specimens.
4. Reinforcement caused a reduction in expansion in prisms and shear specimens stored in the fog room.
5. Expansion of both the prisms and shear specimens increased at the reinforcement ratio decreased.
6. Reinforcement did not necessarily result in a significant reduction in expansion in the blocks.
7. No distinct correlation in the blocks was found between the reinforcement ratio in a given direction and the expansion in that direction.
8. Increased temperature caused an increase in expansion for the prisms.
9. Most blocks stored at ambient temperatures showed similar or greater expansion that those stored at elevated temperatures likely due to the blocks submerged in NaOH at ambient conditions and wrapped in NaOH wetted burlap in the fog room.
10. Little evidence showed that the specimen temperature independently correlated to the expansion rate.
11. Concrete mixed in Batch 3 was found to be the most reactive in shear specimens.
12. No evidence that specimen size plays a role in rate of expansion.
13. Though not fully investigated, the crack indeces values appear to correlate well with the corresponding expansion measurements.

9.1.2 Detailed Observations

1. ASR damage has been definitively produced in the concrete specimens.
2. All unreinforced prisms in the fog room have met the target expansion of 0.5%.
3. All unreinforced shear specimens have met the target 0.5% expansion in at least one direction.
4. No unreinforced blocks in either the lab or the fog room have reached the 0.5% expansion.
5. No control specimen showed greater than .04% expansion proving a successful suppression of ASR expansion using lithium nitrate.
6. In most instances of the reinforced shear specimens, the vertical direction (which is unreinforced) shows

the greatest expansion.

7. Prediction of expansion using ASR Constitutive Law proposed by Larive (1998) reasonably matched the expansion observed in the unreinforced prisms.
8. Reinforced 4"×4"×16" prisms showed an average expansion of 27% of the unreinforced counterpart.
9. Reinforced 6"×6"×14" prisms showed an average expansion of 65% of the unreinforced counterpart.
10. Expansion of reinforced shear specimens expanded 11% of the unreinforced specimens in the longitudinal direction on the top of the specimen due to reinforcement anchorage debonding and subsequent cracking in the specimen.
11. Shear specimen expansion in the vertical (which is unreinforced) is the same for both reinforced and unreinforced specimens.
12. Transverse expansion in the reinforced shear specimens is 77% of the unreinforced expansion in the same direction.
13. Longitudinal expansion measured on the side of reinforced shear specimen is 64% of the unreinforced shear specimens.
14. Definitive conclusions about the effects of reinforcement on expansion in the blocks as many results contradict the predicted result supported by previous research. A theory for the unexpected results is that the expanding concrete has debonded from rebar, therefore acting like an unreinforced specimen with additional pathways for alkali transfer though the space around the rebar created by debonding.
15. In the fog room, blocks with C and D reinforcement have expansion that most match the predicted results.
16. In the fog room, blocks with B and C reinforcement best match predicted results
17. Blocks with B and C are biaxially reinforced. These blocks show definitive evidence of expansion transfer occurring when an increase in expansion is observed in one directions when it is restrained in the other two orthogonal directions.
18. 4"×4"×16" prisms in ambient temperatures of the lab showed an average 58% expansion of their counterpart in the elevated temperature of the fog room.
19. Lab 6"×6"×14" prisms showed an average expansion of 66% of the unreinforced fog room counterpart.
20. Most blocks in the lab expanded produced similar (within 10% less) or greater expansion than the blocks in the fog room with the same reinforcement layout. No trend with respect to reinforcement configuration or measurement direction could be found to describe the behavior. The only difference that is believed to impact the results is that the blocks in the lab are submerged in NaOH while fog room blocks are wrapped in burlap wetted with NaOH.
21. There is no definitive correlation to temperature and expansion rate.
22. Batch 3 is found to be the most reactive in the shear specimens. However, this could be due to the frequent evaporation of the NaOH requiring refilling which supplied the specimens with NaOH at 1.0 molarity. NaOH in pans that did not require frequent refills saw a decrease in molarity over time which could reduce expansion.
23. In most blocks and prisms in lab and fog room, no batch was distinctly more expansive. The exception is that batch 2 in lab P16 prisms was more reactive than other batches.
24. Batch 2 is found to be comparatively to the other two batches expansive despite having a significantly lower slump at the time of casting. Batch 2 had a slump of 2.25 inches compared to 5.5 inch and 6.0 inch slump of Batch 1 and 3, respectively.
25. There is no discernible correlation between specimen size and expansion. Greater expansion in fog

room prisms is because prisms are submerged in NaOH while block and shear specimens are wrapped and wetted.

9.2 Conclusions

For over a year, much work has been done to cast reactive concrete specimens and promote alkali-silica reaction expansion in them. Very rarely have this many specimens of this size been cast and cured at one time to study the effects of ASR. Typically small cylinders or prisms are cast and stored in containers to develop ASR reactions. Due to the large size of the shear specimens, a unique sprinkler system was developed to wet the burlap covered specimens to prevent alkali leaching. Despite challenges of intermittently working fog room facilities, detaching datum discs, and working in an environment with a high volume of caustic solution, substantial ASR expansion was created and a large amount of useful data was collected. This data set provides a basis for analysis on the effects of temperature, reinforcement, and size.

Once the substantial amount of data was collected, MATLAB programs were written to import, organize, and plot the data and provide tools to produce synthesized results. One tool enabled plotting the expansion of one or more specimens over time or comparing specimens to one another enabling the possibility of over 1,400 plots to choose from. Additionally, processed data was exported into spreadsheets for further of other factors such as temperature effect on expansion rate or batch comparisons.

Finally, once all this relevant data had been plotted, an analysis of all the plots was completed to see what conclusions could be made. From these plots, a number of definitive and not so definitive observations were made to understand the effect of temperature, reinforcement, and size in ASR afflicted concrete. From this analysis, a number of recommendations on how to improve on this research are given.

9.3 Recommendation for Future Work

Note: As important as those suggestions are, none of them is critical.

In future work, it is suggested that a more detailed experiment be completed to study the effects of temperature, size, and reinforcement on ASR Expansion in concrete. In this experiment, the prisms showed good results that correlated with predictions. However, the blocks did not show as good of results. It is recommended that further research using blocks to quantify the effects of reinforcement, temperature, and size on ASR expansion be completed. Many improvements can be made to this experiment to produce better results.

When studying temperature effects, ensuring that the way in which blocks are wetted with NaOH is consistent for both elevated and ambient temperatures. Also, it should be assured that a reliable source of heat can be provided to blocks at elevated temperatures at all times over the course of the experiment.

For the effect of reinforcement, having a greater number of blocks at each reinforcement configuration in would allow averages to be taken to provide more consistent results. At least three blocks of each reinforcement layout would be sufficient to verify that all blocks are providing results similar to one another and that there are no outliers in each group. When comparing triaxially reinforced blocks (such as blocks D with #4 bars and E with #3 bars), it may be better to have a larger difference in rebar sizes such as using #3 and #5 bars. Additionally, it may be helpful to have the same larger difference in reinforcement for blocks that are triaxially reinforced with two different rebar sizes(such as in F reinforcement). This also may be able to more clearly show the effects of increasing reinforcement ratios in specimens reinforced in

two and three dimensions.

To further study size effects, a greater number of specimens gradually increasing size is needed to make a more definitive statement about its effect. In this experiment, data from specimens that were cast to study reinforcement and temperature effects was also used to investigate size effects. However, specimens were not specifically cast for the purpose of studying this variable. Carefully designing the size, number, and orientation of the specimens will provide better insight into how a specimen's cross-sectional area or volume will effect its expansion. Additionally, as with studying temperature effects, it is important that all specimens are stored and cured in the same manner.

Finally, a interesting outcome of this analysis is finding that batch 2, which had a significantly lesser slump than batch 1 and 3 showed similar levels of expansion throughout the experiment. It would be interesting to further and more deliberately study the effects of slump on ASR expansion.

Bibliography

ASTM C1260 (2000). *C1260-94 Standard Test Method for Potential Alkali Reactivity of Aggregates (Mortar-Bar Method)*. Annual Book of ASTM Standards.

ASTM C1293 (2008). "1293". In: *Standard Test Method for Concrete Aggregates by Determination of Length Change of Concrete Due to Alkali Silica Reaction*.

ASTM, C39 (2016). "39, Standard test method for compressive strength of cylindrical concrete specimens". In: *Annual book of ASTM standards* 04.02.

Bérubé, M.A. et al. (2005). "Evaluation of the expansion attained to date by concrete affected by alkali-silica reaction. Part III: Application to existing structures". In: *Canadian Journal of Civil Engineering* 32.3, pp. 463–479.

Blanks, R.F. and H.S. Meissner (1946). "The expansion test as a measure of alkali-aggregate reaction". In: *Journal Proceedings*. Vol. 42. 4, pp. 517–540.

Dunant, Cyrille F and Karen L Scrivener (2012). "Effects of uniaxial stress on alkali–silica reaction induced expansion of concrete". In: *Cement and concrete research* 42.3, pp. 567–576.

Fournier, B. et al. (2009). "Effect of environmental conditions on expansion in concrete due to alkali–silica reaction (ASR)". In: *Materials Characterization* 60.7, pp. 669–679.

Gautam, BP et al. (2017). "Multiaxial Expansion-Stress Relationship for Alkali Silica Reaction-Affected Concrete." In: *ACI Materials Journal* 114.1.

Hobbs, D.W. (1988). *Alkali-Silica Reaction in Concrete*. London: Thomas Telford.

Ideker, J.H. et al. (2012). "Do current laboratory test methods accurately predict alkali-silica reactivity?" In: *ACI Materials Journal* 109.4.

Katayama, T. (2017). "Estimation of Residual Expansion". In: *RILEM TC 259-ISR report: Diagnostic & Prognosis of AAR in Existing Structures*. In Preparation.

Larive, C. (1998). *Apports Combinés de l'Experimentation et de la Modélisation à la Comprehension del'Alcali-Réaction et de ses Effets Mécaniques*. Tech. rep. *In French*. Paris: *Ecole Normale des Ponts et Chaussées*.

LCPC (1997). *Détermination de l'indice de fissuration d'un parement de béton; Méthode d'essai LCPC N0. 47*. Tech. rep. 47. Paris, France: Laboratoire Central des Ponts et Chaussées.

Leemann, A. and M. Griffa (2013). *Diagnosis of alkali-aggregate reaction in dams*. Tech. rep. Publication 290934. SFOE-Project SI/500863-01. EMPA, Laboratory for Concrete/Construction Chemestry. URL: http://www.bfe.admin.ch/dokumentation/energieforschung/index.html?lang=de&publication=11174.

Lindgård, Jan et al. (2010). "The EU "PARTNER" Project-European standard tests to prevent alkali reactions in aggregates: final results and recommendations". In: *Cement and Concrete Research* 40.4, pp. 611–635.

Lindgård, Jan et al. (2012). "Alkali–silica reactions (ASR): literature review on parameters influencing laboratory performance testing". In: *Cement and Concrete Research* 42.2, pp. 223–243.

Morenon, Pierre et al. (2017). "Impact of stresses and restraints on ASR expansion". In: *Construction and Building Materials* 140, pp. 58–74.

Multon, S. and F. Toutlemonde (2006). "Effect of Applied Stresses on Alkali-Silica Reaction Induced Expansions". In: *Cement and Concrete Research* 36.5, pp. 912–920.

Musaoglu, O., L. Turanli, and A. Saritas (2014). "Assessing the Effects of Mechanical Preventive Measures on Alkali-Silica Reaction Expansion with Accelerated Mortar Bar Test". In: *Journal of Testing and Evaluation* 42.6, pp. 1–10.

Saouma, V.E. and L. Perotti (2006). "Constitutive Model for Alkali Aggregate Reactions". In: *ACI Materials Journal* 103.3, pp. 194–202.

Saouma, V.E., R. Sparks, and D. Graff (2016). *Development Of ASR Concrete Mix for Large Scale Testing*. Tech. rep. Report to the Nuclear Regulatory Commission, Grant No. NRC-HQ-60-14-G-0010. University of Colorado, Boulder.

Saouma, V.E et al. (2016). "Effect of alkali–silica reaction on the shear strength of reinforced concrete structural members. A numerical and statistical study". In: *Nuclear Engineering and Design* 310, pp. 295–310.

Stanton, T.E. (1940). "Expansion of Concrete Through Reaction Between Cement and Aggregate". In: *Proceedings of ASCE* 66, pp. 1781–1811.

Swamy, R.N. and M.M. Al-Asali (1988). "Influence of Alkali-Silica Reaction on the Engineering Properties of Concrete". In: *Alkalies in Concrete, ASTM STP 930*. Ed. by V.H. Dodson. Philadelphia, PA, pp. 69–86.

A Individual Expansion Curves

Below is a complete inventory of the individual expansion curves created during the data analysis process. For a review of the conventions used in the plots, see Section 6.1.1.

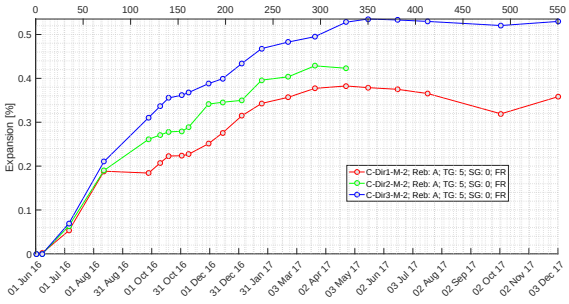

(a) Block 1; FR, Batch 2, Rebar A, TS 5, SG 0

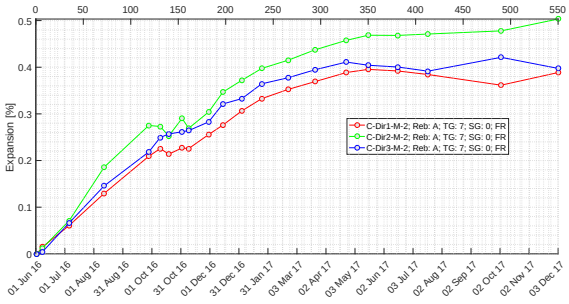

(b) Block 6; FR, Batch 2, Rebar A, TS 7, SG 0

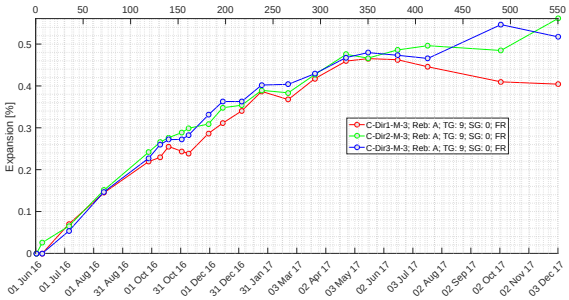

(c) Block 11; FR, Batch 3, Rebar A, TS 9, SG 0

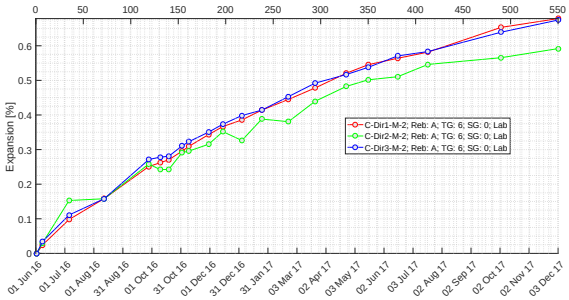

(d) Block 2; Lab, Batch 3, Rebar A, TS 6, SG 0

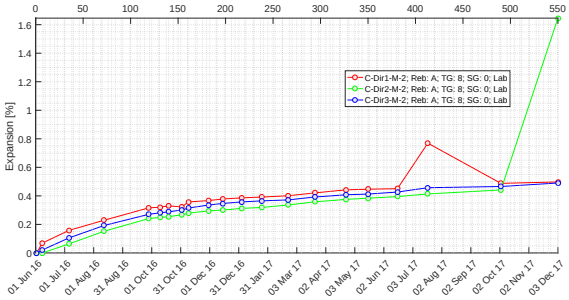

(e) Block 7; Lab, Batch 2, Rebar A, TS 8, SG 0

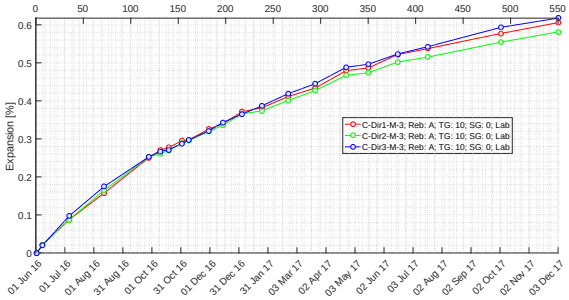

(f) Block 12; Lab, Batch 3, Rebar A, TS 10, SG 0

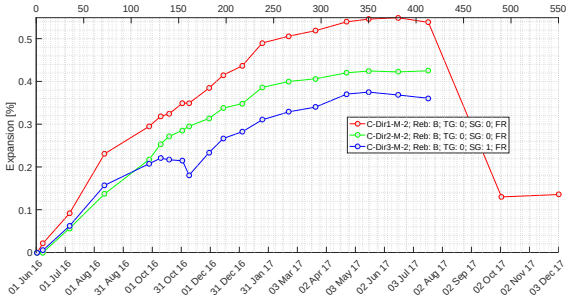

(g) Block 3; FR, Batch 2, Rebar B, TS 0, SG Z

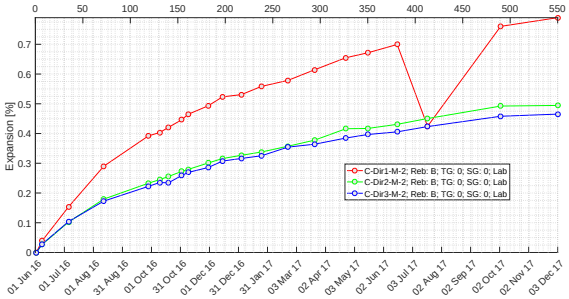

(h) Block 4; Lab, Batch 2, Rebar B, TS 0, SG 0

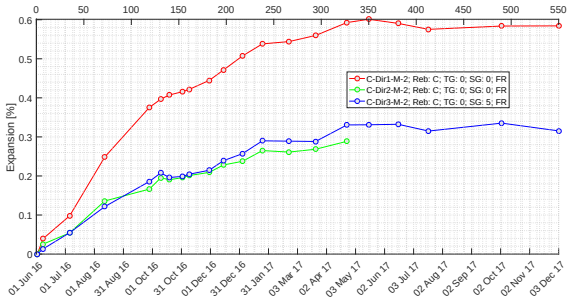

(i) Block 8; FR, Batch 2, Rebar C, TS 0, SG Z

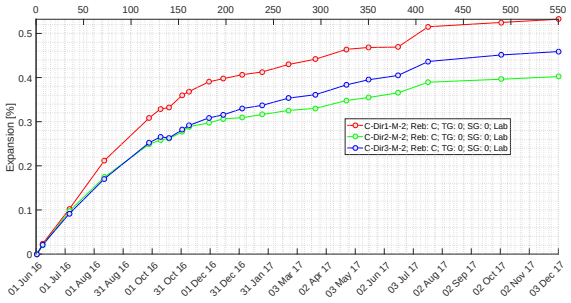

(j) Block 9; Lab, Batch 2, Rebar C, TS 0, SG 0

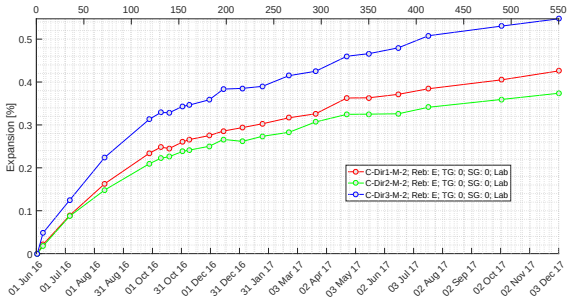

(k) Block 10; Lab, Batch 2, Rebar E, TS 0, SG 0

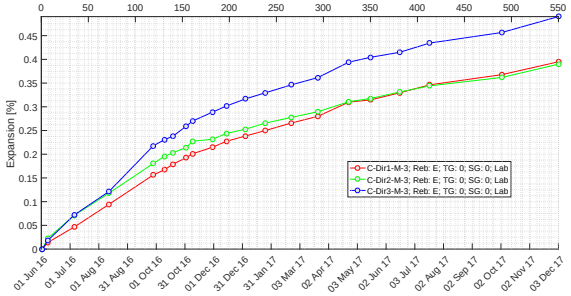

(l) Block 15; Lab, Batch 3, Rebar E, TS 0, SG 0

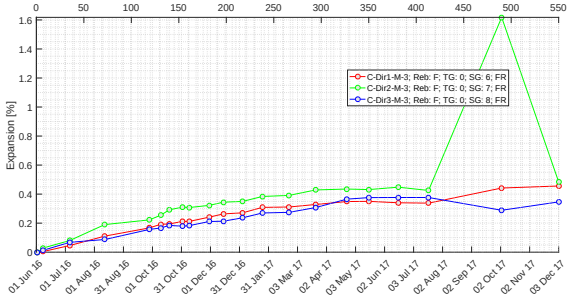

(m) Block 13; FR, Batch 3, Rebar F, TS 0, SG X-Y-Z

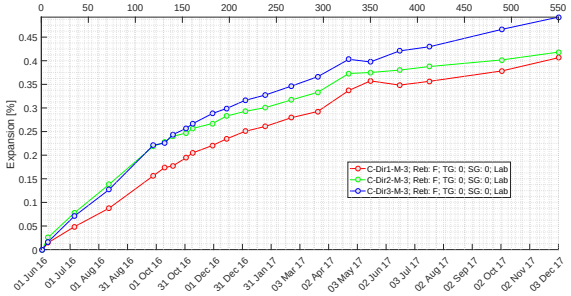

(n) Block 14; Lab, Batch 3, Rebar F, TS 0, SG 0

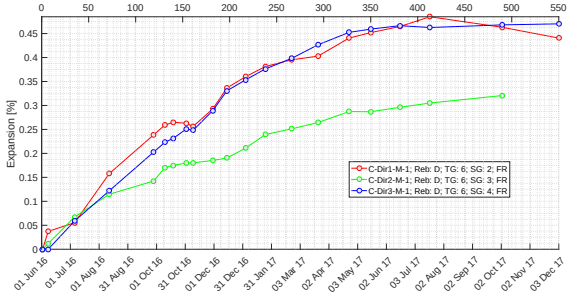

(o) Block 5; FR, Batch 1, Rebar D, TS 6, SG X-Y-Z

Figure A.1: Block specimens

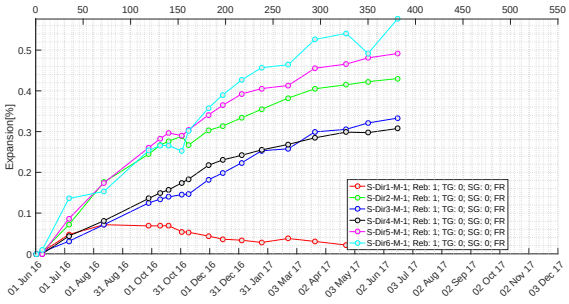

(a) Specimen 1; Reactive, Mix 1, Rebar

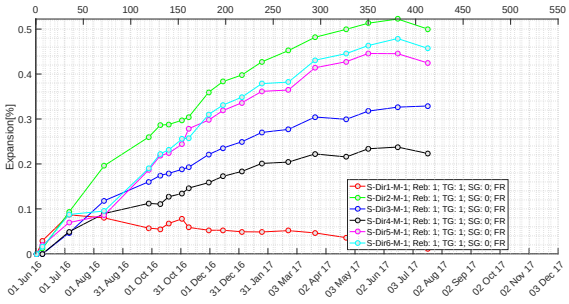

(b) Specimen 2; Reactive, Mix 1, Rebar, TG 1

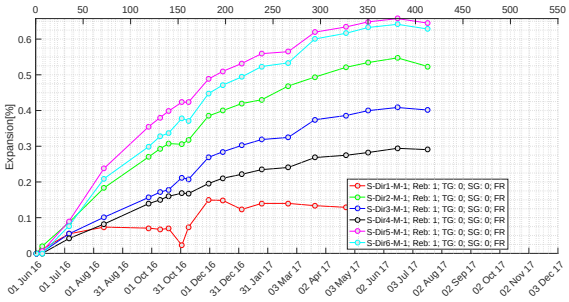

(c) Specimen 3; Reactive, Mix 1, Rebar

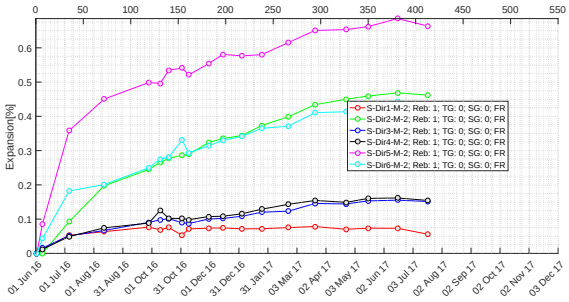

(d) Specimen 5; Mix 2, Reactive, Rebar

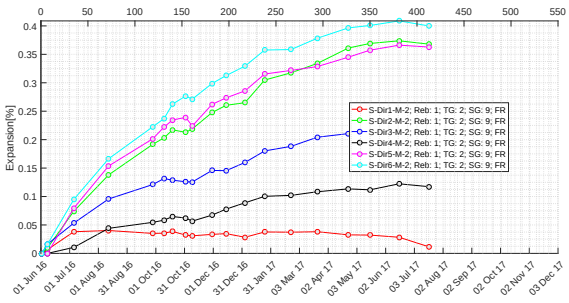

(e) Specimen 6; Reactive, Mix 2, Rebar, TG 2, SG 9

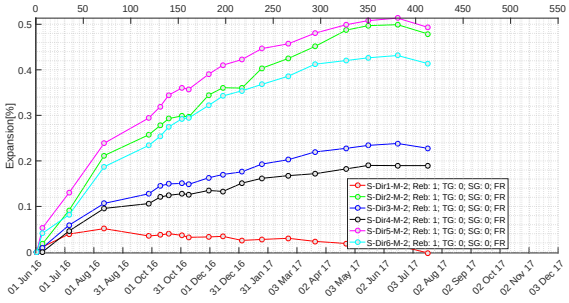

(f) Specimen 7; Reactive, Mix 2, Rebar

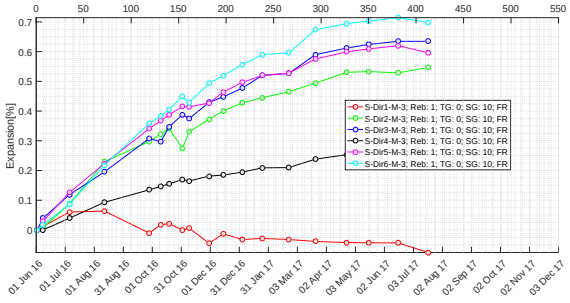

(g) Specimen 9; Reactive, Mix 3, Rebar, SG 10

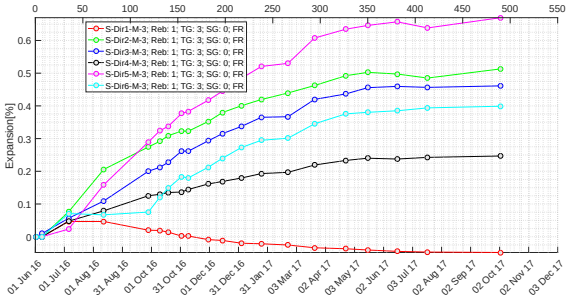

(h) Specimen 10; Reactive, Mix 3, Rebar, TG 3

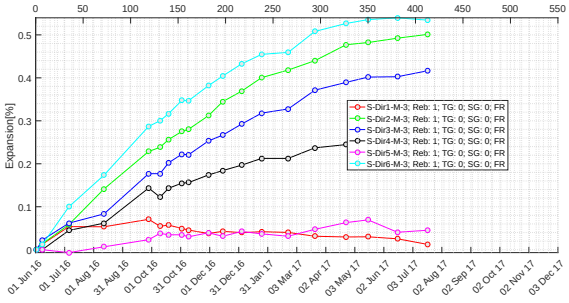

(i) Specimen 11; Reactive, Mix 3, Rebar

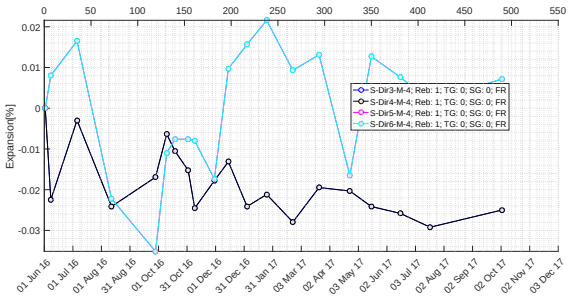

(j) Specimen 13; Non-Reactive, Mix 4, Rebar

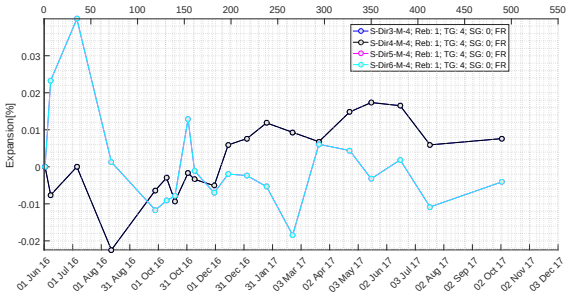

(k) Specimen 14; Non-Reactive, Mix 4, Rebar, TG 4

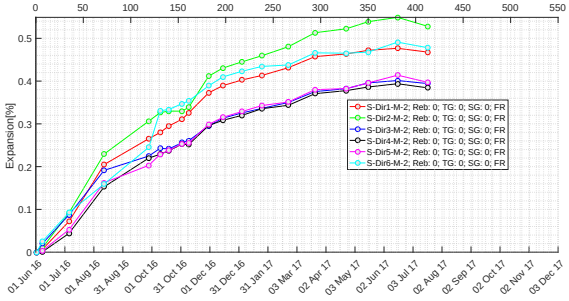

(l) Specimen 4; Reactive, Mix 2, No Rebar

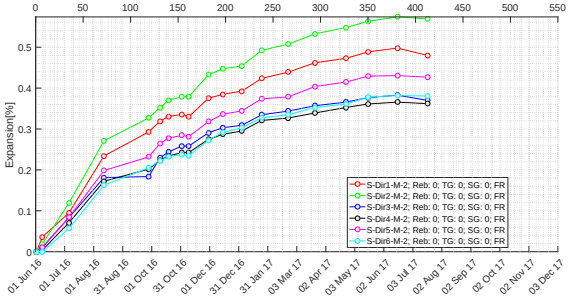

(m) Specimen 8; Reactive, Mix 2, No Rebar

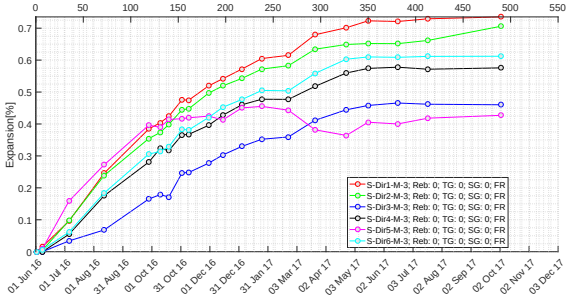

(n) Specimen 12; Reactive, Mix 3, No Rebar

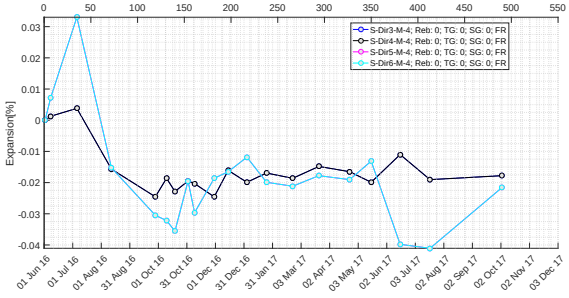

(o) Specimen 15; Non-Reactive, Mix 4, No Rebar

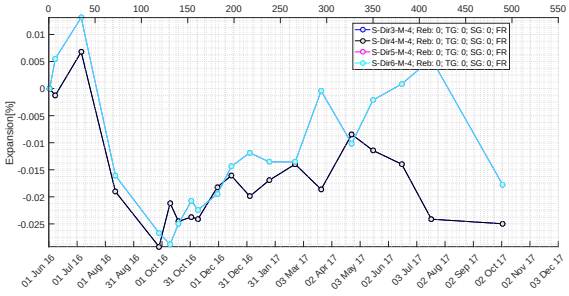

(p) Specimen 16; Non-Reactive, Mix 4, No Rebar

Figure A.2: Shear specimens.